UNIVERSITY OF FORT HARE

University of Fort Hare
Together in Excellence

Faculty of Science & Agriculture

Chemistry Department

Synthesis, Characterisation and Evaluation of functionalized Lignocelluloses-clay nanocomposites for Organic pollutant removal from Water

Donovan M Mafukidze

(Student Number: 200909979)

Prof L.Tichagwa (Supervisor)

Dr M. Lutz (Co-supervisor)

Dr D. M. Katwire (Co-supervisor)

DECLARATION

I declare that this work is the result of my own research except where cited in the references. The dissertation has not been accepted for any degree and is not concurrently submitted in candidature of any other degree.

Signature : …….

Name : ……

Date : ……

DEDICATIONS

This work is dedicated to the Mafukidze and the Kawonza families for their unconditional love and support, and also in loving memory of my dear departed grandparents, Cleopas and Diana Kawonza for the greatness they dreamt and saw in me.

ACKNOWLEDGEMENTS

Firstly I would like to give thanks to the Lord God Almighty for giving me the gift of life and the opportunity to proceed with my studies in good health.

I also want to thank my supervisor Prof L. Tichagwa for her tireless efforts, guidance, support and encouragement. I also extend my gratitude to my co-supervisors Dr M. Lutz and Dr D. M. Katwire for their support, guidance and contributions to my work.

I am grateful for all the contributions to my work given by the following people; Mr T. Bunhu, Mr T. Mcako, Mr K. Tshapu, Mr N. Manene, Mr H. Mungondori, Mr P. Nyamukamba and Miss A. Nel, for their contributions. They all played significant roles in the successful completion of my work. I would also like to thank the University of Fort Hare Chemistry Department as a whole for hosting my research.

It is with a deep sense of gratitude that I thank the National Research Foundation (NRF) and the Govan Mbeki Research and Development Centre (GMRDC) at the University of Fort Hare for the financial support provided.

Last but not least, I would like to give thanks to my family for their love, support and encouragement which kept me motivated. I also thank them for believing in me and standing by my side all the way during the course of my study.

ABSTRACT

PMPSgLig-NaMMT nanocomposites were prepared from methacryloxypropyltrimethoxysilane (MPS), lignocellulose and montmorillonite clay. The potential enhancement of organic pollutant adsorption capabilities of PMPSgLig-NaMMT nanocomposite from water through functionalization was investigated. PMPSgLig-NaMMT was functionalized by esterification and etherification using different methods so as to increase the surface hydrophobicity of the material and hence improve its compatibility with the target pollutants. Specific chemical routes specially tailored for PMPSgLig-NaMMT were established for functionalization mostly based on the common esterification (Fischer esterification) and etherification (Williamson's etherification) reactions. In the functionalization methods, factors such as pH environment, nanocomposite composition, nature of functionalization moiety, and use of or absence of solvents and their variations were studied.

FT-IR, XRD, SEM and TGA were used to characterize the synthesized and functionalized nanoadsorbents. The techniques showed successful functionalization via esterification and etherification methods albeit to different extents, with clear retention of the material's original structure though there were signs of degradation with some methods. Characterization was supported by adsorption studies to validate implications and draw conclusions. The use of 1,10-phenathroline as a model organic pollutant in water in the adsorption studies showed that adsorbents conformed to monolayer adsorption following pseudo-second order kinetics for adsorption of organic pollutants accurately represented. Most importantly the studies revealed the significant impact of the nanocomposite composition on the overall absorbent performance. Adsorption studies also showed that functionalization via esterification methods gave rise to better adsorbents.

LIST OF ABBREVIATIONS

PMPS*g*Lig-NaMMT	Poly (methacryloxypropyl trimethoxysilane) grafted lignocellulose-sodium montmorillonite
Comp	Composite (PMPS*g*Lig-NaMMT) with a lignocellulose to sodium montmorillonite clay ratio of 2:1 respectively
Comp (1:1)	PMPS*g*Lig-NaMMT nanocomposite with a lignocellulose to sodium montmorillonite clay ratio of 1:1 respectively
Comp (1:2)	PMPS*g*Lig-NaMMT nanocomposite with a lignocellulose to sodium montmorillonite clay ratio of 1:2 respectively
Comp (2:1)	PMPS*g*Lig-NaMMT nanocomposite with a lignocellulose to sodium montmorillonite clay ratio of 2:1 respectively
DBTDL	Dibutyltin dilaurate
DMSO	Dimethylsulfoxide
Est (BCl)	Aliphatic functionalized nanocomposite ester (butyryl chloride functionalized)
Est (DBTDL)	Aliphatic functionalized nanocomposite ester (dibutyltin dilaurate catalysed functionalized)
Est (DBTDL 1:1)	Aliphatic functionalized nanocomposite ester (dibutyltin dilaurate catalysed functionalized) based on Comp (1:1)
Est (DBTDL 1:2)	Aliphatic functionalized nanocomposite ester (dibutyltin dilaurate catalysed functionalized) based on Comp (1:2)
Est (DBTDL 2:1)	Aliphatic functionalized nanocomposite ester (dibutyltin dilaurate catalysed functionalized) based on Comp (2:1)

Est (H_2SO_4)	Aliphatic functionalized nanocomposite ester (sulphuric acid catalysed functionalized)
Est (Na)	Aliphatic functionalized nanocomposite ester (sodium metal catalysed functionalized)
Eth (Alip-P)	Aliphatic functionalized nanocomposite ether (pentane solvent)
Eth (Alip-SF)	Aliphatic functionalized nanocomposite ether (solvent free)
Eth (Alip-T)	Aliphatic functionalized nanocomposite ether (toluene solvent)
Eth (Arom)	Aromatic functionalized nanocomposite ether
Eth (H_2SO_4)	Aliphatic functionalized nanocomposite ether (sulphuric acid catalysed functionalized)
Eth (Na)	Aliphatic functionalized nanocomposite ether (sodium metal catalysed functionalized)
EtOH	Ethanol
FT-IR	Fourier transform infrared
Lig	Lignocellulose
MMT	Montmorillonite
MPS	Methacryloxypropyl trimethoxysilane
NaMMT	Sodium montmorillonite
SEM	Scanning electron microscopy
TGA	Thermogravimetric analysis

THF	Tetrahydrofuran
UV/Vis	Ultra-violet/Visible spectroscopy
XRD	X-ray diffraction

LIST OF FIGURES

LIST OF TABLES

TABLE OF CONTENTS

CHAPTER 1

INTRODUCTION

1.1 Overview

Water is sometimes referred to as the "universal solvent" because of its ability to dissolve more substances than any other liquid. This ability may be attributed to the polar nature of the water molecules. Its good solvent properties make it a very important substance in living organisms and their environment where it serves as a transport medium for valuable chemicals, minerals and nutrients; and also as a reaction medium. Apart from its solvent properties water is a temperature buffer and metabolite in living organisms, and also provides a living environment for some organisms. The important role it plays in living organisms makes it a vital necessity for their survival, especially for human beings, and hence it is an extremely important part of everyday life.

However the remarkable solvent properties are not only limited to the dissolution of biologically valuable substances, but also applies to harmful entities too during pollution, and has led to natural sources of clean consumable water being significantly limited. Science and technology are therefore at the forefront in the development of methods for treating water from various sources and recycling waste water to produce clean safe water for consumption and use. Various waste water treatment methods are currently available which include chemical precipitation (United States of America. U.S. EPA, Office of Water Washington, D.C. 2000), reverse osmosis, evaporation, electrodialysis, phytoextraction and ultrafiltration (Li *et al.*, 2003; Sprynskyy *et al.*, 2006; Mobasherpour *et al.*, 2011). Other methods such as advanced oxidation technology, electrochemical methods, microbiological decomposition, ozonation, coagulation and membrane filtration (Lata *et al.*, 2008; Lin *et al.*, 2008; Zhang *et al.*, 2011) are also applied in water treatment for the specific removal of organic pollutants.

Adsorption technology has also made its mark on water treatment where it has proven to be efficient in the removal of both organic and inorganic pollutants from waste water (Nigam et al, 1996; Robinson *et al*, 2001; Annadurai *et al*, 2002). Adsorption methods have been found to provide cost effective solutions to waste water decontamination and have provided a step towards one of the United Nations' Millennium Development Goals (Millennium Declaration, 2000).

1.2 Study Introduction and Motivation

Simultaneous adsorption of methyl orange and metal cations by PMPSgLig-NaMMT was observed to result in the increase of methyl orange adsorption by the adsorbent material (Bunhu and Tichagwa, 2012). A hypothetical explanation of this observation could be that, metal cation adsorption resulted in an increase in positive charge on the adsorbent surface which in-turn resulted in an enhanced electrostatic attraction of methyl orange molecules which encouraged close packing of the molecules in a relatively uniform orientation. The adsorbed molecules hence created a hydrophobic film on the surface of the adsorbent which resulted in an enhanced adsorption of subsequent methyl orange molecules through hydrophobic interactions. Taking this into consideration, enhancing the hydrophobicity of the adsorbent surface would be expected to significantly improve the material's organic pollutant adsorption capabilities from water for a wider range of organics.

This study seeks to develop nanocomposites based on PMPSgLig-NaMMT which have an affinity for organic pollutant molecules of different types. This was to be achieved by modification of the material's surface through functionalization to make the material more hydrophobic and hypothetically a better adsorbent for organic pollutants which are generally hydrophobic. Functionalization of the nanocomposite adsorbent by etherification and

esterification reactions may give rise to high performance organic pollutant removing adsorbents.

The study also combines three concepts of great interest in Chemistry namely; nanotechnology, green chemistry and water treatment. The nano-nature of the adsorbent material gives it a large surface area which is very essential for high adsorbent performance while the natural and relatively abundant raw materials for the synthesis of the nanocomposite adsorbent material suggests that application of the material may provide an effective low cost sustainable method to treat water contaminated with organic pollutants. PMPSgLig-NaMMT nanocomposite material is a relatively new material whose chemistry and full potential for application are still yet to be studied. This study therefore seeks to take a step forward in understanding the potentials in water treatment of the derivatives of the nanocomposite material based on the material's abilities already reported (Bunhu and Tichagwa, 2012). New materials are therefore to be developed based on the nanocomposite which proved to be an effective adsorbent for both organic and inorganic pollutants in water. Taking all this into consideration this study is motivated by the need to unlock the full potential of this new adsorbent material in water treatment.

1.3 Problem Statement

Bunhu and Tichagwa (2012) observed that addition of some heavy metals such as Pb^{2+} and Cd^{2+} to methyl orange (model organic pollutant) contaminated water, notably enhanced the adsorption of the dye by PMPSgLig-NaMMT nanocomposite adsorbent (Figure 1.3). However direct application of the observation would achieve the intended goal of dye removal, but would also defeat the overall intension of water purification due to the toxicity of the heavy metals. On the other hand the enhanced adsorption may also be hypothetically related to the polar nature of the dye molecules. In this respect the PMPSgLig-NaMMT

nanocomposite has proven to be a successful adsorbent for both organic and inorganic pollutants from water; however optimization of organic pollutant removal may be conditionally limited to polar organics in the presence of metal cations.

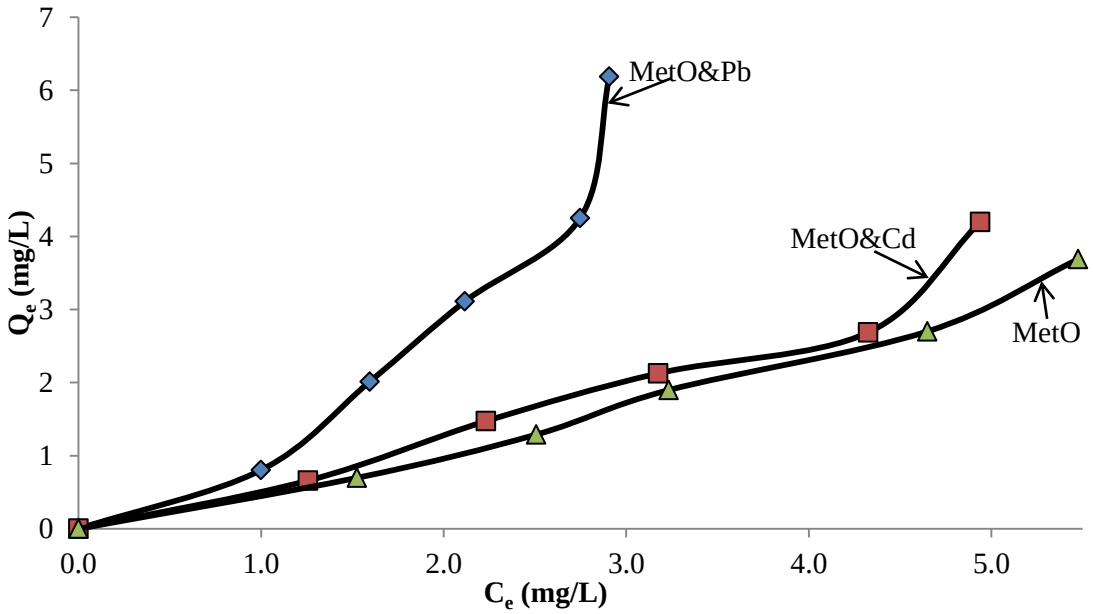

Figure 1.1: Isotherms for MetO, MetO & Cd and MetO & Pb adsorption onto PMPSgLig-NaMMT nanocomposite (Bunhu and Tichagwa, 2012).

With this in mind it is envisaged to improve the adsorption of organic compounds by modifying the nanocomposite surface and widen the range of organic compounds the adsorbent is highly effective on.

1.4 Aim and Objectives

1.4.1 Aim

To produce effective modified lignocelluloses-clay nanocomposites for organic pollutant removal from water through adsorption.

1.4.2 Objectives

- To modify lignocelluloses and montmorillonite clay and characterize the products.

- To prepare PMPSgLig-NaMMT nanocomposites of different compositions and characterize them.
- To functionalize PMPSgLig-NaMMT nanocomposites in order to increase hydrophobicity through esterification and/or etherification using different methods and characterize the products.
- To use the as prepared nanocomposites as adsorbents for the removal of organic pollutants (exemplified by 1,10-phenanthroline) from water.
- To evaluate the adsorption through the generation of adsorption isotherms and application of adsorption model equations.
- To determine the kinetics of the adsorption processes by the prepared nanocomposite adsorbents.
- To establish the effect of nature of functionalization environment (acidic or basic or no direct pH influencing) on the adsorbent performance.
- To establish the significance of the solvent used during functionalization on the adsorbent performance.
- To determine the significance of the nature (aliphatic or aromatic) of functionalization moiety on the performance of the product adsorbents.
- To identify and recommend the most preferable method for functionalization together with possible adjustments for optimization.

1.5 Scope of the Study

This study seeks to explore the possible avenues through which PMPSgLig-NaMMT nanocomposite adsorbent, developed in the research group (Bunhu and Tichagwa, 2012), can be modified for enhanced removal of organic pollutants from water by adsorption. The study focused on the means by which the material was made to be more compatible with organic

compounds and specifically the chemical routes taken to reach the final products. The effects of the functionalization method (etherification or esterification), environment of the functionalization process (acidic or basic), nature of functionalization moiety (aliphatic or aromatic) and use of different solvents on the adsorption performance of the adsorbent material (which included adsorption capacity, rate of adsorption and mode of adsorption) were determined. Adsorption studies were used to clarify implications of material modification as indicated by characterization hence studies did not put much attention on variations in adsorption conditions such as temperature and pH although these conditions were similar to the reported study.

1.6 Outline of Dissertation

This dissertation consists of three sections presented in the form of seven chapters. The first section is made up of Chapters 1 and 2, which introduce the study and give the literature review on relevant concepts to the study. The introduction presents a background and motivations for the study including the aim, objectives and the dissertation outline. On the other hand the literature review presents a build-up of concepts of interest in the research which range from adsorption technology and water treatment to functionalization of lignocellulosic materials.

The second section consists of Chapters 3, 4 and 5; and mostly involves the experimental part of the preparation of the nanocomposite adsorbents. Chapter 3 gives details of the materials and chemicals selected for use and characterization techniques used. Chapter 4 describes and presents methodology and results of raw material pretreatment and preparation of the unfunctionalized nanocomposite adsorbents together with the adsorbents' characterisation. Chapter 5 presents the details of functionalization methodologies through esterification and

etherification of the prepared nanocomposites for optimized organic pollutant adsorption and their characterisation.

The third and final section consisting of Chapters 6 and 7, provides an evaluation of the performance of the prepared adsorbents and study conclusions. Adsorbent performances will be evaluated from results from adsorption studies which will be described and presented in Chapter 6 in this section of the dissertation. In Chapter 7 a general summary overview of the study results is given upon which conclusions and recommendations for future work will be made.

1.7 References

Annadurai, G.; Juang, R. S.; Lee, D. J. **(2002)** Use of cellulose-based wastes for adsorption of dyes from aqueous solutions. *Journal of Hazardous Materials*. B92. p. 263–274.

Bunhu, T. and Tichagwa, L. **(2012)** Adsorption of Methyl Orange, Pb^{2+} and Cd^{2+} from Aqueous Solution by Composites of Lignocellulose-Montmorillonite Modified with MethacryloxypropylTrimethoxySilane. *Macromol. Symp*. 313-314 (1) p. 146–156.

Lata, H.; Garg, V. K. and Gupta, R. K. **(2008)** Adsorptive removal of basic dye by chemically activated Parthenium biomass: equilibrium and kinetic modelling. *Desalination.* 219. p. 250–261.

Li, Y. H.; Ding, J.; Luan, Z.; Di, Z.; Zhu, Y.; Xu, C.; Wu, D.; Wei, B. **(2003)** Competitive adsorption of Pb, Cu and Cd ions from aqueous solutions by multiwalled carbon nanotubes. *Carbon.* 41. p. 2787–2792.

Lin, J. X.; Zhan, S. L.; Fang, M. H.; Qian, X. Q.; Yang, H. **(2008)** Adsorption of basic dye from aqueous solution onto fly ash. *Journal of Environmental Management*. 87. p. 193–200.

Mobasherpour, I.; Salahi, E. and Pazouki, M. **(2012)** Comparative of the removal of Pb^{2+}, Cd^{2+} and Ni^{2+} by nano crystallite hydroxyapatite from aqueous solutions: Adsorption isotherm study. *Arabian Journal of Chemistry*. 5. p. 439-446.

Nigam, P.; Banat, I. M.; Singh, D.; Marchant, R. **(1996)** Microbial process for the decolorization of textile effluent containing azo, diazo and reactive dyes. *Process Biochemistry*. 31 (5) p. 435-442.

Robinson, T.; McMullan, G.; Marchant, R.; Nigam, P. **(2001)** Remediation of dyes in textile effluent: A critical review on current treatment technologies with a proposed alternative. *Bioresource Technology*. 77. p. 247-255.

Sprynskyy, M.; Buszewski, B.; Terzyk, A. P.; Namieśnik, J. **(2006)** Study of the selection mechanism of heavy metal (Pb^{2+}, Cu^{2+}, Ni^{2+}, and Cd^{2+}) adsorption on clinoptilolite. *Journal of Colloid and Interface Science*. 304. p. 21–28.

United Nations. **(2000)** *Goal 7: 2013 Fact Sheet - Ensure environmental sustainability.* [Online] Available from: http://www.un.org/millenniumgoals/bkgd.shtml. [Accessed: 17th February 2014].

United States of America. U.S. EPA, Office of Water Washington, D.C. **(2000)** *Wastewater Technology Fact Sheet: Chemical Precipitation*. Washington, D.C.: U.S. EPA.

Zhang, G.; Li, X.; Li, Y.; Wu, T.; Sun, D.; Lu, F. **(2011)** Removal of anionic dyes from aqueous solution by leaching solutions of white mud. *Desalination*. 274 (1–3) p. 255–261.

CHAPTER 2

LITERATURE REVIEW

2.1 Introduction

Clean safe water is an irreplaceable necessity to the human population which's supply is of distinct importance. Natural sources of clean consumable water have become significantly limited due to population growth and pollution, and waste water treatment has ceased to be an option and has become a practically applied solution. The vital importance of water has resulted in advances in technology aimed at making the availability of clean and safe water to all a reality.

Due to the remarkable solvent properties of water, numerous substances pose as possible contaminants in water that may not be easily removed. As a result different methods have and are being developed for the elimination of various classes of water contaminants. Various waste water treatment methods are currently available and in application for the removal of various pollutants from water. Waste water is usually treated by methods which include evaporation, reverse osmosis, ultrafiltration, electrodialysis, phytoextraction (Li *et al*., 2003; Sprynskyy *et al*., 2006; Mobasherpour *et al*., 2011) and chemical precipitation (USEPA, 2000). However water treatment methods used depend on the targeted pollutants, hence it is practically effective to use a combination of the various methods since pollutants rarely occur in isolation.

Of particular concern is the elimination of organic contaminants, especially persistent organic pollutants (POPs) from water, due to their association with many health hazards including being probable human carcinogens and also posing non-cancer health hazards to intellectual functions and the nervous, immune and reproductive systems (Corsolini *et al*., 2005). Organic

pollutants such as dyes and chlorophenols may be removed or rendered harmless by application of methods such as coagulation, membrane filtration, microbiological decomposition, advanced oxidation technology, ozonation and electrochemical methods (Lata *et al*., 2008; Lin *et al*., 2008; Zhang *et al*., 2011). Another important reason for the elimination of these contaminants from water is that, water not only presents a delivery vehicle for the toxins to organisms, but it also presents a distribution medium such that the harmful effects of organics may be observed in distant places from the sources of the pollutants.

For many challenges that Science and technology are finding solutions to, important principles governing the viability of these solutions include the cost and sustainability of the methods involved. As such, development of methods for effective removal of organic pollutants from water is also governed by such principles for possibility of practical application and wide spread use. Adsorption technology has been reported to be a simple operation, cost effective and efficient method for removal of both organic and inorganic pollutants from water (Nigam *et al*., 1996; Robinson *et al*., 2001; Annadurai *et al*., 2002). Adsorption is also proving to be a high potential water treatment method as some of the adsorbents may have simultaneous multipollutant removal capabilities (Bunhu and Tichagwa, 2012). The key to unlocking the potential of this material is found through firstly understanding the general structure of its component materials, lignocellulose and montmorillonite clay.

2.2 Lignocellulose

Lignocellulose is a complex material composed of nanometer-scale cellulose fibrils, hemicelluloses and lignin. In this material cellulose and hemicelluloses (carbohydrate polymers) are tightly bound to the lignin to form the lignocellulose (Carroll and Somerville,

2009). Other organic and inorganic components may also be included in the material structure but lignocellulose constitutes the larger part of the bio-renewable resource, wood.

2.2.1 Cellulose

Cellulose is the most abundant organic polymer on earth (Aygan and Arikan, 2008). It is a linear chain organic polymer composed of several hundred to over ten thousand β(1-4) linked D-glucose monomers (thus it is a polysaccharide), with the formula $(C_6H_{10}O_5)_n$ (Crawford, 1981). Cellulose is characterized by its hydrophilicity, chirality, biodegradability, broad chemical modifying capacity, and its ability to form versatile semi-crystalline fiber morphologies (Klemm *et al*., 2005). The structure of cellulose is composed of long polymer chains of glucose units connected by beta acetal linkages.

Cellulose is relatively crystalline and requires a temperature of 320 ^{0}C and pressure of 25 MPa to make it amorphous in water (Deguchi *et al.,* 2006). Several variable crystalline structures of cellulose can be identified and these correspond to the location of hydrogen bonds between and within the polymer chains as shown in Figure 2.1.

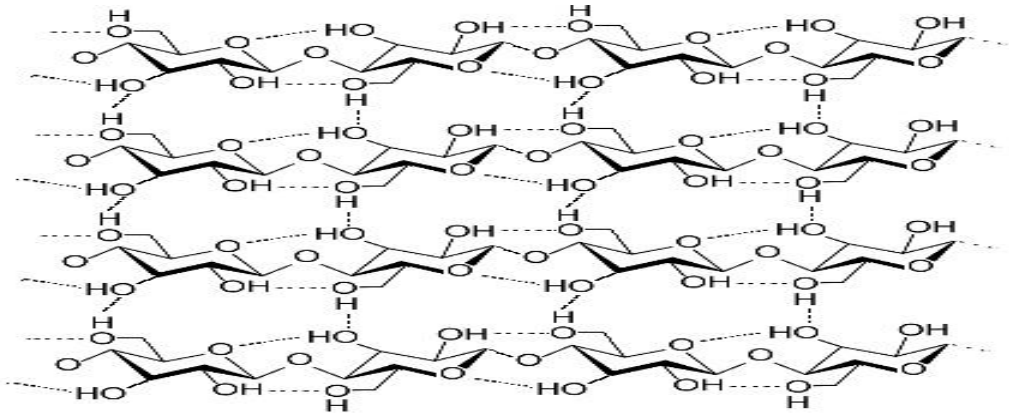

Figure 2.1: Hydrogen bonding in cellulose (Science Encyclopedia, 2014).

Strong hydrogen bonds in between the polymer chains make it insoluble in common solvents like water (Hon, 1991). Cellulose is however soluble in ionic liquids such as cupriethylenediamine (CED), cadmiumethylenediamine (cadoxen), N-methylmorpholine N-oxide and lithium chloride/ dimethylformamide (Stenius, 2000). Natural formation of cellulose makes it a renewable and low cost raw material in medicine, technology and industrial manufacturing.

2.2.2 Hemicellulose

Hemicelluloses (second most abundant biopolymer) are polysaccharides found in plant cell walls. Hemicelluloses have a random, amorphous structure with little strength and are easily hydrolyzed by diluted acid or base as well as a myriad of hemicellulose enzymes. The composition of hemicelluloses consists of relatively short chains (500-3000 sugar units) which are branched. The main industrial applications of hemicelluloses include conversion into sugars, chemicals, fuels and sources of heat energy (Bordenave, 2009).

2.2.3 Lignin

Lignin is the third most abundant natural polymer and is found in all plants, mostly between the cells and within them and in the cell walls where it fills the spaces between cellulose, hemicelluloses and pectin components. Lignin is very resistant to degradation due to the strong chemical bonding observed in its structure. Numerous internal H-bonds are also observed in its structure. Lignin is composed of compounds which are complex, amorphous, 3-dimensional polymers that have a phenylpropane (benzene ring with a 3-carbon tail) monomer structure (Sjöström, 1993).

Protolignins (natural lignins) are formed by removal of water from sugars to create aromatic structures and are grouped into several types characteristic of hardwoods, softwoods and grasses. Within each type there is a lot of variation whereby lignin differs from species to species and from one tissue to the next in the same plant and also even in different parts of the same cell. The main functional groups in lignin include methoxyl, phenolic hydroxyl, benzyl alcohol and carbonyl groups.

2.3 Clay

Clay is a naturally occurring material composed primarily of fine grained minerals, which harden when dried or fired. It mostly consists of phyllosilicates, responsible for plasticity, but may also contain other materials that impart plasticity and hardening when dried or fired. Chemical compositions of clays determine the plasticity of the materials. Clay may also contain other materials that do not impart plasticity and non-crystalline phases (usually organic matter) which are referred to as ‘associated minerals’ and ‘associated phases’ respectively. Clay minerals are generally formed over long periods of time by gradual chemical weathering of rocks by low concentrations of carbonic acid and diluted solutions. Some clay minerals are also formed by hydrothermal activity. Clay type and structure, and therefore also properties and uses, vary according to the nature of the mineral components and composition of the clay (Guggenheim and Martin, 1995).

2.3.1 Montmorillonite Structure and Chemistry

The structure of Montmorillonite clay consists of platelets with an inner octahedral layer sandwiched between two tetrahedral silicate layers as shown in Figure 2.2. The octahedral layers are aluminum oxide sheets where some of the aluminum atoms have been substituted with magnesium atoms.

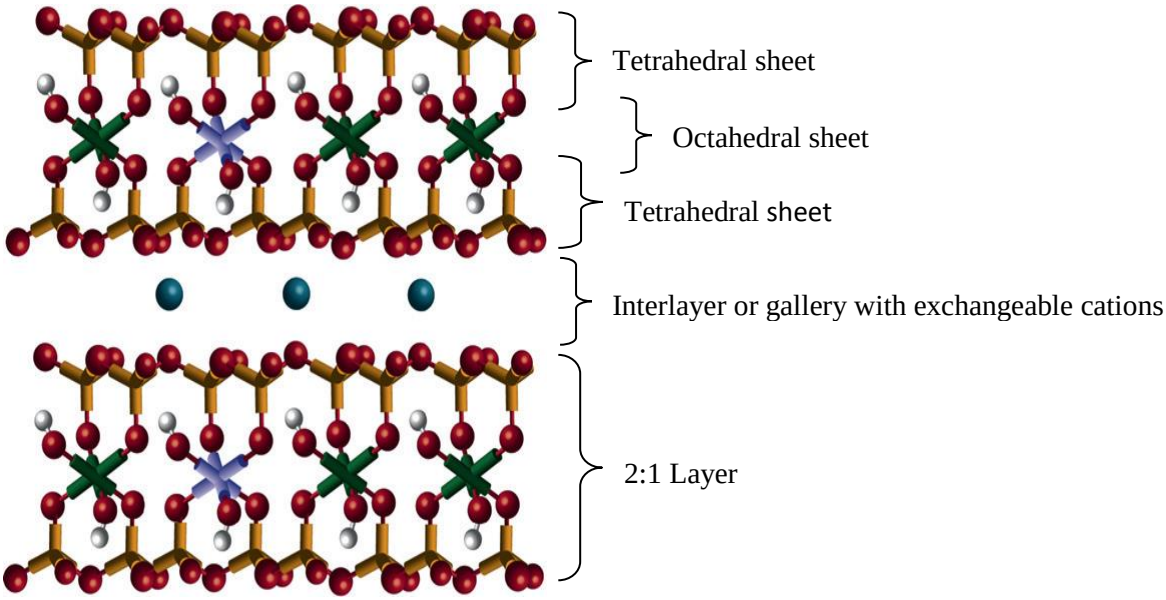

Figure 2.2: Structure of Montmorillonite clay (Paiva et al., 2008).

Silicon may also be substituted in the tetrahedral layers by aluminium (Bleam and Hoffmann, 1988). Taking into account the differences in valence between aluminum and magnesium, and that between silicon and aluminum, substitution creates negative charges distributed within the plane of the platelets. Surface charge on the clay may also arise from acid behavior of the silanol groups in water. The created negative charges are then balanced by positive counter-ions found between the platelets or in the galleries as shown in Figure 2.2. Counter-ions are typically sodium cations and other natural earth metals.

The sodium counter-ions may be hydrated and this results in the expansion of the galleries and swelling of the clay. Sodium ions can be exchanged with organic cations such as those from ammonium salts during lipophilization. Lipophilization occurs by replacing inorganic cations in galleries of the native clay with organic compounds such as alkylammonium surfactant (intercalant) making the hydrophilic layered silicates compatible with hydrophobic polymer matrices. Such modified clay is called lipophilized clay, or organophilic clay or simply organo-clay. Lipophilization enables expansion of the silicate nano-galleries to exfoliate the silicate layers into single layers of a nanometer thickness. Lipophilization is thus

sometimes used as a pre-swelling step in clay nanocomposite preparation. The extent of negative charge of clay is described by the cation exchange capacity (CEC) of the clay. Montmorillonite exhibits two high temperature endothermic reactions in the ranges 500 – 750 ^{0}C and 800 – 900 ^{0}C. These high temperature changes correspond to rupture of two kinds of hydroxyl bonds within the clay structure. In the 500 - 750 ^{0}C range, hydroxyl ions in the octahedral layer are lost resulting in some loss in structural arrangement, which can be regained by rehydration. On the other hand, hydroxyls in the silica sheets are lost in the 800 – 900 ^{0}C temperature range (Tzong, 2010).

2.4 Adsorption Technology and Water Treatment

Adsorption may be defined as the increase in concentration of a particular component at the interface between two phases (Dabrowski, 2001; Noll *et al.*, 1992) (Figure 2.3).The process mainly differs from absorption in that, adsorption creates a film of adsorbate on the adsorbent surface, while in absorption a fluid (absorbate) permeates or is dissolved into a liquid or solid(absorbent). Adsorption is a surface based process while absorption depends on the volume of the material. Both processes are however encompassed by the term sorption.

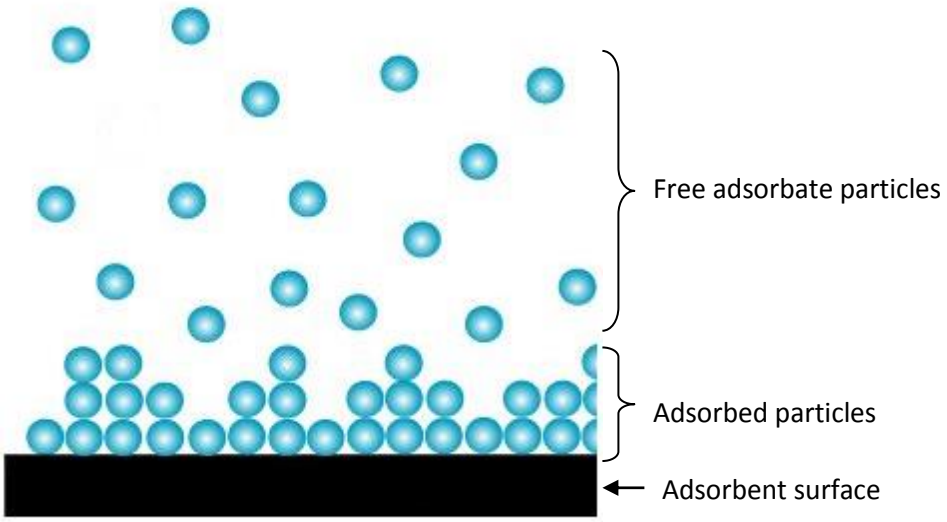

Figure 2.3: Adsorption onto a solid surface (Thermodynamik, 2009).

The reverse of adsorption is referred to as desorption. Atoms on the surface of a material are not completely surrounded by other atoms unlike in bulk material where all bonding requirements of constituent atoms are fulfilled by other atoms in the material, hence the surface atoms can attract external molecules or atoms (adsorbate) in an effort to fulfil these bonding requirements (Stadie, 2013). The nature of the bonding however depends on the species involved. The adsorption processes may be classified as either physisorption (characteristic of weak Van der Waals forces) or chemisorption (characteristic of covalent bonding).

In adsorption studies, isotherms are usually used to describe the adsorption. In isotherms, the amount of adsorbate on the adsorbent is expressed as a function of its pressure (for gases) or concentration (for liquids) at constant temperature. For comparison of different materials, the amount adsorbed is usually normalized by the mass of adsorbent. Adsorption may be classified as monolayer, whereby adsorbate particles are only adsorbed onto the adsorbent surface, and multilayer, where adsorption continues to occur onto the surface of adsorbed particles after (sometimes even before) the adsorbent surface area has been saturated by the adsorbate. Due to the many factors which determine how adsorption occurs in different situations, a number of mathematical models such as the Freundlich and Langmuir, have been proposed to fit isotherms for different modes of adsorption. Adsorption isotherms also enable the determination of the adsorption capacities of adsorbents.

Adsorption onto a surface is due to a number of interactions between the chemical groups on the surface of the adsorbent and the adsorbate particles. The interactions vary with adsorbent and also depend on the pH of the medium, salt concentration and presence of ligands in the medium. Adsorbent-adsorbate interactions include complexation, ion-exchange, chelation/coordination, acid-base interactions, electrostatic interactions, physical adsorption, precipitation, hydrophobic interactions and hydrogen bonding (Crini, 2005). Adsorption

technology has been applied in water purification, where one, two or more of the mentioned interactions occurs in the decontamination of polluted water. Industrial application of adsorption technology is however hindered by the high costs of adsorbent material currently available for commercial use. To counteract this drawback, alternative low-cost adsorbents are being developed and optimized for the purpose. Such adsorbents include zeolites, fly ash, agricultural lignocellulosic waste and clay minerals (Annadurai, Juang and Lee, 2002; Lin and Juang, 2002; Shukla *et al*., 2002; Babel and Kurniawan, 2003; Jain *et al*., 2003; Taty-Costodes *et al*., 2003; Mohan and Pittman, 2006; Mohan and Pittman, 2007).

Adsorbents used in water treatment are generally classified into three broad groups, namely organic, biological and mineral (inorganic) adsorbents (Knaebel, n.d.). Organic adsorbents include polymeric materials such as polysaccharides. Mineral adsorbents constitute those materials derived from mineral deposits like activated carbon (from coal), zeolites and clay. On the other hand, biological adsorbents include bacterial or fungi biomass, agricultural waste biomass and wood biomass (Tobin *et al*., 1984; Antizar-Ladislao *et al*., 2004; Denizli *et al*., 2005; Li *et al*., 2003; Wilke *et al*., 2006; Halttunen *et al*., 2007; Tong *et al*., 2007; Yu *et al*., 2007). Another class of adsorbents is composed of adsorbents produced by the combination of various adsorbent materials together with other material to enhance or modify adsorption properties of an adsorbent material (Montarges *et al*., 1998; Jeong *et al*., 2007; Salipira *et al*., 2007; Jin *et al.*, 2007). The adsorbents that have been used in water treatment include activated carbon, zeolites, polymeric materials, clays, nanotubes and lignocellulosic adsorbents (Li *et al*., 2003; Crini, 2005; Savage *et al.*, 2005; Lin *et al*., 2006; Salipira *et al*., 2007).

2.5 Nanomaterials in Adsorption Technology

Adsorption is usually used as a polishing step to remove organic and inorganic pollutants during water and wastewater treatment. However the efficiency of common adsorbents is mostly restricted by the lack of selectivity, surface area or active sites and the adsorption kinetics (Knaebel, n.d.; Guerrant and Salmon, 1928; Kavaklı *et al*., 2004; Jafar Ahamed and Shajudha Begum, 2012; Reza, Ali and Mansoureh, 2013). A significant step towards solving the problems associated with common adsorbents used in water treatment is the introduction of nanotechnology through the application of nano-adsorbents. In general nanotechnology is defined as the science and engineering involved in the design, synthesis, characterization, and application of materials and devices whose smallest functional organization in at least one dimension is on the nanometer scale (Silva, 2004). Nano-adsorbents present high specific surface area and associated sites for sorption including short intraparticle diffusion distance, and tunable pore size and surface chemistry (Xiaolei *et al*., 2012). Some current and potential applications for nano-adsorbents have been summarized in Table 2.1.

A special class of nano-adsorbents that has been showing interesting and promising application is that of the nanocomposite adsorbents. This class of adsorbents consists of materials composed of particle-filled polymers whereby at least one of the dimensions of the dispersed particles is in the nano-range (1-100nm). Nanoparticle introduction into a bulky material can significantly alter the properties of the material and such materials have been observed to exhibit interesting properties such as resistance to chemical attack and thermal degradation as well as mechanical strength (Zhao *et al.*, 2006) and have been ideally applied in the development of structural material. Polymer-clay nanocomposites have been applied in water treatment as adsorbents (Khaydarov *et al.*, 2010) and in preparation of nanofiltration membranes (Jeong *et al.*, 2007).

Table 2.1: Examples of some current and potential applications for nano-adsorbents (Xiaolei et al, 2012).

Nano-adsorbent	Desirable nanomaterial properties	Enabled technologies
Carbon nanotubes (CNT)	High specific surface area, highly accessible adsorption sites, diverse contaminant-CNT interactions, tuneable surface chemistry, easy reuse	Adsorption of recalcitrant contaminants, contaminant preconcentration or detection
Nanoscale metal oxide	High specific surface area, short intraparticle diffusion distance, more adsorption sites, compressible without significant surface area reduction, easy reuse, some are super paramagnetic	Adsorptive media filters, slurry reactors
Nanofibers with coreshell structure	Tailored shell surface chemistry for selective adsorption, reactive core for degradation, short internal diffusion distance	Reactive nano-adsorbents

Nanocomposite adsorbents prepared using carbon nanotubes and synthetic polymers have been investigated for removal of various pollutants from water and observed to be relatively more effective than conventional adsorbents (Montarges *et al.*, 1995; Lin *et al.*, 2006; Salipira *et al.*, 2007) and hence show a great potential for application in water treatment and purification. However the viability of practical application of these adsorbents is challenged by the relatively high costs involved in the acquisition of carbon nanotubes and the synthetic

polymers, and also the relatively non-biodegradability of many synthetic polymers which may present an environmental hazard. In light of these challenges, the concept of nanocomposite adsorbents for water treatment needs to be developed beyond the idea of efficiency only to also being 'green' and financially feasible for practical application.

One approach that is being considered and investigated is the modification of the concept of polymer-clay nanocomposites where the synthetic polymers are replaced by abundant, renewable and biodegradable materials such as lignocellulose from plant biomass (Bunhu and Tichagwa, 2012). The relative abundance of the adsorbent components and their biodegradability would be expected to render the nanocomposite adsorbents affordable and relatively environmentally friendly. Lignocellulose also possesses many functional groups which may serve as adsorption sites for various pollutants from water and they also present the possibility of further modification of the nanocomposites such as functionalization for adsorption of a particular pollutant. Many clays, especially smectites have been investigated for their potential as adsorbents for water treatment and purification, but montmorillonite has received more attention due to its adsorption-advantageous properties of high surface area, high cation-exchange capacity, swelling properties in water and its potential for ion-exchange (Ahmaruzzaman, 2008).

2.6 Polymer-Clay Nanocomposites

Incorporation of nanometer scale (<100 nm) sized material in a polymer matrix gives rise to polymer nanocomposites which have improved strength, thermal stability, toughness, stiffness, barrier properties and flame retardancy compared to the pure polymer matrix. Nanocomposites may be classified according to their nanofiller dimensionality i.e. zero-dimensional (nanoparticle), one-dimensional (nanofiber), two-dimensional (nanolayer), and three-dimensional (interpenetrating network) nanocomposites (Schmidt, 2002).

Subject to the nature of the layered silicate, organic cation and/or polymer matrix, and the preparation technique, three key categories of composites may be acquired when layered clay is associated with a polymer (Figure 2.4). Phase separated composites (polymer is unable to intercalate between the silicate sheets) (Figure 2.4a) may be obtained, whose properties remain similar to the usual microcomposites. Apart from this category of composites, two types of nanocomposites can be obtained from layered silicates.

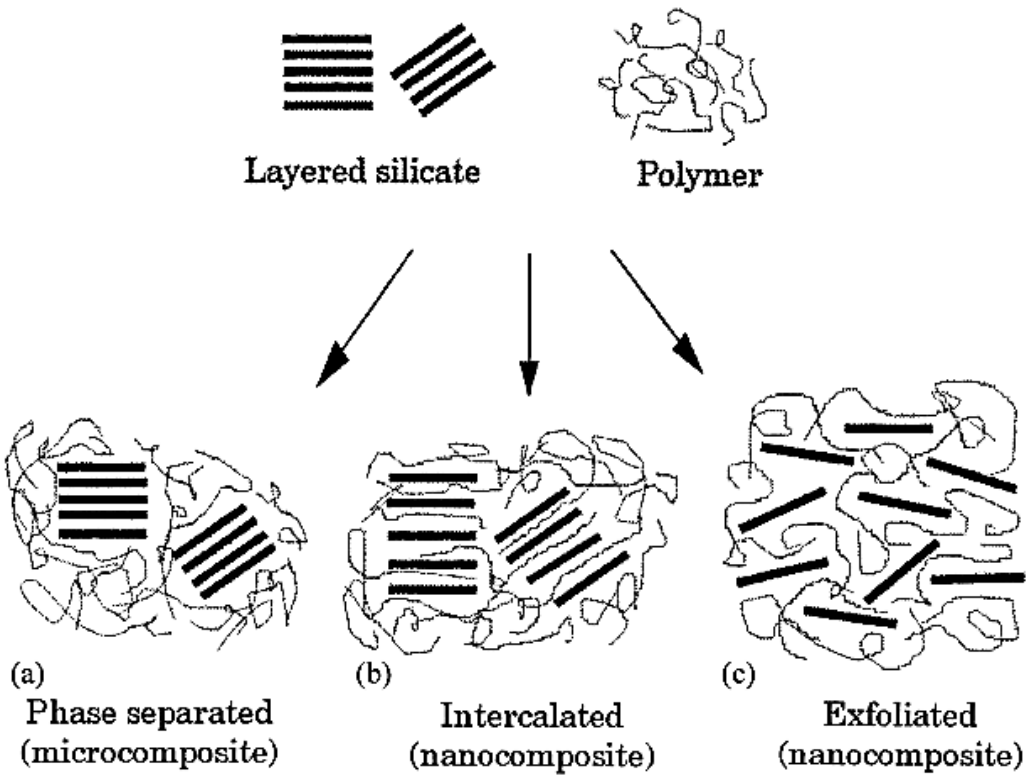

Figure 2.4: Scheme of different types of composites arising from the interaction of layered silicates and polymers: (a) phase separated microcomposite; (b) intercalated nanocomposite and (c) exfoliated nanocomposite (Dubois and Alexandre, 2000).

The layered nanocomposites may be classified as either intercalated (where polymer chains alternate with the inorganic layers in a fixed composition ratio and have a defined number of inter-lamellar space polymer layers) (Figure 2.4b) or exfoliated (where the number of

polymer chains between layers is continuously variable and the layers are greater than 10 nm apart) (Figure 2.4c).

Intercalated and exfoliated nanocomposite structures may be characterized and distinguished using XRD (for identification of intercalation and exfoliation) and TEM (for determination of morphology) analysis. In intercalated nanocomposites, the repetitive multilayer structure is well maintained and the interlayer spacing can be determined.

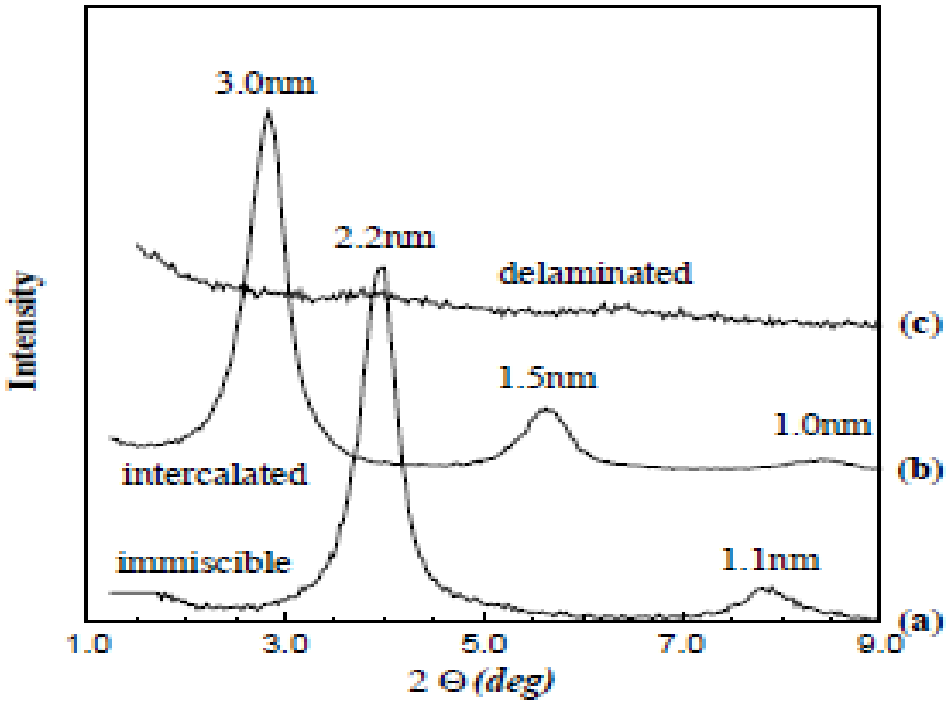

Figure 2.5: XRD patterns of: (a) phase separated microcomposite (organo-modified fluorohectorite in a HDPE matrix); (b) intercalated nanocomposite (same organomodified fluorohectorite in a PS matrix) and (c) exfoliated nanocomposite (the same organo-modified fluorohectorite in a silicone rubber matrix) (Giannelis, Krishnamoorti and Manias, 1999).

Intercalation of polymer chains usually increases the interlayer spacing which leads to a shift of the diffraction peak towards lower angle values (Figure 2.5b). In exfoliated structures no diffraction peaks are visible in the XRD diffractograms (Figure 2.5c) either as a result of a much too large spacing between the layers of ordered exfoliated structures or the

nanocomposites do not show any order. When the layers don't show any order TEM is used to characterize the nanocomposite morphology. Other intermediate structures can exist which show both intercalation and exfoliation and in such cases, a broadening of the diffraction peak is usually observed and the overall structure is defined using TEM. Exfoliated nanocomposite systems usually lead to better mechanical properties than intercalated nanocomposites (Dubois and Alexandre, 2000).

2.7 Synthesis of Layered Nanocomposites

Several approaches have been considered for preparation of polymer-layered silicate nanocomposites and these include four main processes, exfoliation-adsorption, *in situ* intercalative polymerization, melt intercalation and template synthesis (Oriakhi, 1998).

2.7.1 Exfoliation-adsorption

In this method a layered silicate is delaminated into single layers using a solvent in which the polymer or a prepolymer (in case of insoluble polymers) is soluble. Due to the weakness of the forces that hold the layers together, layered silicates are easily dispersed in an adequate solvent. The polymers then adsorb onto the separated layers and are sandwiched as the layers reassemble, following solvent evaporation to form, in the best situation, an ordered multilayer structure (Dubois and Alexandre, 2000; Beyer, 2002). This method can be further divided into three types as follows:

1. *Exfoliation-adsorption from polymers in solution*

The method is mostly used with water-soluble polymers to produce intercalated nanocomposites (Lerner and Oriakhi, 1997; Lagaly, 1999) based on poly(ethylene oxide) (Parfitt and Greenland, 1970; Zhao, Urano and Ogasawara, 1989; Ruiz-Hitzky *et al*.,1995;

Billingham, Breen and Yarwood, 1997; Ogata, Kawakage and Ogihara, 1997), poly(vinyl alcohol) (Greenland, 1963; Ogata, Kawakage and Ogihara, 1997), poly(vinylpyrrolidone) (Levy and Francis, 1975) or poly(acrylic acid) (Billingham, Breen and Yarwood, 1997). In the method steric restrictions from the polymer matrix prevent restacking of all the silicate layers and some of them remain exfoliated (Lagaly, 1986). Polymer intercalation using this technique can also be done in organic solvents.

2. *Exfoliation-adsorption from prepolymers in solution*

This method is usually applied with polymeric materials and conjugated polymers that are infusible and insoluble in organic solvents whereby soluble polymeric precursors are intercalated in the layered silicate and then thermally or chemically transformed into the desired polymer (Yano *et al*., 1993; Yano, Usuki and Okada, 1997).

3. *Exfoliation-adsorption by emulsion polymerization*

This technique has been mainly developed to introduce intercalation of water insoluble polymers within Na-montmorillonite which is well known to readily delaminate in water (Lee and Jang, 1996; Lee and Jang, 1998; Noh and Lee, 1999) and a surfactant is usually used to aid the dispersion of the polymer in the aqueous phase.

2.7.2 *In situ* Intercalative Polymerization

In this technique for nanocomposite synthesis, the layered silicate is mechanically mixed with the specifically required monomer for production of the intended polymer. The monomer then intercalates within the interlayer galleries of the silicate and facilitates separation of its layers giving rise to the swelling of the clay. Polymerization of the monomer then occurs at this site as a result of initiation by either of a number of methods such as heating, radiation and diffusion to give rise to linear or cross linked polymer matrices. Chain growth in the filler

galleries gives rise to filler exfoliation and formation of the nanocomposite (Dubois and Alexandre, 2000; Rehab and Salahuddin, 2005). The method has been used in the synthesis of thermoplastic, thermoset and elastomeric nanocomposites (Dubois and Alexandre, 2000).

2.7.3 Melt Intercalation

The method involves heat treatment, statically or under shear of a mixture of a polymer and layered silicate above the softening point (glass transition temperature) of the polymer. During the heat treatment, polymer chains diffuse from the bulk polymer melt into the nano-galleries between the layers, producing an expanded polymer-silicate structure. Based on a theoretical model (Vaia and Giannelis, 1997) the outcome of nanocomposite formation via polymer melt intercalation depends on energetic factors that may be obtained from the surface energies of the polymer and the layered silicate. Sufficient compatibility of the polymer and filler layer, results in the entry of the polymer into the interlayer spaces of the filler and the formation of either an intercalated or exfoliated nanocomposite. In this technique, no solvent is required (Dubois and Alexandre, 2000).

2.7.4 Template Synthesis

In this technique the silicates are formed *in situ* in an aqueous solution containing the polymer and the silicate building blocks. The polymer facilitates the nucleation and growth of the inorganic host crystals due to self-assembly forces and gets trapped within the layers as they grow (Dubois and Alexandre, 2000). This method is particularly adapted to water soluble polymers, and some attempts have been achieved with polymers such as poly(vinylpyrrolidone), hydroxypropylmethylcellulose, poly(acrylonitrile), poly(dimethyldiallylammonium) and poly(aniline) (Carrado and Xu, 1998). The method has been mostly used for the synthesis of double-layer hydroxide-based nanocomposites

(Oriakhi, I.V. Farr, M.M. Lerner, 1997; Wilson Jr *et al*., 1999), but is far less developed for layered silicates.

2.8 Lignocellulose-Clay Nanocomposites

Lignocellulose-montmorillonite nanocomposites have been widely researched for application in structural materials mainly in the furniture industry as well as the packaging industry (Zhao *et al.,* 2006). However, the literature available on the use of the lignocellulose-clay nanocomposites as adsorbent materials for the removal of inorganic and organic pollutants from aqueous solutions is limited. An improvement in the mechanical and tensile strength as well as the thermal stability of the resultant nanocomposites has been observed (Liao *et al.*, 2005). The nanocomposites have been prepared and used for structural materials like furniture boards and flooring materials. The advantages of using wood (lignocellulosic biomass) include low density, low equipment abrasiveness, relatively low cost, and good biodegradability. Lignocellulose-clay nanocomposites are usually prepared using the melt intercalation method (Fornes *et al.*, 2002; Jiang *et al.*, 2004; Liao *et al.*, 2005; Zhao *et al.*, 2006; Kord *et al*., 2010).

However, considering the application of the lignocellulose-clay nanocomposites in this study, it would be important to preserve the adsorption sites of the lignocellulose and the interlayer galleries of the clay particles (especially when a polymer is used) in order to allow for maximum interaction with pollutant molecules after nanocomposite synthesis (Bunhu, 2011). Covalent bonding should be targeted to link lignocellulose and clay to avoid leaching of the polymers (especially water soluble polymers like poly (methacrylic acid)) into solution which would cause secondary pollution problems. In view of these emphasized concerns and the inaccessibility of the melt blending equipment, this technique could not be applied in this study.

Bunhu (2011) studied the application of lignocellulose-clay nanocomposites as adsorbents for removal of heavy metals and organic dyes from water. In the study a variety of nanocomposites were prepared using a modified form of *in-situ* intercalative polymerization so as to circumvent the above mentioned concerns. However a distinctly outstanding nanoadsorbent, PMPS*g*Lig-NaMMT, was developed as was made note of in Sections 1.2 and 1.3 and drew attention, hence became the basis of this study.

2.8.1 PMPS*g*Lig-NaMMT Nanocomposite

PMPSgLig-NaMMT nanocomposite was synthesized by Bunhu and Tichagwa (2012) and was observed to successfully adsorb both organic and inorganic pollutants from water. On the other hand simultaneous adsorption proved to have a positive effect on the adsorption properties of the material. The details of the synthesis of PMPS*g*LigNaMMT as reported by Bunhu and Tichagwa (2012) are given in Section 4.1. Bunhu and Tichagwa (2012) also reported on the characterization of PMPS*g*Lig-NaMMT nanocomposite where their results from FT-IR, XRD, TGA and TEM described the nanocomposite as consisting of polymerized MPS (PMPS) as part of its structure as it couples the lignocellulose and NaMMT, and is intercalated among other properties which confirmed success in material formation.

PMPS*g*Lig-NaMMT consisting of coupled lignocellulose and NaMMT has its surface mostly characterized by hydroxyl functional groups. However the hydroxyl groups on NaMMT are relatively few (Rausell-Colom and Serratosa, 1987) as compared to those on lignocellulose and are even fewer in the nanocomposite as they are also used for grafting of the MPS during nanocomposite synthesis (Bunhu and Tichagwa, 2012). Taking this into consideration functionalization of PMPS*g*Lig-NaMMT may mostly be considered to be based on reactions of the lignocellulose component. The lignocellulose hydroxyl functional group abundance

may serve as an abundant source of adsorption sites and possible functionalization sites. In this study the abundance of hydroxyl groups is used to modify the nanocomposite adsorbent.

2.9 Lignocellulose and Lignocellulose Derivatives Functionalization

The concept of functionalization brings about specificity and selectivity in adsorbents and it involves the modification of the material surface. The modification to functionalize the material has three challenges namely; selection of appropriate moiety to graft and bring about the desired surface properties, method of grafting the selected moiety without affecting its desired properties and design of the process in such a way that the originally attractive properties of the material are not affected significantly. Considering this, a logical starting point for the functionalization process may be the characterization of the material surface to identify the possible methods for grafting. The numerous hydroxyl groups in lignocellulose mainly characterize the lignocellulose surface functionally, and its functionalization may reasonably be based on alcohol reactions. On the other hand maximum functionalization of lignocellulose is hindered by the compact structure of the material which reduces availability of surface functional groups (Petridis and Smith, 2008; Zhao, Zhang and Liu, 2012). However appropriate pretreatment of the lignocellulose prior to nanocomposite formation can enhance the availability of surface functional groups which would in turn enhance both grafting and coupling during nanocomposite synthesis and functionalization.

Lignocellulose retreatment mostly involves partial degradation of the hemicellulose and lignin components to reduce cellulose crystallinity and increase the material porosity (Stroeve *et al*., 2009) thereby enhancing the availability of the surface functional groups. Considering the effects of pretreatment, lignocellulose functionalization can be observed to be more centered on the reactions of the cellulose component of the material. The structure of cellulose is unique and simple, and this notably influences its chemical reactions. The

hydroxyl groups at the ends of the cellulose chain show different behavior (C-1 end has reducing properties, while C-4 end hydroxyl group is nonreducing) and laterally protruding hydroxyl groups are capable of making both inter- and intramolecular hydrogen bonds. Intramolecular hydrogen bonding between neighboring anhydroglucose rings increases the linear stability of the polymer chain and affects the reactivity of the hydroxyl groups, mainly of the C-3 hydroxyl group. The cellulose surface mainly consists of hydrogen atoms bonded directly to carbon and is therefore hydrophobic. These properties of cellulose give rise to its supramolecular structure which determines several of its chemical and physical properties (Varshney and Naithani, 2011).

The degree of polymerization (DP) or molecular weight distribution usually distinctly influences the mechanical, solution, biological, and physiological properties of cellulose and gives useful information for the designing of active cellulose derivatives (Hon, 1996). Solid state cellulose consists of highly ordered crystalline regions scattered between less ordered amorphous areas in which the hydroxyl groups are more easily available for reaction than in the more highly ordered crystalline areas, which are less reactive (Coffey *et al*., 1995). The degree of crystallinity (DC) (ratio of amorphous cellulose to crystalline cellulose) depends upon the species and pretreatment of the sample (Fink *et al*., 1995) and it plays an important part in chemical functionalization of cellulose. Cellulose contains 31.48% by weight of hydroxyl groups (one primary and two secondary per glucose unit) and availability of these gives rise to vast prospects for preparation of useful derivatives. On the other hand reactivity of these hydroxyl groups differs depending on the reaction medium in which functionalization is carried out example, the order of reactivity for etherification performed in an alkaline medium is 2 > 6 > 3 while the primary hydroxyl group (OH-6) is the most active in esterification (Hon, 1996).

The nature, distribution, and homogeneity of substituent groups determine the properties of derivatives. (Nicholson and Meritt, 1985). The degree of substitution (DS) (average number of hydroxyl groups replaced by the substituents) in cellulose has a maximum of three, but may be less in lignocellulose and its derivatives. Chemical functionalization of cellulose includes hydroxyl reactions such as esterification, etherification, intermolecular crosslinking reactions, and macrocellulosic free radical reactions, mostly in the making of graft cellulose copolymers (Arthur, 1986) to increase the cellulose value. Cellulose derivatives are grouped according to the processes and substituents, for instance, esters cellulose acetate through esterification and ethers methyl cellulose through etherification. Chemical functionalization continues to play a leading part in improving the overall utilization of cellulosic polymers such as lignocellulose and the accessibility to hydroxyl groups and their reactivity open prospects for preparation of specific molecular structures for future applications.

The modification of the surface of cellulosic materials to make them more compatible with non-polar polymers has been established effectively by making the structures more hydrophobic. This is usually achieved by creating hydrophobic ester or ether derivatives of cellulose (Mark, 1980; Woodhams, Thomas and Rodgers, 1984; Boldizar *et al*., 1987; Zadorecki and Michell, 1989; Bledzki and Gassan, 1999; Pasquini *et al*., 2008; Thielemans *et al*., 2008). This approach is generally centred on using surfactant-type structures (molecules having at least one polar end group, capable of reacting with the cellulosic surface hydroxyl groups, and long hydrophobic extensions) to make it compatible with non-polar matrices like polyolefins (Trejo-O'Reilly, Cavaillé and Gandini, 1997; Trejo-O'Reilly *et al*., 1998; Gandini and Belgacem, 1998; Abdelmouleh *et al*., 2002; Gopalan *et al*., 2003; Abdelmouleh *et al*., 2004).

2.10 References

Abdelmouleh, M.; Boufi, S.; Belgacem, M. N.; Duarte, A. P.; Salah, A. B.; Gandini, A. **(2004)** Modification of cellulosic fibres with functionalized silanes: Development of surface properties. *Int. J. Adhesion Adhesives* 24 (1). p. 43-54.

Abdelmouleh, M.; Boufi, S.; Salah, A. B.; Belgacem, M. N.; Gandini, A. **(2002)** Interaction of silane coupling agents with cellulose. *Langmuir* 18 (8). p. 3203-3208.

Ahmaruzzaman, M. **(2008)** Adsorption of phenolic compounds on low-cost adsorbents: a review. *Colloid Interface Sci.*, 143. p. 48-67.

Ahmaruzzaman, M. **(2008)** Adsorption of phenolic compounds on low-cost adsorbents: a review. *Colloid Interface Sci.*, 143. p. 48-67.

Annadurai, G., Juang, R. S. and Lee, D. J. **(2002)** Use of cellulose-based wastes for adsorption of dyes from aqueous solutions. *J. Hazard mater*. 92 (3). p. 263-274.

Antizar-Ladislao, B. and Galil, N. I. **(2004)** Biosorption of phenol and chlorophenols by acclimated residential biomass under bioremediation conditions in a sandy aquifer. *Water Research*. 38. p. 267–276.

Arthur, J. C Jr. **(1986)** In: Allen, G. and Bevington, J. C. (eds) *Comprehensive polymer science*. Vol 6. Pergamon: Oxford.

Aygan, A. and Arikan, B **(2008)** A new halo-alkaliphilic, thermostable endoglucanase from moderately halophilic Bacillus sp.C14 isolated from van soda lake. *Int. J. Agri. Biol*., 10 (369). p. 74.

Babel, S. and Kurniawan, T. A. **(2003)** Low-cost adsorbents for heavy metals uptake from contaminated water: A review. *J. Hazard mater*. 97 (1-3). p. 219-243.

Beyer, G. **(2002)** Nanocomposites: A new class of flame retardants for polymers. *Plast. Add. & Comp*. 4 (10). p. 22-27.

Billingham, J.; Breen, C. Yarwood, J. **(1997)** Adsorption of polyamine, polyacrylic acid and polyethylene glycol on montmorillonite: an in situ study using ATR-FTIR. *Vibr. Spectrosc*. 14. p. 19-34.

Bleam, W. F. and Hoffmann, R. **(1988)** Isomorphous substitution in phyllosilicates as an electronegativity perturbation: Its Effect on bonding and charge distribution. *Inorg. Chem*. 27 (18). p. 3180-3186.

Bledzki, A. and Gassan, J. **(1999)** Composites reinforced with cellulose based fibres. *Progress in Polymer Science*. 24. p. 221–274.

Boldizar, A.; Klason, C.; Kubát, J.; Näslund, P.; Sáha, P. **(1987)** Prehydrolyzed cellulose as reinforcing filler for thermoplastics. *International Journal of Polymeric Materials*. 11. p. 229–262.

Bordenave, N. **(2009)** Hemicelluloses. [Online] October 2009. Available from: http://www.cfs.purdue.edu/class/f&n630/pdf_full/hemicelluloses_NB.pdf. [Accessed: 20th November 2013].

Bunhu, T. **(2011)** *Preparation and evaluation of polymer-grafted lignocellulose-montmorillonite nanocomposites for the adsorption of heavy metals (Pb^{2+} and Cd^{2+}) and dyes (methyl orange and neutral red) from aqueous solution.* A Thesis Submitted in partial fulfilment of the Requirements of University of Fort Hare for the Degree of Doctor of Philosophy in Chemistry. Alice: University of Fort Hare.

Bunhu, T. and Tichagwa, L. **(2012)** Adsorption of Methyl Orange, Pb2+ and Cd2+ from Aqueous Solution by Composites of Lignocellulose-Montmorillonite Modified with MethacryloxypropylTrimethoxySilane. *Functional polymeric material and composites*. 313-314. p. 146-156.

Carrado, K.A. and Xu, L. Q. **(1998)** In-situ synthesis of polymer-clay nanocomposites from silicate gels. *Chem. Mater*. 10. p. 1440-1445.

Carroll, A. and Somerville, C. **(2009)** *Cellulosic Biofuels: Annual Review of Plant Biology*. 60. p. 165-182.

Chang, J. H. A.; An, Y. U.; Kim, S. J.; Im, S. **(2003)** Poly(butylene terephthalate)/organoclay nanocomposites prepared by in situ interlayer polymerization and its fiber (II). *Polymer*. 44. p. 5655-5661.

Coffey, D. G., Bell, D. A. and Henderson, A. **(1995)** *Food polysaccharides and their application*. New York: Marcel Dekker.

Corsolini, S. **(2005)** Persistent organic pollutants in edible fish: A human and environmental health problem. *Microchemical Journal.* 79. p. 115– 123.

Crawford, R. L. **(1981)** *Lignin biodegradation and transformation*. New York: John Wiley and Sons.

Crini, G. **(2005)** Recent developments in polysaccharide-based materials used as adsorbents in wastewater treatment.Progress in Polymer Science. 30. p. 38–70.

Dabrowski, A. **(2001)** Adsorption - from theory to practice. *Adv. Colloid Interface. Sci. 93*. p. 135-224.

Deguchi, S; Tsujii, K. and Horikoshi, K. **(2006)** Cooking cellulose in hot and compressed water. *Chemical Communications*. 31. p.3293-3295.

Denizli, A.; Cihangir, N.; Tüzmen, N.; Alsancak, G. **(2005)** Removal of chlorophenols from aquatic systems using the dried and dead fungus *Pleurotus sajor caju*. *Bioresource Technology*. 96. p. 59–62.

Dubois, P. and Alexandre, M. **(2000)** Polymer-layered silicate nanocomposites: preparation, properties and uses of a new class of materials. *Material Science and Engineering*. 28. p. 1-63.

Fink, H. P., Hofmann, D. and Philipp, B. **(1995)** Some aspects of lateral chain order in cellulosics from X-ray scattering. *Cellulose*. 2. p.51–70.

Fornes, T. D.; Yoon, P. J.; Hunter, D. L.; Keskkula, H.; Paul, D. R. **(2002)** Effect of organoclay structure on nylon 6 nanocomposite morphology and properties. *Polymer*. 43 (22). p. 5915-5933.

Gandini, A. and Belgacem, M. N. **(1998)** Recent advances in the elaboration of polymeric materials derived from biomass components. *Polym. Int*. 47 (3). p. 267-276.

Giannelis, E. P.; Krishnamoorti, R. and Manias, E. **(1999)** Polymer-silica nanocomposites: model systems for confined polymers and polymer brushes. *Adv. Polym. Sci*. 118. p. 108-147.

Gopalan, N. K.; Dufresne, A.; Gandini, A.; Belgacem, M. N. **(2003)** Crab shell chitin whiskers reinforced natural rubber nanocomposites: Effect of chemical modification of chitin whisker. *Biomacromolecules.* 4 (6). p. 1835-1842.

Greenland, D. J. **(1963)** Adsorption of polyvinylalcohols by montmorillonite. *J. Colloid Sci*. 18. p. 647-664.

Guerrant, N. B. and Salmon, W. D. **(1928)** Some factors affecting the adsorption of quinine, oxalate, and glucose by fullers' earth and norit. *J. Biol. Chem*. 80. p. 67-89.

Guggenheim, S. and Martin. R. T.; **(1995)** Clay and Clay Minerals. *The Clay Minerals Society*. 43 (2) p. 255-256.

Halttunen, T., Salminen, S. and Tahvonen, R. **(2007)** Rapid removal of lead and cadmium from water by specific lactic acid bacteria. *International Journal of Food Microbiology*. 114. p. 30–35.

Hon, D. N. and Shiraishi, N. **(1991)** *Wood and Cellulosic Chemistry*. New York: Marcel Dekker, Inc.

Hon, D. N. S. **(1996)** *Chemical modification of lignocellulosic material*. New York: Marcel Dekker.

Jafar Ahamed, A. and Shajudha Begum, A. **(2012)** Adsorption of copper from aqueous solution using low-cost adsorbent. *Arch. Appl. Sci. Res*. 4 (3). p.1532-1539.

Jain, A. K.; Gupta, V. K.; Bhatnagar, A.; Suhas. **(2003)** Utilization of industrial waste products as adsorbents for the removal of dyes. *J Hazard mater.* 101 (1). p. 31-42.

Jeong, B. H.; Hoek, E. M. V.; Yan, Y.; Subramani, A.; Huang, X.; Hurwitz, G.; Ghosh, A. K.; Jawor, A. **(2007)** Interfacial polymerization of thin film nanocomposites: A new concept for reverse osmosis membranes. *Journal of Membrane Science*. 294. p. 1–7.

Jiang, H. and Kamdem, D. P. **(2004)** Development of Poly(vinyl chloride)/Wood Composites.A Literature Review. *Journal of Vinyl & Additive Technology.* 10 (2). p. 59-69.

Jin, S.; Fallgren, P. H.; Morris, J. M.; Chen, Q. **(2007)** Removal of bacteria and viruses from waters using layered double hydroxide nanocomposites. *Science and Technology of Advanced Materials*. *8*. p. 67–70.

Kavaklı, P. A.; Seko, N.; Tamada, M.; Güven, O. **(2004)** Adsorption Efficiency of a New Adsorbent Towards Uranium and Vanadium Ions at Low Concentrations. *Separation Science and Technology*. 39 (7). p. 1631–1643.

Klemm, D.; Heublein, B.; Fink, H. P.; Bohn, A. **(2005)**, Cellulose: Fascinating Biopolymer and Sustainable Raw Material. *Angew. Chem*. Int. Ed. 44. p. 3358–3393.

Knaebel, K. S. **(n.d.)** *Adsorbent selection*. Dublin: Adsorption Reserch, Inc.

Kord, B.; Hemmasi, A. H. and Ghasemi, I. **(2010)** Properties of poly (propylene)/wood flour/organomodified montmorillonite nanocomposites. *Wood Science Technology*. p. 1-9. DOI 10.1007/s00226-010-0309-7.

Lagaly, G. **(1986)** Smectic clays as ionic macromolecules. In: Wilson, A. D. and Prosser, H. J. (eds). *Development in Ionic Polymers*. London: Elsevier.

Lagaly, G. **(1999)** Introduction: from clay mineral-polymer interactions to clay mineral-polymer nanocomposites. *Appl. Clay Sci*. 15. p. 1-9.

Lata, H.; Garg, V. K. and Gupta, R. K. **(2008)** Adsorptive removal of basic dye by chemically activated Parthenium biomass: equilibrium and kinetic modelling. *Desalination*. 219. p. 250–261.

Lee, D. C. and Jang, L. W. **(1996)** Preparation and characterization of PMMA-clay hybrid composite by emulsion polymerization, *J. Appl. Polym. Sci*. 61. p. 1117-1122.

Lee, D. C. and Jang, L. W. **(1998)** Characterization of epoxy-clay hybrid composite prepared by emulsion polymerization. *J. Appl. Polym. Sci*. 68. p. 1997-2005.

Lerner, M. and Oriakhi, C. **(1997)** Polymers in Ordered Nanocomposites. In: Goldstein, A. (ed.). *Handbook of Nanophase Materials*. New York: Marcel Dekker, Inc.

Levy, R. and Francis, C. W. **(1975)** Interlayer adsorption of polyvinylpyrrolidone on montmorillonite. *J. Colloid Interface Sci*. 50. p. 442-450.

Li, Y. H.; Ding, J.; Luan, Z.; Di, Z.; Zhu, Y.; Xu, C.; Wu, D.; Wei, B. **(2003)** Competitive adsorption of Pb, Cu and Cd ions from aqueous solutions by multiwalled carbon nanotubes. *Carbon*. 41. p. 2787–2792.

Li, Y. H.; Wang, S.; Luan, Z.; Ding, J.; Xu, C.; Wu, D. **(2003)** A dsorption of cadmium (II) from aqueous solution by surface oxidized carbon nanotubes. *Carbon*. 41. p. 1057–1062.

Li, Z. and Yuan, H. **(2006)** Characterization of cadmium removal by *Rhodotorula sp. Y11*. *Applied Microbiology and Biotechnology*. 73. p. 458–463.

Liao, H. T. and Wu, C. S. **(2005)** Preparation of poly(ethylene-octene) elastomer/clay/wood flour nanocomposites by a melting method. *Macromolecular Material Engineering*. 290. p. 695–703.

Lin, J. X.; Zhan, S. L.; Fang, M. H.; Qian, X. Q.; Yang, H. **(2008)** Adsorption of basic dye from aqueous solution onto fly ash. *Journal of Environmental Management*. 87. p. 193–200.

Lin, S. H. and Juang, R. S. **(2002)** Heavy metal removal from water by sorption using surfactant modified montmorillonite. *J. Hazard mater*. 92 (3). p. 315-326.

Lin, Y., Cui, X. and Bontha, J. **(2006)** Electrically controlled anion exchange based on polypyrrole and carbon nanotubes nanocomposite for perchlorate removal. *Environmental Science and Technology*. 40 (12). p. 4004-4009.

Mark, H. **(1980)** Fifty years of cellulose research. *Cellulose Chemical Technology*. 14. p. 569–581.

Mobasherpour, I.; Salahi, E. and Pazouki, M. **(2011)** Comparative of the removal of Pb^{2+}, Cd^{2+} and Ni^{2+} by nano crystallite hydroxyapatite from aqueous solutions: Adsorption isotherm study. *Arabian Journal of Chemistry*.

Mohan, D. and Pittman, C. U. **(2006)** Activated carbons and low cost adsorbents for remediation of tri- and hexavalent chromium from water. *J. Hazard mater.* 137 (2). p. 762-811.

Mohan, D. and Pittman, C. U. **(2007)** Arsenic removal from water/wastewater using adsorbents - A critical review. *J. Hazard mater*. 142 (1-2). p. 1-53.

Nicholson, M. D. and Meritt, F. M. **(1985)** Cellulose ethers. In: Nevell, T. P. and Zeronian, S. H. (eds) *Cellulose chemistry and its applications*. Chichester: Ellis Horwood.

Nigam, P.; Banat, I. M.; Singh, D.; Marchant, R. **(1996)** Microbial process for the decolorization of textile effluent containing azo, diazo and reactive dyes. *Process Biochemistry*. 31 (5). p. 435-442.

Noh, M. W. and Lee, D. C. **(1999)** Synthesis and characterization of PS-clay nanocomposite by emulsion polymerization. *Polym. Bull*. 42. p. 619-626.

Noll, K. E.; Vassilios, G. and Hou, W. S. **(1992)** Adsorption Technology for Air and Water Pollution Control. p. 21-22.

Ogata, N.; Kawakage, S. and Ogihara, T. **(1997)** Poly(vinyl alcohol)-clay and poly(ethylene oxide)-clay blend prepared using water as solvent. *J. Appl. Polym. Sci*. 66. p. 573-581.

Oriakhi, C. **(1998)** Nano sandwiches. *Chem. Br*. 34. p. 59-62.

Oriakhi, C. O.; Farr, I. V. and Lerner, M. M. **(1997)** Thermal characterization of poly(styrene sulfonate)/layered double hydroxide nanocomposites. *Clays and Clay Minerals*. 45. p. 194-202.

Paiva, L. B.; Morales, A. R. and Valenzuela-Díaz, F. R. **(2008)** Organoclays: characteristics, preparation methods, intercalation compounds and characterization techniques. *Cerâmica*. 54. (330) p. 213-226.

Parfitt, R. L. and Greenland, D. J. **(1970)** Adsorption of poly(ethylene glycols) on montmorillonites, *Clay Mineral*. 8. p. 305-323.

Pasquini, D.; Teixeira, E. M.; Curvelo, A. A. S.; Belgacem, M. N.; Dufresne, A. **(2008)** Surface esterification of cellulose fibres: Processing and characterisation of low-density polyethylene/ cellulose fibres composites. *Composites Science and Technology*. 68. p. 193–201.

Petridis, L. and Smith, J. C. **(2008)** Cellulosic ethanol: Progress towards a simulation model of lignocellulosic biomass. *J. Phys.* [Online] Conf. Ser. 125. Available from: http://iopscience.iop.org/1742-6596/125/1/012055. [Accessed: 30 March 2014].

Rausell-Colom, J. A. and Serratosa, J. M. **(1987)** Reactions of clays with organic substances. In: A.C.D. Newman (ed). *Chemistry of Clays and Clay Minerals*, New York: Wiley-Interscience.

Rehab, A. and Salahuddin, N. **(2005)** Nanocomposite materials based on polyurethane intercalated into montmorillonite clay. *Mater. Sci. Eng*. A 399. p. 368-376.

Reza, A., Ali, M. and Mansoureh, N. **(2013)** Application of chemically modified beach sand as low cost efficient adsorbent for dye removal. *Current Chemistry Letters*. 2. p. 215–223.

Robinson, T.; McMullan, G.; Marchant, R.; Nigam, P. **(2001)** Remediation of dyes in textile effluent: a critical review on current treatment technologies with a proposed alternative. *Bioresource Technology*. 77. p. 247-255.

Ruiz-Hitzky, E. **(1995)** Nanocomposite materials with controlled ion mobility. *Adv. Mater*. 7 (2). p. 180-184.

Salipira, K. L.; Mamba, B. B.; Krause, R. W. Malefetse, T. J.; Durbach, S. H. **(2007)** Carbon nanotubes and cyclodextrin polymers for removing organic pollutants from water. *Environmental Chemical Letters*. 5. p. 13–17.

Savage, N.; Diallo, M. S. **(2005)** Nanomaterials and water purification: opportunities and challenges. *Journal of Nanoparticle Research*. 7. p. 331–342.

Schmidt, D., Shah, D., Giannelis E. P. **(2002)** New advances in polymer/ layered silicate nanocomposites. Current Opinion in Solid State and Materials Science. 6. p. 205- 212.

Science Encyclopedia. **(2014)** *Cellulose - Structure Of Cellulose.* [Online] Available from: http://science.jrank.org/pages/1333/Cellulose-Structure-cellulose.html. [Accessed: 24th May 2014].

Shukla, A. **(2002)** The role of sawdust in the removal of unwanted materials from water. *J. Hazard mater*. 95 (1-2). p. 137-152.

Sjöström, E. **(1993)** *Wood Chemistry - Fundamentals and Applications*. 2nd edition. San Diego: Academic Press.

Sprynskyy, M.; Buszewski, B.; Terzyk, A. P.; Namieśnik, J. **(2006)** Study of the selection mechanism of heavy metal (Pb^{2+}, Cu^{2+}, Ni^{2+}, and Cd^{2+}) adsorption on clinoptilolite. *Journal of Colloid and Interface Science*. 304. p. 21–28.

Stadie, N. P. **(2013)** *Synthesis and Thermodynamic Studies of Physisorptive Energy Storage Materials*. A Thesis Submitted in partial fulfilment of the Requirements of California Institute of Technology for the Degree of Doctor of Philosophy. Pasadena, California: California Institute of Technology.

Stenius, P. (ed.) **(2000)** *Forest Products Chemistry*. Papermaking Science and Technology. Vol. 3. Finland: Finnish Paper Engineers' Association and TAPPI.

Stroeve, P.; Kumar, P.; Barrett. D. M.; Delwiche, M.J. et al. **(2009)** Methods for Pretreatment of Lignocellulosic Biomass for Efficient Hydrolysis and Biofuel Production. *Ind. Eng. Chem. Res.*

Taty-Costodes, V. C. **(2003)** Removal of Cd(II) and Pb(II) ions, from aqueous solutions, by adsorption onto sawdust of pinus sylvestris. *J. Hazard mater.* 105 (1-3). p. 121-142.

Thermodynamik **(n.d)** *Forschung: Hydrogen storage in novel carbon materials.* [Online] Available from: http://www.td.mw.tum.de/tum-td/de/forschung/themen/Hydro_Storage. [Accessed: 22th November 2013].

Thielemans, B.; Ly, B.; Dufresne, A.; Chaussy, D.; Belgacem. M. N. **(2008)** Surface functionalization of cellulose fibres and their incorporation in renewable polymeric matrices. *Composites Science and Technology*. 68. p. 3193–3201.

Tobin, J. M., Cooper, D. G. and Neufeld, R. J. **(1984)** Uptake of metal ions by rhizopus arrhizus biomass. *Applied and Environmental Microbiology*. p. 821-824.

Tong, M. Yu, J.; Sun, X.; Li, B. **(2007)** Polymer modified biomass of baker‘s yeast for treating simulated wastewater containing nickel and lead. *Polymers for Advanced Technologies*. 18. p. 829–834.

Trejo-O’Reilly, J. A., Cavaillé, J. Y. and Gandini, A. **(1997)** The surface chemical modification of cellulosic fibres in view of their use in composite materials. *Cellulose.* 4. p. 305-320.

Trejo-O’Reilly, J. A.; Cavaille, J. Y.; Belgacem, N. M.; Gandini**, A. (1998)** Surface energy and wettability of modified cellulosic fibres for use in composite materials. *Adhesion*. 67. p. 359-374.

Tzong-Yuan, J.; Yung-Chung, C., Cheng-Che, T., Shenghong, A., Dai, Tzong-Ming, W., Ru-Jong, J., **(2010)** Nanoscale Organic/Inorganic Hybrids Based on Self-Organized Dendritic Macromolecules on Montmorillonite. *Applied clay science*. 48. p. 103-110.

United States of America. U.S. EPA, Office of Water Washington, D.C. **(2000)** *Wastewater Technology Fact Sheet: Chemical Precipitation*. Washington, D.C.: U.S. EPA.

Vaia, R. A. and Giannelis, E. P. **(1997)** Polymer melt in organically modified layered silicates: model predictions and experiment. *Macromolecules*. 30. p. 8000-8009.

Varshney, V. K. and Naithani, S. **(2011)** Chemical Functionalization of Cellulose Derived from Nonconventional Sources. In: S. Kalia *et al*. (eds). *Cellulose Fibers: Bio- and Nano-Polymer Composites.* Berlin Heidelberg: Springer.

Wilke, A., Buchholz, R. and Bunke, G. **(2006)** Selective biosorption of heavy metals by algae. *Environmental Biotechnology*. 2 (2). p. 47-56.

Wilson, O.C Jr.; Olorunyolemi, T.; Jaworski, A.; Borum, L.; Young, D.; Siriwat, A.; Dickens, E.; Oriakhi, C.; Lerner, M. **(1999)** Surface and interfacial properties of polymer-intercalated layered double hydroxide nanocomposites. *Appl. Clay Sci*. 15. p. 265-279.

Woodhams, R. T., Thomas, G. and Rodgers, D. K. **(1984)** Wood fibers as reinforcing fillers for polyolefins. *Polymer Engineering & Science*. 24. p. 1166–1171.

Yano, K.; Usuki, A. and Okada, A. **(1997)** Synthesis and properties of polyimide-clay hybrid films. *J. Polym. Sci. A: Polym. Chem.* 35. p. 2289-2294.

Yano, K.; Usuki, A.; Okada, A.; Kurauchi, T.; Kamlgalto, O **(1993)** Synthesis and properties of polyimide-clay hybrid. *J. Polym. Sci.: Part A: Polym. Chem*. 31. p. 2493-2498.

Yu, J.; Tong, M.; Sun, X.; Li, B. **(2007)** Poly (methacrylic acid) modified biomass for enhancement adsorption of Pb2+, Cd^{2+} and Cu^{2+}. *Journal of Chemical Technology and Biotechnology*. 82. p. 558–565.

Zadorecki, P. and Michell, A. J. **(1989)** Future prospects for wood cellulose as reinforcement in organic polymer composites. *Polymer Composites*. 10. p. 69–77.

Zhang, G.; Li, X.; Li, Y.; Wu, T.; Sun, D.; Lu, F. **(2011)** Removal of anionic dyes from aqueous solution by leaching solutions of white mud. *J. Desal*. 274 (1). p. 255-261.

Zhao, X., Zhang, L. and Liu, D. **(2012)** Biomass recalcitrance. Part I: The chemical compositions and physical structures affecting the enzymatic hydrolysis of lignocellulose. *Biofuels, Bioprod. Bioref*. 6 (4). p. 465-482.

Zhao, X.; Urano, K. and Ogasawara, S. **(1989)** Adsorption of polyethylene glycol from aqueous solutions on montmorillonite clays. *Colloid Polym. Sci*. 267. p. 899-906.

Zhao, Y.; Wang, K.; Zhu, F.; Ping Xue, P.; Jia, M. **(2006)** Properties of poly(vinyl chloride)/wood flour/montmorillonite composites: Effects of coupling agents and layered silicate. *Polymer Degradation and Stability*. 91. p. 2874-2883.

CHAPTER 3

EXPERIMENTAL: MATERIALS AND GENERAL PROCEDURES

3.1 Introduction

This chapter presents the materials used and experimental details of the study. It also gives some specific details of the characterization techniques used including sample preparation.

3.2 Materials and Chemical reagents

Platanus x hispanica (London plane) tree leaves were used as the source of the biopolymer lignocellulose. The tree leaves were collected from the University of Fort Hare (UFH) Alice campus grounds. Montmorillonite clay (91.44 meq/100g) was purchased from Bao Bio Holdings (Pty) Ltd. These two materials formed the primary raw materials for the synthesis of the nanocomposite adsorbent under study. Methacryloxypropyltrimethoxysilane (3-(trimethoxysilyl) propyl methacrylate) (≥98.0% Sigma) was used as the coupling agent in the nanocomposite synthesis while dibutyltin dilaurate (95.0% Aldrich) was used as the catalyst in the coupling reaction.

Ethanol (99.8%), acetone (99.5% Spellbound Laboratory Solutions) and diethyl ether (ether) (99.0%) purchased from Merck Chemicals (Pty) Ltd together with tetrahydrofuran (THF) (99.9% Sigma-Aldrich), *n*-pentane (99.0% BDH Chemicals Ltd) and toluene (99.8% Associated Chemical Enterprises (ACE) (Pty) Ltd) were used in this study at various stages as solvents where ethanol, acetone, THF and ether were used as Soxhlet extraction solvents. On the other hand ethanol, *n*-pentane and toluene were used as synthesis solvents. Deionized water was used in combination with ethanol (1:1, V:V mixture) as extraction solvents and in synthesis. Deionized water was also used in the preparation of artificially polluted water with

1,10-Phenanthroline (99% SAARCHEM (Pty) Ltd) as the model organic contaminant in the study.

Table 3.1: Chemical names, formulae, molecular structures and molecular masses of used in the study.

Chemical name	Molecular mass /gmol^{-1}	Molecular formula	Chemical structure
3-(Trimethoxysilyl) propyl methacrylate	248.35	$C_{10}H_{20}O_5Si$	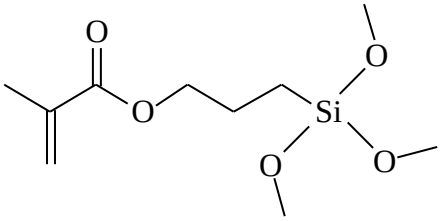
1,10-Phenanthroline	180.21	$C_{12}H_8N_2$	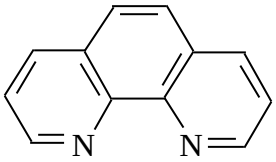
1-Chlorobutane	92.57	C_4H_9Cl	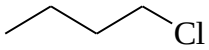
Butyryl chloride	106.56	C_4H_7ClO	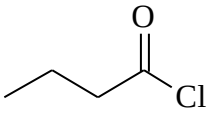
***n*-Butyryl acid**	88.11	$C_4H_8O_2$	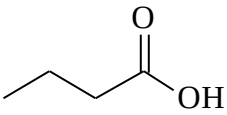
1-Bromo-3-phenyl propane	199.09	$C_9H_{11}Br$	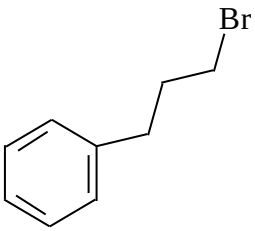
Butan-1-ol	74.12	$C_4H_{10}O$	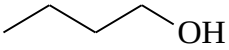
Dimethylsulfoxide	78.13	C_2H_6SO	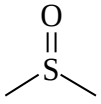

Other used materials were 1-Chlorobutane (99.0% Riedel-de Haën), butyryl chloride (98.0 % Sigma-Aldrich), *n*-butyryl acid (99.0% BDH Chemicals Ltd) and 1-bromo-3-phenyl propane (98.0 % Sigma-Aldrich) which were used as the functionalization moiety reagents. Pyridine (99.0% Merck Chemicals (Pty) Ltd) and potassium iodide (99.5% SAARCHEM (Pty) Ltd) were also used in the functionalization reactions. Silver (I) oxide (≥99.99% Sigma-Aldrich), metallic sodium (SAARCHEM (Pty) Ltd) and sulphuric acid (98.0% RADCHEM) were used to catalyse the functionalization reactions while dimethylsulfoxide (>99.0% Merck-Schuchardt) was used as an antioxidant in one of the reactions.

3.3 Characterization Techniques

This section describes the analytical techniques that were used for the characterization of the nanocomposite adsorbents prepared. The samples were characterized using Fourier transform infrared spectroscopy (FT-IR), X-ray diffraction (XRD) analysis, scanning electron microscopy (SEM) and thermogravimetric analysis (TGA). In this section the technique (ultra-violet/visible spectroscopy (UV/Vis)) used for the quantitative analysis of 1,10-phenanthroline in water during adsorption studies is also described. FT-IR, XRD and TGA were carried out at the University of Fort Hare Alice campus Chemistry Department, while SEM was carried out at the University of Western Cape Electron Microscopy Unit in the Physics Department.

3.3.1 Fourier Transform Infrared Spectroscopy (FT-IR)

Infrared spectroscopy is the study of relationships between matter and electromagnetic radiation. Atoms in molecules constantly vibrate with regular frequencies in the same range as infrared radiation. Vibrations which are followed by an alteration in dipole moment result in absorption of infrared radiation. Plotting the amount of radiation absorbed by a substance

against the incident wavelength gives a graph that reflects the presence of specific chemical bonds and can hence be used for structural identification by indication of the presence of key functional groups. Spectra associated with atoms result from electrons moving from one electronic energy level to another while inter-atomic spectra are mostly characterized by either bond stretching or bending vibration modes (Nicholls, 1976).

In FT-IR spectroscopy a beam of infrared energy is emitted from a glowing black-body source and passes through an aperture which controls the amount of energy reaching the sample and, eventually the detector. The beam enters an interferometer where spectral encoding occurs and the resulting interferogram signal enters the sample compartment where it is transmitted through or reflected off of the surface of the sample, depending on the type of analysis being done. Specific frequencies of energy, which are exclusively characteristic of the sample, are absorbed and the beam finally passes to the detector for final measurement. The measured signal is then digitized and sent to the computer where the Fourier transformation (mathematical decoding of interferogram signal) occurs and the final infrared spectrum is presented ready for user interpretation and any necessary manipulation (ThermoNicolet, 2001).

In this study infrared spectra were recorded using a PerkinElmer System 2000 FTIR. Each sample was properly mixed with potassium bromide (KBr) in a 1:100 sample:KBr ratio and ground thoroughly using pestle and mortar. An adequate amount of the ground sample was pelletized using a hydraulic pelletizer to give a transparent pellet, and then the samples were run against an air background. 8 scans were carried out for each sample in the wavenumber range 4000 cm^{-1} to 370 cm^{-1} with a resolution of 4 cm^{-1}.

3.3.2 X-ray Diffraction (XRD)

XRD is a rapid and non-destructive technique used to obtain structural information about crystalline solids from diffraction patterns. An electron in an alternating electromagnetic field oscillates with the same frequency as the field. When an X-ray beam hits an atom, the electrons around the atom oscillate with the same frequency as the incoming beam. Destructive interference (combining waves are out of phase and there is no resultant energy leaving the solid sample) occurs in almost all directions. In crystals regular arrangement of atoms results in constructive interference and waves will be in phase and there will be well defined X-ray beams leaving the sample in various directions. Bragg's Law gives the conditions for constructive interference as:

$$n\lambda = 2d\mathrm{Sin}\Theta \qquad (3.1)$$

where, λ is the wavelength of the X-rays, d is the distance between different plane of atoms in the crystal lattice and θ is the angle of diffraction. The diffracted radiation is very intense in certain directions which correspond to constructive interference from waves reflected from the layers of the crystal and gives a diffraction pattern (Scintag Inc., 2013).

The instrument consists of an X-ray source, a goniometer (device for restricting wavelength range), sample holder, radiation detector, and signal processor and readout. When an X-ray beam hits a crystal (sample), the beam is scattered in a manner characteristic of the atomic structure to give a unique pattern of peaks at different angles and intensity (Scintag Inc., 2013). Conversion of the diffraction peaks to d-spacings allows identification of the sample because each crystalline material has a set of unique d-spacings. X-ray powder diffraction **(**polycrystalline X-ray diffraction**)** is mainly used for sintered samples, metal foils, coatings and films, finished parts, etc. It is usually used to determine phase composition (commonly called phase ID), quantitative phase analysis, unit cell lattice parameters, crystal structure,

average crystallite size of nanocrystalline samples, crystallite microstrain and texture, and residual stress (Technology of Materials, 2014).

X-ray diffractograms of the samples in this study were obtained using a Bruker-AXS D8 Advance diffractometer (Cu Kα radiation with λ = 1.5406 Å) equipped with a PSD Lynx-Eye Si-strip detector (with 196 channels), at room temperature. This technique allowed for crystal phase identification and estimation of d-spacing and crystallite sizes. The x-ray diffraction analysis was carried out in locked couple mode with an accelerating voltage 40 kV and applied current of 40 mA.

3.3.3 Scanning Electron Microscopy (SEM)

Scanning electron microscopy (SEM) is a technique for high-resolution imaging of surfaces using a focused beam of high-energy electrons to generate signals at the surface of solid specimens that reveal information about the sample such as external morphology (texture), chemical composition, and crystalline structure and orientation of materials making up the sample (Swapp, 2013; MEE, Inc., 2014). Data is collected over a selected area of the surface of the sample, and a 2-dimensional image is generated that shows spatial variations in these properties.

Accelerated electrons have substantial quantities of kinetic energy, and when targeted at a solid sample the energy is emitted as a variety of signals produced by electron-sample interactions when the incident electrons are decelerated in the sample. The signals include secondary electrons (that produce SEM images), backscattered electrons (BSE), diffracted backscattered electrons (EBSD that are used to determine crystal structures and orientations of minerals), photons (characteristic x-rays that are used for elemental analysis and continuum x-rays), visible light (cathodoluminescence–CL), and heat. Secondary electrons

(for showing morphology and topography on samples) and backscattered electrons (for illustration of contrasts in composition in multiphase samples) are commonly used for imaging samples. X-ray generation is a result of inelastic collisions of the incident electrons with electrons in orbitals of atoms in the sample. SEM analysis on the same materials can be repeated.

The important parts of all SEM instruments include an electron source (gun), electron lenses, sample stage, detectors for all signals of interest, display/data output devices and infrastructure requirements (power supply, vacuum system, cooling system, vibration-free floor and room free of ambient magnetic and electric fields). SEM instruments have at least one detector (usually a secondary electron detector) and the precise abilities of the instrument are critically reliant on the detectors it houses. Sample preparation includes acquisition of a sample that will fit into the SEM chamber and some accommodation to prevent charge build-up on electrically insulating samples. An electrically conductive coating should be applied to electrically insulating samples for study in conventional SEM's, unless the instrument is capable of operation in a low vacuum mode. The choice of material for conductive coatings depends on the data to be acquired: carbon is most desirable if elemental analysis is a priority, while metal (usually gold) coatings are most effective for high resolution electron imaging applications (Goldstein et al., 2003; Swapp, 2013; LTI, 2014).

In this study SEM analysis was performed on a JEOL JSM-6390LV scanning electron microscope fitted with a secondary electron detector. All samples were coated with gold prior to SEM analysis.

3.3.4 Thermogravimetric Analysis (TGA)

TGA is an analytical technique that measures the variation of a sample’s weight with temperature in a controlled atmosphere. TGA is primarily used to determine the composition

of material and determine their thermal stability. The technique characterizes materials that show weight change due to decomposition, oxidation or dehydration. Chemical bond formation and breaking at elevated temperatures may result in sample weight change which is observed by a sensitive analytical balance.

Samples are deposited in a crucible that is placed in a furnace on a quartz beam connected to an automatic recording balance. Change in the weight of the sample results in a deflection of the beam and movement of the beam is determined by a pair of photosensitive diodes (position sensor). Restoration of the beam to the original null position is achieved by means of a feedback current from the photodiodes to the coil of the balance, which is proportional to the change in the sample's weight (Willard et al., 1988). A wide range of materials can be characterized using TGA and these include nanocomposites and clays. TGA has been successfully used to determine the thermal stability of polymer-clay nanocomposites, the amount of clay integrated per given amount of polymer, as well as the formation of metal oxide pillars (Kloprogge, J. T. et al, 1994; Chae, H. J. et al, 2001).

In this study thermo gravimetric analysis was carried out on a PerkinElmer TGA 7 thermo gravimetric analyser. Analysis was carried out under a nitrogen atmosphere at 20.0 ml/min in the temperature range from 20 °C to 900 °C at 10 °C/min ˚C.

3.3.5 Ultraviolet/Visible Spectroscopy (UV/Vis)

Ultraviolet/visible absorption spectroscopy is the measurement of the reduction in intensity of a beam of light after it passes through a sample or after reflection from a sample surface. In a molecule the atomic orbitals of atoms in a bond are merged to form molecular orbitals which can be occupied by electrons of different energy levels. Ground state molecular orbitals can be excited to anti-bonding molecular orbitals. When these electrons are provided with energy

in the form of light radiation, they get excited from the highest occupied molecular orbital (HOMO) to the lowest unoccupied molecular orbital (LUMO) and the resulting species is known as the excited state or anti-bonding state. An electron in a bonding σ orbital of a molecule is excited to the corresponding anti-bonding orbital by the absorption of radiation.

Ultraviolet and visible radiation interacts with matter which causes electronic transitions (promotion of electrons from the ground state to a high energy state) (Akhter, 2014). Absorption in the visible region results in molecules undergoing electronic transitions and when the absorbance is measured, the concentration of the analyte can be related to the signal transmitted through or absorbed by the sample by the Beer-Lambert law. The Beer-Lambert equation is expressed as follows:

$$A = \epsilon bc \qquad (3.2)$$

where A, ϵ, b and c are the absorption, molar absorptivity (a constant which is characteristic of the absorbing species at a specific wavelength), pathlength of the sample and the concentration respectively. The absorption is therefore directly proportional to concentration for a given set of instrumental conditions (Pavia et al., 2001).

A UV/Vis spectrophotometer comprises of five components: a light (radiation) source (UV and visible), wavelength selector (monochromator), sample containers, detector, signal processor and readout. Two light sources are commonly used in UV/Vis spectrophotometers, an incandescent lamp made from a tungsten filament contained in a glass envelope (used for wavelengths longer than 350 nm) and a medium pressure deuterium arc lamp (used for wavelengths shorter than 350 nm). The monochromators comprise of an entrance slit, a collimating lens, a dispersing device (usually a prism or a grating), a focusing lens and an exit slit used to convert polychromatic radiation (radiation of more than one wavelength) to radiation of only a particular wavelength. There are three common types of detectors that are

used namely, photomultiplier tubes, linear photodiode arrays and charge-coupled devices (CCDs) (Sheffield Hallam University, 2014).

In this study the determination of the concentration of 1,10-phenanthroline in the solutions was carried out on a CECIL CE 2021 (2000 series) UV/Vis spectrophotometer at a wavelength of 285 nm. Before analysis with UV/Vis spectrophotometry, the sample solutions were filtered through acrodisc syringe filters (0.45 μm supor membrane) of low protein binding to remove solid particles. The sample solutions were analyzed using a quartz cell of 1 cm path length.

3.4 References

Akhter. **(2014)** *Ultra violet (UV) spectroscopy, introduction,principle instrumentation,different types of uv transition.* [Online] Available from: http://www.slideshare.net/mariomS7/uvvis-spectroscopy. [Accessed: 15th May 2014].

Chae, H. J.; Nam, I. S.; Ham, S. W.; Hong, S. B. **(2001)** Physicochemical characteristics of pillared interlayered clays. *Catalysis Today*. *68*. p. 31–40.

Goldstein, J.; Newbury, D.; Joy, D.; Lyman, C.; Echlin, P.; Lifshin, E.; Sawyer, L.; Michael, J. **(2003)** *Scanning electron microscopy and X-ray microanalysis*. 3rd edition. New York: Plenum Press pp.

Kloprogge, J. T.; Booy, E.; Jansen, J. B. H.; Geus, J. W. **(1994)** The effect of thermal treatment on the properties of hydroxy-Al and hydroxy-Ga pillared montmorillonite and beidellite. *Clay Minerals*. *29*. p. 153-167.

Laboratory Testing Inc.(LTI). **(2014)** *Materials Testing (Metallurgical Testing): SEM Analysis*. [Online] Available from: http://www.labtesting.com/services/materials-testing/metallurgical-testing/sem-analysis/. [Accessed: 10th June 2014].

Materials Evaluation and Engineering (MEE), Inc. **(2014)** *Handbook of Analytical Methods for Materials: Scanning Electron Microscopy*. [Online] Available from: http://mee-inc.com/sem.html. [Accessed: 10th June 2014].

Nicholls, R. **(1976)** *Composite Construction Materials Handbook.* Englewood Cliffs, NJ: Prentice-Hall, Inc.

Pavia D.L.,Lampman G. M.,and Kriz, G.S. **(2001)** *Introduction to spectroscopy: A guide for students of organic chemistry*. 3rd edition. Philadelphia: Harcourt College Publishing.

Scintag Inc. **(2013)** *Chapter 7: Basics of X-ray Diffraction.* [Online] Available from: http://hompi.sogang.ac.kr/@bb/bboard.asp?db=catalyst_freeboard3&mode=download&num=5&filename=xrdbasics.pdf. [Accessed: 10th June 2014].

Sheffield Hallam University. **(2014)** *UV-Vis Absorption Spectrosctroscopy: Instrumentation.* [Online] Available from: http://teaching.shu.ac.uk/hwb/chemistry/tutorials/molspec/uvvisab3.htm.[Accessed: 15th May 2014].

Swapp, S. **(2013)** *Geochemical Instrumentation and Analysis: Scanning Electron Microscopy (SEM).* [Online] Available from: http://serc.carleton.edu/research_education/geochemsheets/techniques/SEM.html. [Accessed: 10th June 2014].

Technology of Materials. **(2014)** *What is X-Ray Diffraction?: Analysis of Materials by X-Ray Diffraction (XRD).* [Online] Available from: http://www.xraydiffrac.com/xraydiff.html. [Accessed: 13th June 2014].

ThermoNicolet. **(2001)** *Introduction to Fourier Transform Infrared Spectrometry.* [Online] Available from: http://mmrc.caltech.edu/FTIR/FTIRintro.pdf. [Accessed: 10th June 2014].

Willard, H. H.; Merrit, L. L. (Jr); Dean, J. A.; Settle, F. A. (Jr). **(1988)** *Instrumental Methods of Analysis*. 7th edition. Belmont, California: Warsdworth Publishing Company.

CHAPTER 4

PREPARATION AND CHARACTORIZATION OF PMPSgLig-NaMMT

4.1 Introduction

This chapter describes the detailed procedures carried out in the synthesis of the unfunctionalized PMPS*g*Lig-NaMMT nanocomposite materials as proposed by Bunhu and Tichagwa (2012). The nanocomposites were prepared in three stages, of which the first two involved the preparation of the constituent materials which make up the product nanocomposites. The third stage involves the bringing together of the prepared constituent materials to give the nanocomposite products. The results of these experimental procedures were observed and analyzed through the use of the various characterisation techniques applied on the prepared materials. Characterization of the prepared materials was carried out using FTIR, XRD, SEM and TGA; and the results and discussion of the characterization are reported in Section 4.2. Characterization of the raw materials (raw MMT and unpretreated biomass) was also carried out for comparison purposes.

4.2 Preparation of PMPS*g*Lig-NaMMT nanocomposite

4.2.1 Preparation of NaMMT

Clay, 30 g, (91.44 meq/100 g montmorillonite) was dispersed in 120 mL of 2M NaCl solution in a 250 mL conical flask. The mixture was stirred for 12 hours with a magnetic stirrer at room temperature. The clay was then separated by centrifugation for 30 minutes and the aqueous solution decanted. The separated clay was dispersed again in 60 mL 2M NaCl solution and the mixing and separation repeated. The NaMMT sediment was then washed

several times with deionized water through centrifugation until the supernatant liquid gave a negative result for the $AgNO_3$(aq) Cl^- test (Clark, 2002). Residual water in the NaMMT was then evaporated in a ventilated oven and the NaMMT dried at 105 ^{0}C for 24 hours.

4.2.2 Pretreatment of Lignocellulosic Biomass

Tree leaf biomass was collected, washed with distilled water and dried in a ventilated oven at a temperature of 105 ^{0}C for a period of 48 hours. The dry leaves were reduced to powder using a food blender. Biomass powder was then sieved through a 170 mesh sieve to produce a fine particulate sample for use. Soluble organic and inorganic compounds (including pigments) were removed by Soxhlet extraction using a 1:1 (v/v) EtOH:H_2O solvent combination, at 250 mL of solvent per 10 g of biomass for 24 hours. The Soxhlet extracted biomass was then dried in a ventilated oven at 105 ^{0}C for 24 hours. The biomass was stored in a desiccator ready for use.

4.2.3 Preparation of Nanocomposite

Lignocellulosic biomass together with NaMMT in different proportions (4 g:2 g, 3 g:3 g and 2 g:4 g) were dispersed in 150 mL of a 1:1 (v/v) EtOH: H_2O solvent mixture for 1 hour under high speed magnetic stirring for the preparation of the 2:1, 1:1 and 1:2 Lig:NaMMT ratio nanocomposite samples respectively. MPS, 3.4 mL ($1.4x10^{-2}$ mol), was added to the lignocellulose-NaMMT dispersion and stirred for 10 minutes. Dibutyltin dilaurate catalyst, 0.125 mL ($2.1x10^{-4}$mol) was then added to the dispersion and the mixture was stirred for 10 minutes after which the mixture was allowed to react for 24 hours at a temperature of 70 ^{0}C while stirring continued in a setup as shown in Figure 4.1.

Dibutyl tin dilaurate, 1:1 v/v EtOH: H_2O solvent

NaMMT + Lig + MPS ⟶ **PMPSgLig-NaMMT**

70 ^{0}C (24 hours)

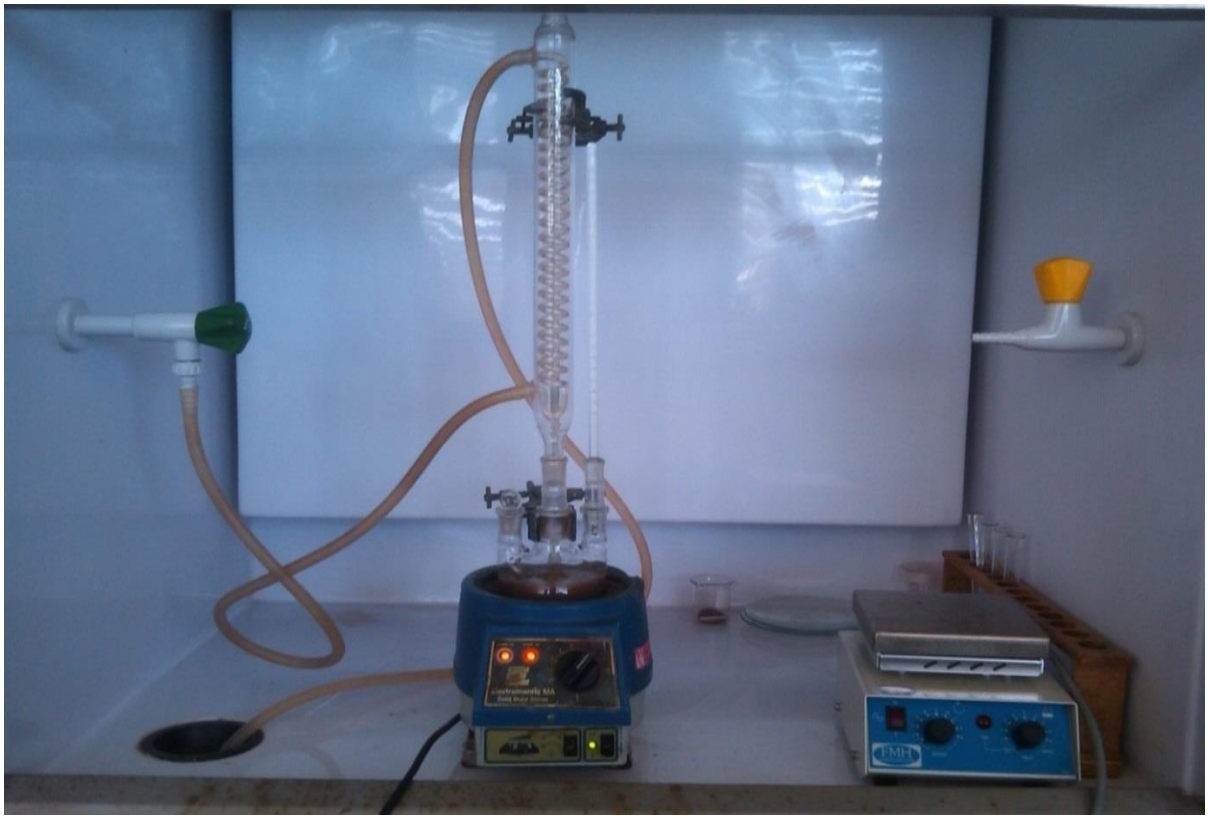

Figure 4.1: PMPSgLig-NaMMT nanocomposite synthesis laboratory reaction setup.

After 24 hours of reaction, the mixture was cooled to room temperature and the PMPSgLig-NaMMT nanocomposites isolated by filtration. Free MPS monomer, homopolymerizsed silane and the catalyst were removed by Soxhlet extraction for 24 hours using THF as the solvent, followed by washing with water. The prepared nanocomposites were then dried in a ventilated oven at 50 ^{0}C for 48 hours and then characterized.

4.3 Results and Discussion

This section describes the results obtained from the characterization of the materials that were prepared in this chapter.

4.3.1 FTIR Analysis

Figure 4.2 shows the FTIR spectra of PMPS*g*Lig-NaMMT nanocomposites and their component materials lignocellulose and NaMMT. In the FTIR spectrum the peaks on the nanocomposite spectra in the range of 1300 - 400 cm^{-1} are mainly attributed to stretching and bending vibrations of Si-O-Al, Si-O-Si, O-Si-O and Al-O groups (Yuan *et al.*, 2006; Manohar *et al.*, 2006; Bhattacharyya *et al.*, 2009), which may be observed to tally with corresponding peaks in the NaMMT spectrum.

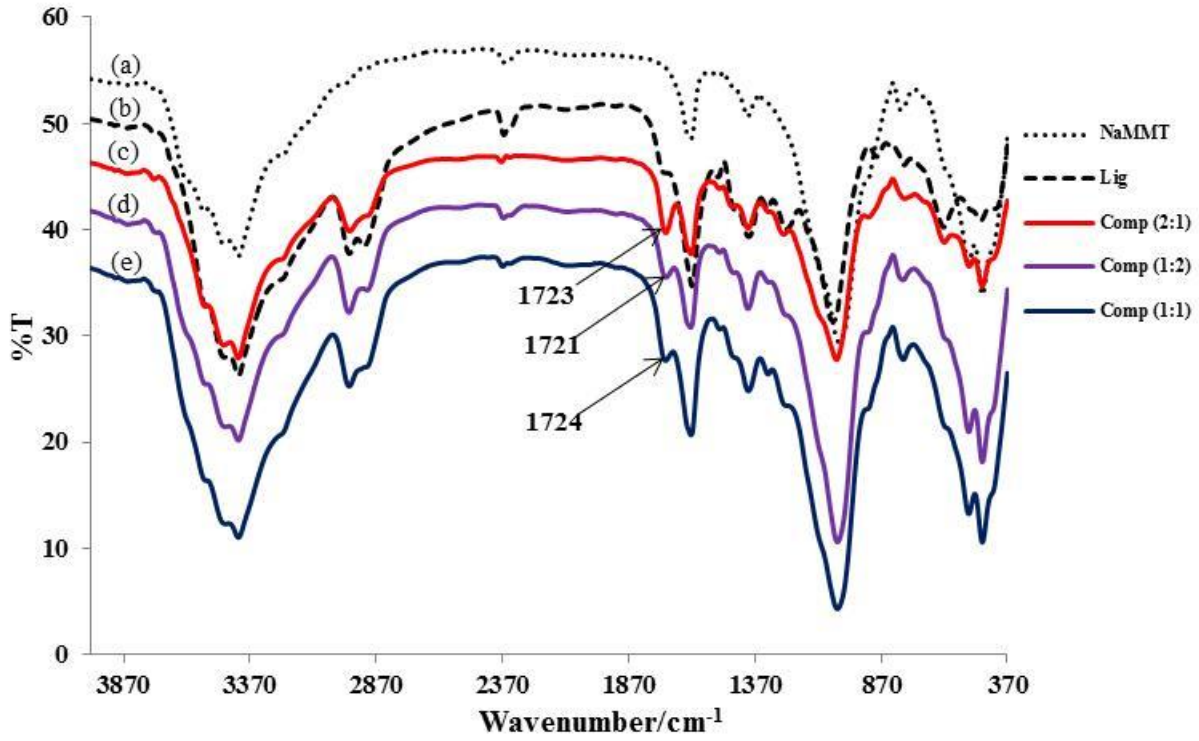

Figure 4.2: IR spectra of (a)NaMMT, (b) lignocellulose and PMPSgLig-NaMMT nanocomposites ((c) Comp(2:1), (d) Comp(1:2) and (e) Comp(1:1)).

This suggests that the main features of NaMMT structure are retained as NaMMT is modified to PMPS*g*Lig-NaMMT. It can also be observed that the deviations of the PMPSgLig-NaMMT spectrum from that of NaMMT in this region correspond and may be attributed to distinct peaks in the lignocellulose spectrum which also suggests that the general structure of lignocellulose is retained in the nanocomposite. In general, peaks from the nanocomposite

components are observed to be retained with little (if any) shifts in position in the nanocomposite which indicates retention of the structure of the raw components.

The peak in the 1639-1650 cm^{-1} range of each spectrum was ascribed to H-O-H bending vibrations in water molecules, which overlapped with that of the C=C stretching vibration. On the other hand peaks at approximately 2950 and 2993; 3415 and 3636 cm^{-1} were attributed to C-H stretching, H-O-H stretching (adsorbed H_2O) and structural O-H stretching vibrations, respectively (Manohar *et al.*, 2006; Bhattacharyya *et al.*, 2009). However most notably and most important was the emergence of a peak in the range 1721-1724 cm^{-1} which was absent in both NaMMT and lignocellulose spectra. This peak corresponds to the unsaturated C=O of the MPS ester group. The peak appeared at higher wavenumbers than the expected 1715 cm^{-1} (McMurry, 2008) possibly due to the saturation of some of the MPS ester during polymerization. Also the peak's intensity was observed to vary with nanocomposite composition of which the intensity was directly proportional to the lignocellulose ratio. However such a trend was not observed with the peak positions in the nanocomposite variations and this may have been due to different random levels of MPS polymerization during synthesis which resulted in different ratios of saturated and unsaturated ester contents hence different and rather random peak positions. Considering that the nanocomposites were Soxhlet extracted with THF to extract any homopolymerized and non-grafted MPS, appearance of the peak in the 1721 - 1724 cm^{-1} range suggests success in MPS grafting and successful coupling of NaMMT and lignocellulose.

4.3.2 XRD Analysis

Figure 4.3 shows the XRD diffractrograms of PMPS*g*Lig-NaMMT nanocomposites, NaMMT and lignocellulose. In the low angle analysis a d_{001} peak shift to lower 2θ values was observed in the PMPS*g*Lig-NaMMT diffractrograms with comparison to that of NaMMT

instrument's software. Table 4.1 summarizes the basal reflection peak 2θ and d-spacing values of NaMMT and the PMPS*g*Lig-NaMMT nanocomposites.

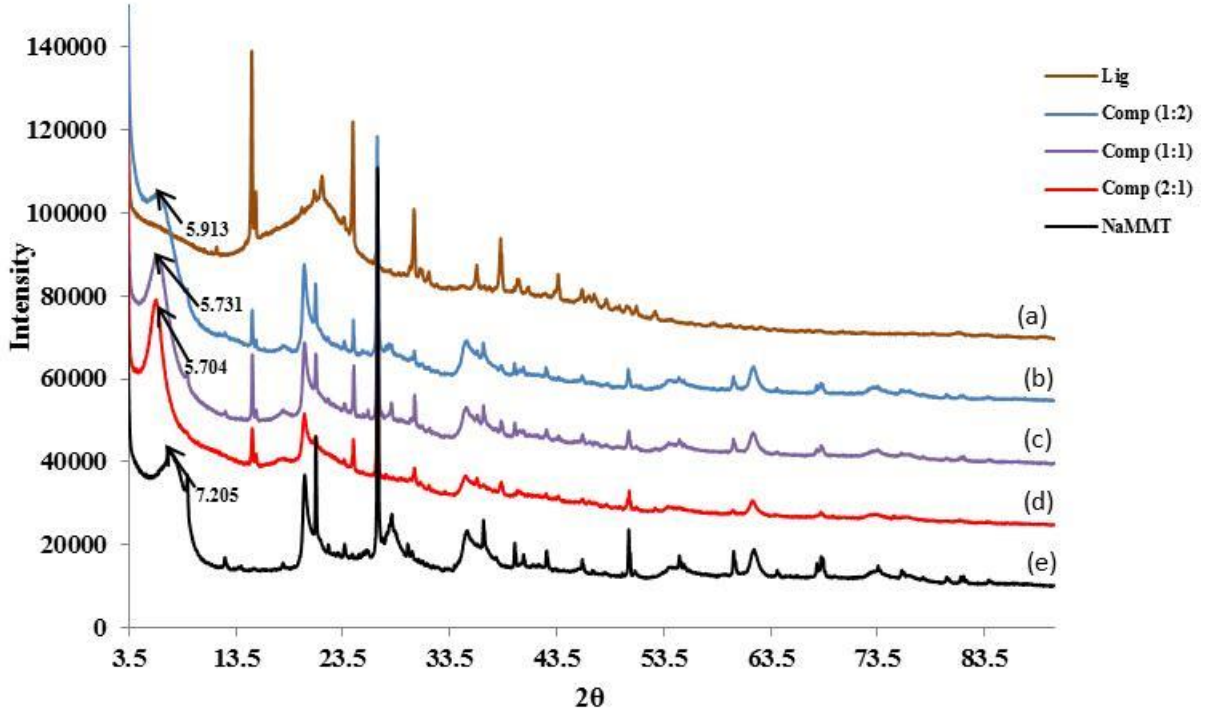

Figure 4.3: XRD diffractograms of (a) lignocellulose, (e) NaMMT and PMPSgLig-NaMMT nanocomposites ((b) Comp(1:2), (c) Comp(1:1) and (d) Comp(2:1)).

The d-spacing values of the nanocomposites were observed to be in the 1-100 nm range, hence by definition the composite materials were classified as nanocomposites.

The wide range XRD analysis on the other hand indicated that the nanocomposites retained the general structure of their component materials, especially NaMMT, with some slight decrease in crystallinity at some 2θ values. This suggested that the nanocomposite was layered similarly to the NaMMT due to the retention of its general structure in the nanocomposite. Emergence of peaks in the PMPS*g*Lig-NaMMT spectra corresponding to peaks in lignocellulose suggested that lignocellulose and NaMMT were successfully coupled as these peaks correspond to some crystalline phases only observed in the lignocellulose and not NaMMT.

Table 4.1: Summary of nanocomposite basal reflection peak 2θ and d-spacing values

Sample ID	Basal reflection peak (2θ)	d-spacing (nm)	Δ d-spacing (nm)
NaMMT	7.27	1.216	-
Comp (1:1)	6.09	1.451	0.235
Comp (1:2)	6.30	1.402	0.186
Comp (2:1)	6.05	1.462	0.246

4.3.3 SEM Analysis

Figure 4.4 shows the SEM micrographs of PMPS*g*Lig-NaMMT nanocomposites and their components lignocellulose and NaMMT nanoclay. Figure 4.4 (a) is the micrograph for NaMMT which appears as flakes of the nanoclay.

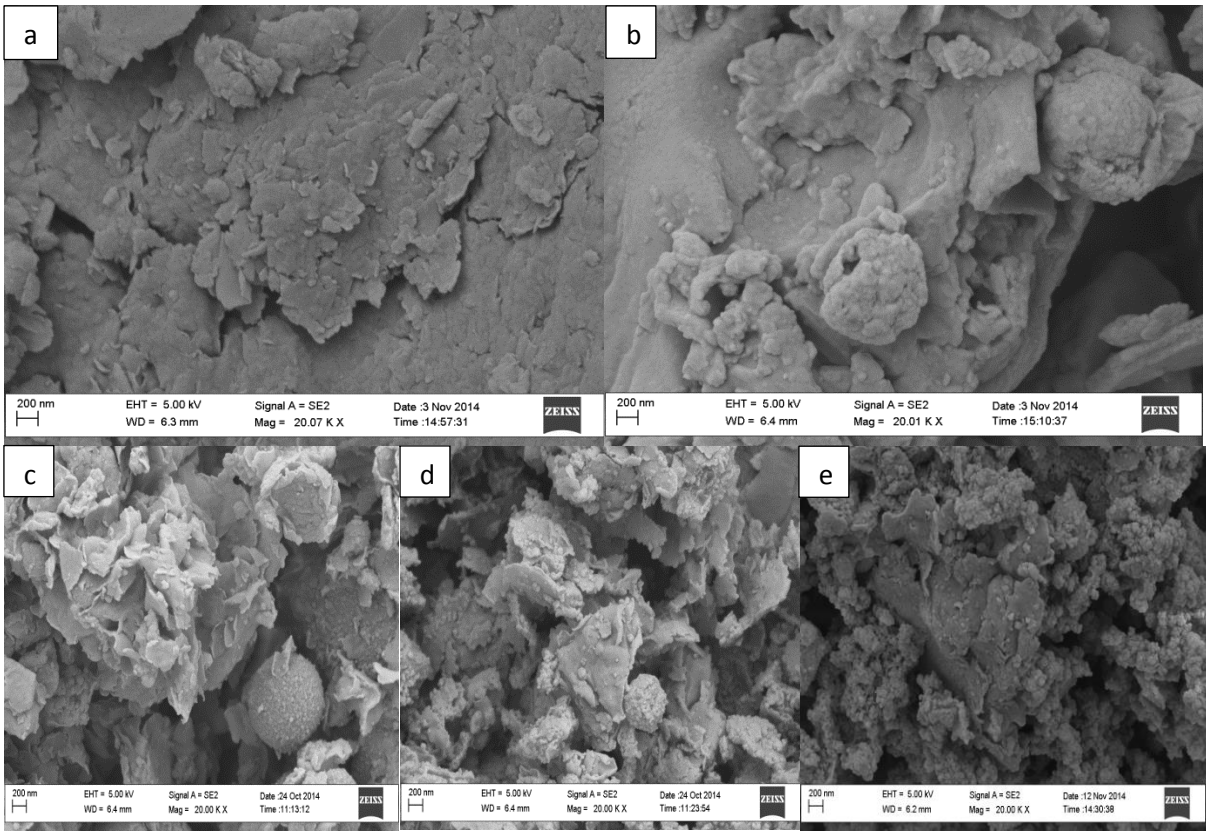

Figure 4.4: SEM micrographs of (a) NaMMT, (b) lignocellulose, (c) Comp (1:1), (d) Comp (1:2) and (e) Comp (2:1).

In Figure 4.4 (b) the micrograph shows the relatively larger lignocellulose particles with relatively smooth surfaces at this magnification. In Figures 4.4 (c), (d) and (e) the micrographs show the two components combined together in the nanocomposites with varying Lig:NaMMT ratios. The micrographs also show that the reaction processes broke down the clay aggregates to smaller particles and also relatively separated the lignocellulose aggregates to separate particles, which was consistent with the finer particle sizes of the products observed as compared to that of the lignocellulose. However due to the inhomogeneity of the lignocellulose and clay particle shapes and sizes, the variation in composition could not be easily distinguished at a glance although a variation could be observed in the micrographs when closely compared. The micrographs also support the suggestion by FT-IR results that the two components were successfully coupled.

4.3.4 Thermogravimetric Analysis

Figure 4.5 shows the thermograms of PMPS*g*Lig-NaMMT nanocomposites and their constituent materials, lignocellulose and NaMMT clay. The thermograms obtained from the five samples show an initial weight loss towards the 100 ^{0}C temperature region which can be explained by the loss of surface moisture from the samples. A distinctly notable weight loss in the range 200 - 400 ^{0}C for lignocellulose may be attributed to the pyrolysis of its hemicellulose and cellulose components. The gradual further weight loss may be attributed to the pyrolysis of the lignin component of the lignocellulose which generally decomposes steadily in the range 400 - 600 ^{0}C, but may also decompose at higher temperatures (Grandmaison *et al.,* 1987; Aggarwal *et al.,* 1997; Beall, 2007; Yang and Wu, 2009; Sebio-Puñal *et al*., 2012; Sen *et al*., 2014).

On the other hand, only a slight loss in weight apart from the loss due to moisture content was observed in the NaMMT clay thermogram at temperatures beyond 600 ^{0}C.

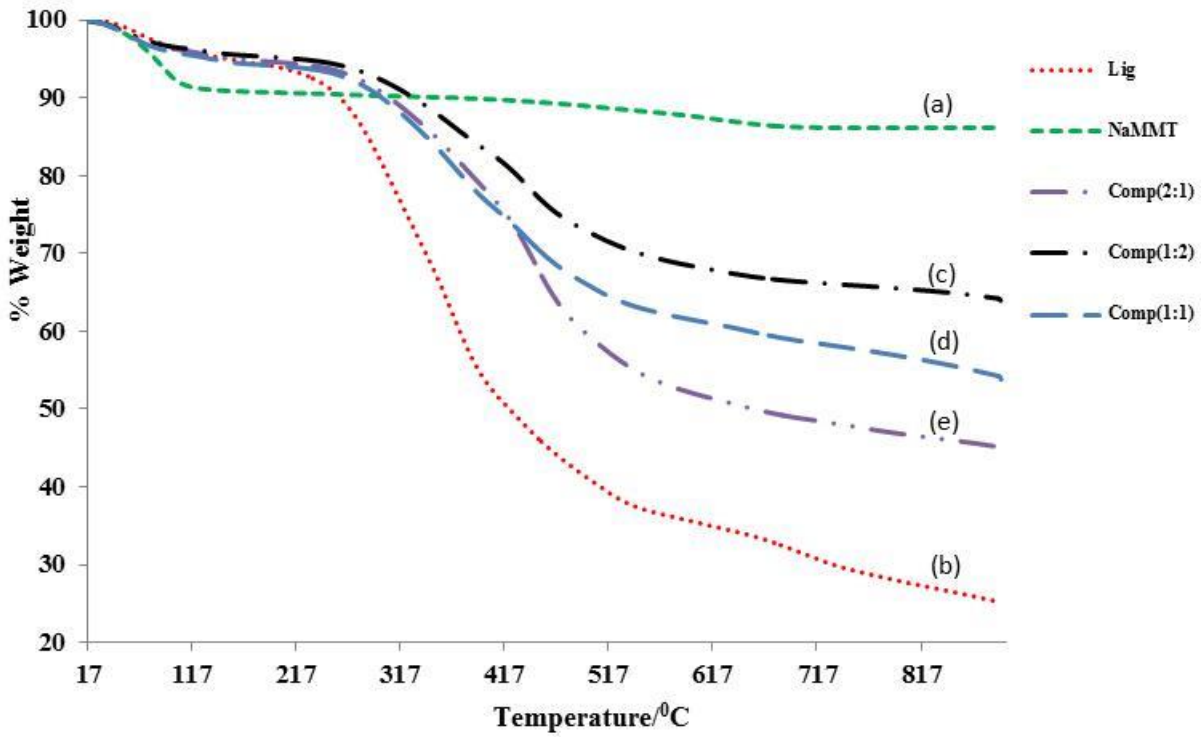

Figure 4.5: Thermograms of (a) NaMMT, (b) lignocellulose, (c) Comp (1:1), (d) Comp (1:2) and (e) Comp (2:1).

The gradual loss was attributed to dehydration of the hydrated cations in the interlayer and the dehydroxylation of the montmorillonite, which is not easily lost at low temperatures (Singla *et al*., 2012). The low overall gradual loss in weight in the NaMMT clay indicated relatively high thermal stability of NaMMT clay as compared to the lignocellulose. However the thermograms for PMPS*g*Lig-NaMMT nanocomposites indicate interesting thermal properties of the material which can be explained by reference and comparison to the thermal properties of lignocellulose and NaMMT clay. The thermograms of PMPS*g*Lig-NaMMT were observed to be between that of lignocellulose and that of NaMMT clay, with their general shape mostly similar to that of lignocellulose, but slightly shifted to the right and upwards.

Decomposition temperatures and general thermogram shapes were comparable to that of lignocellulose, but indicate higher thermal stability which may be attributed to the presence

of the more thermally stable NaMMT clay of which stability was directly proportional to NaMMT content in the nanocomposites. In general the mass loss was mostly due to decomposition of the lignocellulose components and the grafted and polymerized MPS, hence the greater the lignocellulose ratio in the sample, the greater the weight loss observed. The change in decomposition temperature of lignocellulose in PMPS*g*Lig-NaMMT suggests that in the nanocomposites, lignocellulose and NaMMT clay may not only just be present together (mixture), but there may be some form of interaction between them. Considering that lignocellulose is organic and NaMMT is inorganic (hence relatively incompatible) and that MPS (a coupling agent) was present, an explanation for the interaction between lignocellulose and NaMMT clay may be their coupling by MPS. This suggestion serves to support the notion that MPS was successfully grafted and polymerized in the coupling of lignocellulose and NaMMT clay during nanocomposite synthesis.

4.4 Conclusion

Results from FT-IR spectra, XRD diffractograms and TGA thermograms of PMPS*g*Lig-NaMMT nanocomposites and their constituent materials suggested and gave evidence that lignocellulose and NaMMT were successfully coupled by the MPS coupling agent. XRD also confirmed the product materials to be nanocomposites. SEM micrograms of the product and their components further supported the notion of successful coupling of the two component materials, to give rise to the conclusion that PMPS*g*Lig-NaMMT nanocomposites of varying compositions were successfully synthesized with significant retention of constituent materials' properties.

4.5 References

Aggarwal, P. and Dollimore, D. **(1997)** The use of the temperature signal and its derivative in a TG-DTA simultaneous unit. *Journal of thermal analysis and calorimetry*. 50 (5-6). p. 719-726.

Beall, F. C. **(2007)** Thermogravimetric Analysis of Wood Lignin and Hemicelluloses. *Wood and Fiber Science.* 1 (3). p.215-226.

Bhattacharyya, K. G. and Gupta, S. S. **(2009)** Calcined tetrabutylammonium kaolinite and montmorillonite and adsorption of Fe(II), Co(II) and Ni(II) from solution. *Applied Clay Science*. *46*. p. 216–221.

Bunhu,T., and Tichagwa, L. **(2012)** Adsorption of methyl orange, Pb^{2+} and Cd^{2+} from aqueous solution by composites of lignocellulose-montmorillonite modified with methacryloxypropyl trimethoxysilane. *Macromol. Symp*. 313-314 (1). p. 146-156.

Clark, J. **(2002)** *Testing For Halide Ions.* [Online] October 2012. Available from: http://www.chemguide.co.uk/inorganic/group7/testing.html. [Accessed: 20th May 2013].

Grandmaison, J.; Thibault, J.;Kaliaguine, S.; Chantal, P. **(1987)** Fourier transform infrared spectrometry and thermogravimetry of partially converted lignocellulosic materials. *Anal. Chem.* 59. p. 2153-2157.

Manohar, D. M.; Noeline, B. F. and Anirudhan, T. S. **(2006)** Adsorption performance of Al-pillared bentonite clay for the removal of cobalt (II) from aqueous phase. *Applied Clay Science*. 31. p. 194-206.

McMurry, J. **(2008)** *Organic Chemistry.* 7th edition. Chicago :Thomson - Brooks/Cole. p. 423-433.

Sebio-Puñal, T. and **(2012)** Thermogravimetric analysis of wood, holocellulose, and lignin from five wood species. *Journal of Thermal Analysis and Calorimetry*. 109(3). p. 1163-1167.

Sen, A.; Van den Bulckeb, J.; Defoirdtb, N.; Van Ackerb, J.; Pereira, H. **(2014)** Thermal behaviour of cork and cork components. *Thermochimica Acta* .582. P.94-100.

Singla, P.; Mehta, R. and Upadhyay, S. N. **(2012)** Clay Modification by the Use of Organic Cations. *Green and Sustainable Chemistry*. 2. p.21-25.

Tarascon, J.; Barpanda, P.; Recham, N.; Chotard, J.; Djellab, K.; Walker, W.; Armand, M. **(2010)** Structure and electrochemical properties of novel mixed $Li(Fe_{1-x}M_x)SO_4F$ (M = Co, Ni, Mn) phases fabricated by low temperature ionothermal synthesis. *J. Mater. Chem*. 20 (9). p. 1659-1668.

Yang, Q. and Wu, S. **(2009)** Thermogravimetric characteristics of wheat straw lignin.*Cellulose Chem.Technol*. 43 (4-6). p.133-139.

Yanga,H. C.;Choa, Y. J.; Eunb, H. C.; Kima, E. H. **(2007)** Destruction of chlorinated organic solvents in a two-stage molten salt oxidation reactor system. *Chemical Engineering Science*. 62. p. 5137-5143.

Yuan, P.; He, H.; Bergaya, F. A.; Wu, D.; Zhou, Q.; Zhu, J. **(2006)** Synthesis and characterization of delaminated iron-pillared clay with meso–microporous structure. *Microporous and Mesoporous Materials*. *88.* p. 8–15.

CHAPTER 5

FUNCTIONALIZATION AND CHARACTERIZATION OF PMPSgLig-NaMMT

5.1 Introduction

This chapter describes the detailed procedures carried out in an attempt to achieve functionalization. It is however of great importance to note that the procedures described in this chapter have been specifically tailored for application on the specific nanocomposite material of interest based on literature reference of relatively similar material and general chemistry reactions. The specific conditions used may not necessarily represent the optimum conditions for the processes. The procedures described in this chapter were designed to cover the application of the commonly known methods for esterification and etherification where the –OH groups in both lignocellulose and NaMMT components of the nanocomposite material took the role of alcohols. The Comp (2:1) nanocomposite sample was used in the study as the parent nanocomposite except where specified.

Evolution of methods reported in literature to the designed procedures was based on the challenges and observations noted from preliminary trials using common procedures and conditions for esterification and etherification reactions, such as the possibility of alteration of the material structure and properties as a result of pH conditions of the reaction system. In this chapter success and shortfalls of the various methods were identified and possible explanations given by analysis of results from the various characterization techniques applied on the products and these were reported in Section 5.4.

5.2 Functionalization by Esterification

5.2.1 Acid Catalyzed Reaction

PMPS*g*Lig-NaMMT (3.00 g) was stirred in 200 ml of deionized water for 5 minutes then filtered over fritted glass. The swollen substrate was washed on the filter with ethanol then stirred in 80 ml of ethanol for 5 minutes and filtered. The solid was then washed on the filter with *n*-butyric acid and stirred in 50 ml of the carboxylic acid for 10 minutes and filtered. A mixture composed of *n*-butyric acid (25.78 ml), acetic anhydride (9.45 ml) and H_2SO_4 catalyst (9.00 µl, 98 %) was heated at 90°C for 1 hour. Solvent-exchanged PMPSgLig-NaMMT was then added to the reaction medium. The whole mixture was stirred at approximately 110°C for 2 hours. At the end of the reaction, 150 ml of ethanol was added to precipitate the solubilized fraction. The solid was separated by filtration over fritted glass and purified by Soxhlet extraction with ethanol for 8 hours. The purified product was then dried at 80 °C for 48 hours and characterized.

5.2.2 Base Catalyzed Reaction

PMPS*g*Lig-NaMMT (3.00g) was dispersed in 40 ml of pyridine and stirred for 10 minutes followed by cautious addition of 40 ml of butyryl chloride. The mixture was allowed to react for 30 minutes and 400 ml of a 1:1 (v/v) EtOH:H_2O mixture was added to the resulting product, followed by stirring for 1 hour. The resulting gooey product was then allowed to settle for 30 minutes. The solvent mixture was decanted off followed by addition of 150 ml of ethanol to the product, stirred for 20 minutes and then filtered. The product was then washed on the filter first with ethanol and then with copious amounts of deionized water. The functionalized composite was then dried in a ventilated oven at 80 ^{0}C for 48 hours and characterized.

5.2.3 DBTDL Catalyzed Reactions

PMPS*g*Lig-NaMMT was solvent exchanged as described in Section 5.2.1. The solvent-exchanged PMPS*g*Lig-NaMMT was added to 40 ml of *n*-butyric acid and stirred for 20 minutes under high speed magnetic stirring. The catalyst, DBTDL (0.125 ml), was then added to the dispersion, mixed for 10 minutes and the mixture allowed to react under reflux for 2 hours while stirring. At the end of the reaction the solid was allowed to cool, separated by filtration over fritted glass and purified by Soxhlet extraction with ethanol for 24 hours. The purified product was then dried at 80 °C for 48 hours and characterized.

5.2.4 Sodium Metal Catalyzed Reactions

PMPS*g*Lig-NaMMT nanocomposite (3.00 g) was dispersed in 25 ml of *n*-pentane and stirred continuously. Approximately 3.00 g of freshly cut, divided (about 10 pieces) sodium metal chips in 15 ml of *n*-pentane were then added to the dispersion and allowed to react for 24 hours (reaction time may vary depending on the sizes of the sodium chips) at room temperature, after which all unreacted sodium chips were removed. Butyryl chloride (40 ml) was then cautiously added to the dispersion and stirring continued for about 3 hours to complete the reaction. The product was then filtered and dispersed in 400 ml of a 1:1 (v/v) EtOH:H_2O mixture, stirred for 30 minutes and then filtered. The product was then washed on the filter first with diethyl ether and then with copious amounts of deionized water. The functionalized composite was then dried in a ventilated oven at 80 ^{0}C for 48 hours and characterized.

5.3 Functionalization by Etherification

5.3.1 Base Catalyzed Reactions

5.3.1.1 Solvent Free Reaction

PMPS*g*Lig-NaMMT was solvent exchanged as described in Section 5.2.1, with the final stage being done using *n*-chlorobutane. Potassium iodide (1.83 g) and silver oxide (0.13 g) were added to *n*-chlorobutane (40 ml) and stirred for about 20 minutes under high speed magnetic stirring to give the reaction medium. The solvent-exchanged PMPS*g*Lig-NaMMT was then added to the reaction medium. The whole mixture was stirred at approximately 25 °C for 8 hours. At the end of the reaction the solid was separated by filtration and purified by Soxhlet extraction with acetone for 5 h followed by washing with copious amounts of deionized water. The purified product was then dried at 80 °C for 48 hours and characterized.

5.3.1.2 Reaction in Solvent

PMPS*g*Lig-NaMMT (3.00 g) was dispersed in 50 ml of toluene and mixed by high speed magnetic stirring for 20 minutes. *n*-Chlorobutane (1.16 ml) with potassium iodide (1.83 g)/1-bromo-3-phenylpropane (1.68 ml) and silver oxide (0.13 g) were then added to the mixture and mixing continued. The mixture was then allowed to react for 8 hours at approximately 25 ^{0}C. The resulting product was filtered off and washed by Soxhlet extraction with acetone for 5 hours then with water for 5 hours. The reaction was also repeated for *n*-chlorobutane using *n*-pentane as the solvent. The product from the reaction in pentane was dried in an oven at 80 ^{0}C for 1 hour followed by washing with diethyl ether and then Soxhlet extracted with water for 5 hours. The functionalized composites were then dried in a ventilated oven at 80 ^{0}C for 48 hours and characterized.

5.3.2 Acid Catalyzed Reaction

PMPS*g*Lig-NaMMT was solvent exchanged as described in Section 5.2.1, with the final stage being done using butan-1-ol. The solvent-exchanged PMPS*g*Lig-NaMMT was then added to 40 ml of butan-1-ol and the mixture stirred at approximately 100 °C for 5 minutes. At the end of 5 minutes of mixing at 100 °C, 8.80 µl of concentrated (98 %) H_2SO_4 was added to the reaction mixture and stirring continued for 2 hour. At the end of the reaction the solid was separated by filtration and washed with acetone followed by washing with deionized water. The purified product was then dried at 80 °C for 48 hours and characterized.

5.3.3 Sodium Metal Catalyzed Reactions

PMPS*g*Lig-NaMMT nanocomposite (3.00 g) was dispersed in 25 ml of *n*-pentane and stirred continuously. Approximately 3.00 g of freshly cut, divided (about 10 pieces) sodium metal chips in 15 ml of *n*-pentane were then added to the dispersion and allowed to react for 48 hours at room temperature, after which all unreacted sodium chips were removed. The alkyl halide (10 ml of *n*-chlorobutane) was then added to the dispersion and stirring was continued for about 5 hours at room temperature to ensure a complete reaction. DMSO (20 ml) was then added to the dispersion and stirring continued for 3 hours. The product was then filtered and then Soxhlet extracted for 3 hours using acetone, after which the solvent was changed to water and the Soxhlet extraction continued for another 24 hours (until fresh water passes the product and remains clear). The product was then dried in a ventilated oven at 80 ^{0}C for 48 hours.

5.4 Results and Discussion

This section describes the results obtained from the characterization of the materials that were prepared in this chapter.

5.4.1 FTIR Analysis

5.4.1.1 Functionalization by Esterification

Figure 5.1 displays the FTIR spectra of the ester derivatives of PMPSgLig-NaMMT nanocomposite relative to the parent nanocomposite. The spectra show that the derivatives retained their main structural and functional properties which suggested that the material was relatively stable and resistant to all functionalization treatments applied.

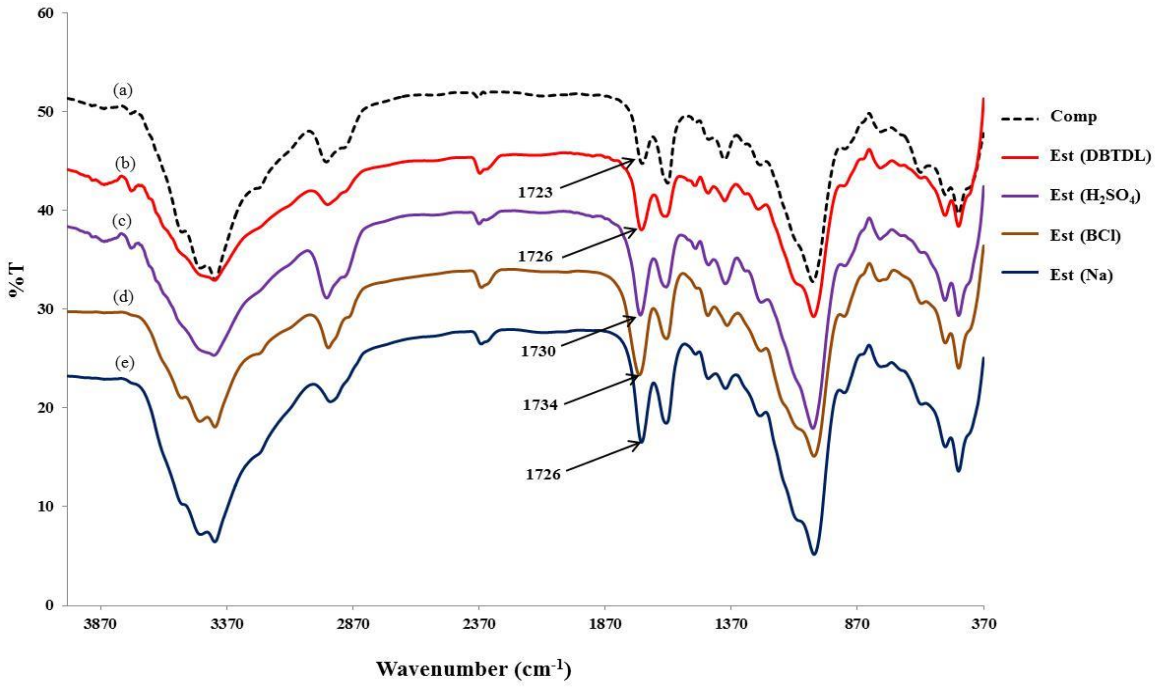

Figure 5.1: FTIR spectra of (a) Comp, (b) Est (DBTDL), (c) Est (H_2SO_4), (d) Est (BCl) and (e) Est (Na) nanocomposites.

Varying intensities of the H-O-H bending peak (1639-1650 cm^{-1}) suggested varying levels of water exclusion after functionalization as material became relatively more hydrophobic. A

decrease in O-H band intensity coupled with the increase in the C-O stretch around 1057 cm^{-1} suggested success in functionalization.

On the other hand relatively non trended variation in the alkyl C-H sp^3 peaks around 2993 cm^{-1} was attributed to the balance between partial lignocellulose degradation (peak diminish) and functionalization (peak enhancement). However a significantly important observation was made on the ester C=O stretching peak of the derivatives. This peak in all derivatives was observed to be more intense and shifted towards the left (1726-1734 cm^{-1}) with reference to the peak in the parent nanocomposite (1723 cm^{-1}), which both indicated an increase in ester presence, especially saturated ester (McMurry, 2008). Extent of peak shift was used as a relative measure of the esterification functionalization where the order descended in the following order Est (BCl) > Est (H_2SO_4) > Est (DBTDL) > Est (Na).

5.4.1.2 Functionalization by Etherification

Figure 5.2 shows the FTIR spectra of the etherified derivatives with that of the unfunctionalized parent nanocomposite. In the spectra no significant peak changes apart from some slight variations in peak intensities which can be attributed to the materials inhomogeneity, could be observed mainly because functionalization did not introduce a distinctly new bonding relationship. The C-O (1000-1300 cm^{-1}) and C-O-C (1220 cm^{-1} asymmetry and 850 cm^{-1} symmetry) stretches characteristic of the ether functionalization were masked by the already existing C-O groups of the lignocellulose structure such that in the absence of other distinguishing groups it was relatively difficult to confirm functionalization with reasonable confidences.

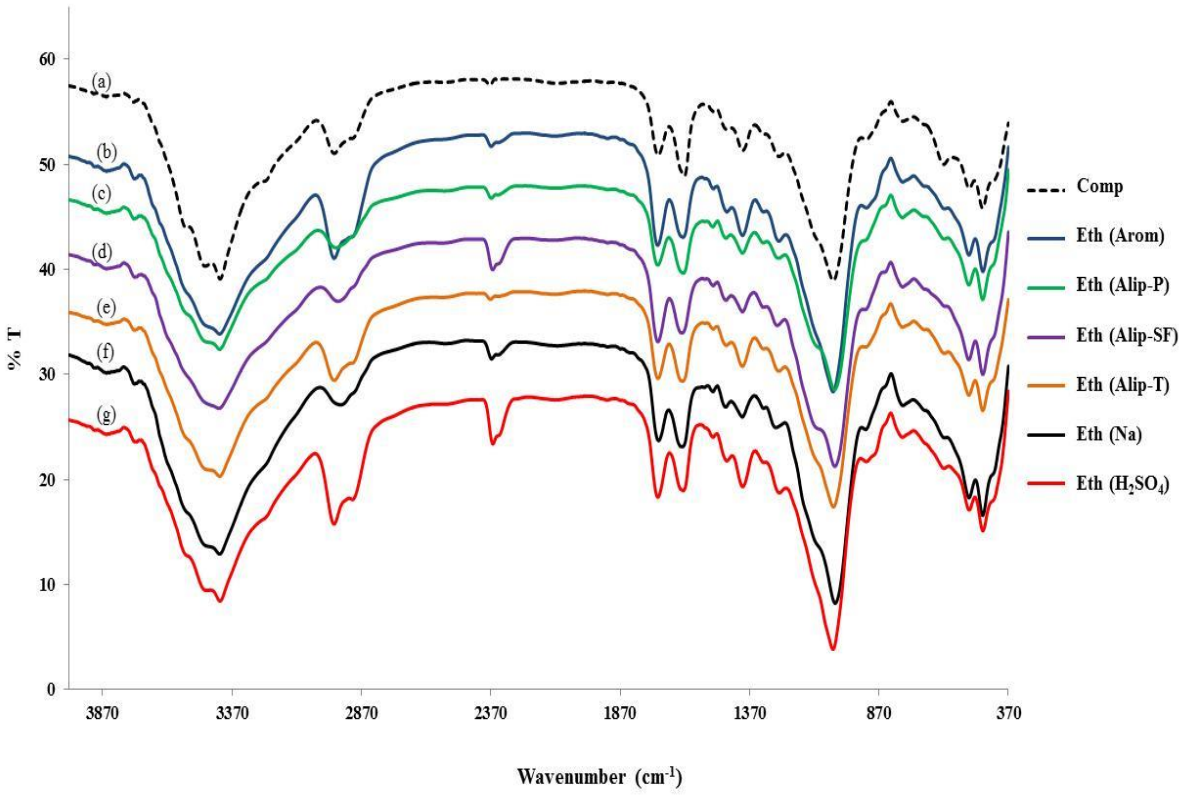

Figure 5.2: FTIR spectra of (a) Comp, (b) Eth (Arom), (c) Eth (Alip-P), (d) Eth (Alip-SF), (e) Eth (Alip-T), (f) Eth (Na) and (g) Eth (H_2SO_4) nanocomposites.

In general similar observations regarding the H-O-H bending, O-H bend, C-O stretch and alkyl C-H stretch peak intensities, 1640, 1330-1430, 1000-1300 and 2950 cm^{-1} respectively, were made as those observed with the ester derivatives. However the exclusion of water appeared to be more pronounced as the H-O-H bending peak (1639-1650 cm^{-1}) was notably diminished as can be observed in Figure 5.2 when the peak is compared with ester C=O stretch peak (1723 cm^{-1}) which had a relatively constant intensity in all samples unlike in the esters where the peak intensity diminishing could easily have been mistaken for the C=O stretch peak intensification.

5.4.1.3 Effects of Nanocomposite Composition

Figure 5.3 shows the FTIR spectra of DBTDL catalyzed ester derivatives of varying Lig: NaMMT ratios together with corresponding parent nanocomposites. Observations similar to those made in Sections 5.3.1.1 and 5.3.1.2 regarding the H-O-H bending, O-H band, C-O stretch and alkyl C-H peak intensities were also made with the nanocomposites of varying composition and their derivatives. However H-O-H bending peak intensities were observed to diminish after functionalization in a trend that appeared to be related to the material composition. This trend suggested that the greater the ratio of Lignocellulose in the material, the greater the exclusion of water after functionalization.

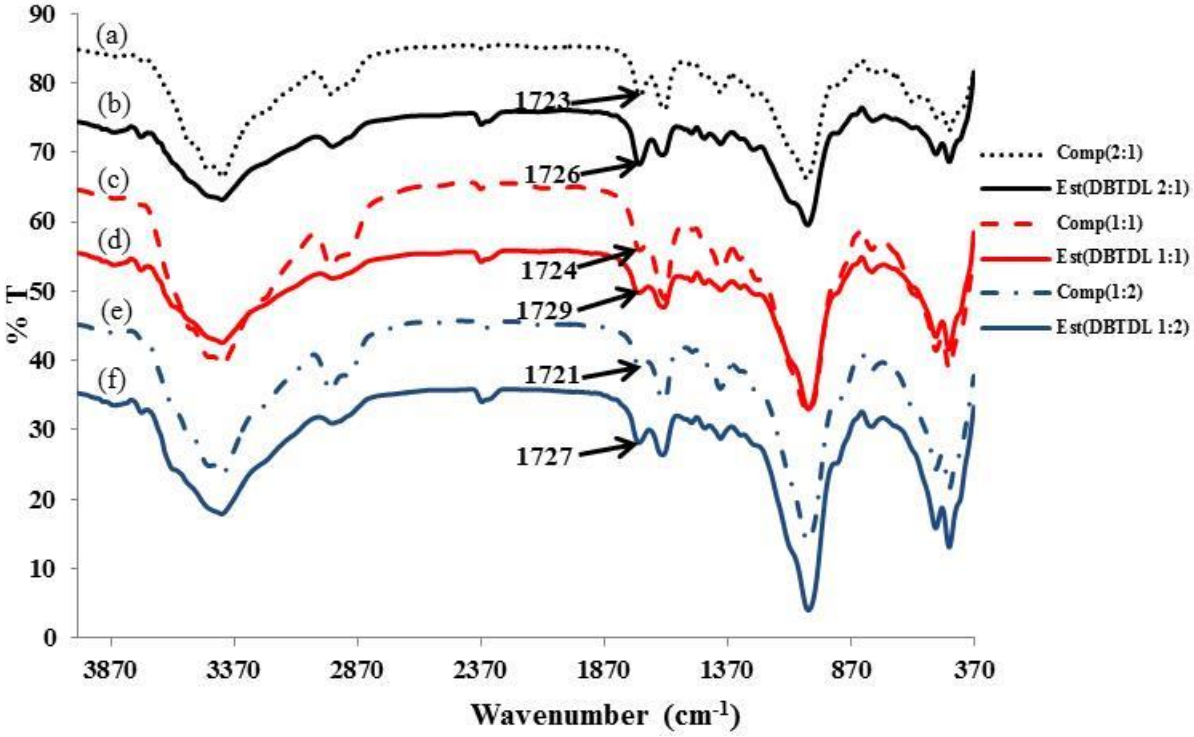

Figure 5.3: FTIR spectra of (a) Comp (2:1), (b) Est (DBTDL 2:1), (c) Comp (1:1), (d) Est (DBTDL 1:1), (e) Comp (1:2) and (f) Est (DBTDL 1:2) nanocomposites.

For all three composition variations a peak shift towards higher wavenumbers was observed for the ester C=O stretch peak after functionalization, which supported the idea of successful functionalization. However an interesting observation that was made was that the magnitude

of peak shift appeared to be directly proportional to the NaMMT content of the nanocomposites which suggested that more functionalization may havesignificantly occurred on the NaMMT component.

5.4.2 XRD Powder Analysis

5.4.2.1 Functionalization by Esterification

Figure 5.4 shows the diffractograms for the ester derivatives of PMPSgLig-NaMMT nanocomposite. Wide angle analysis of the diffractograms revealed that the general structure of the nanocomposites was retained after functionalization.

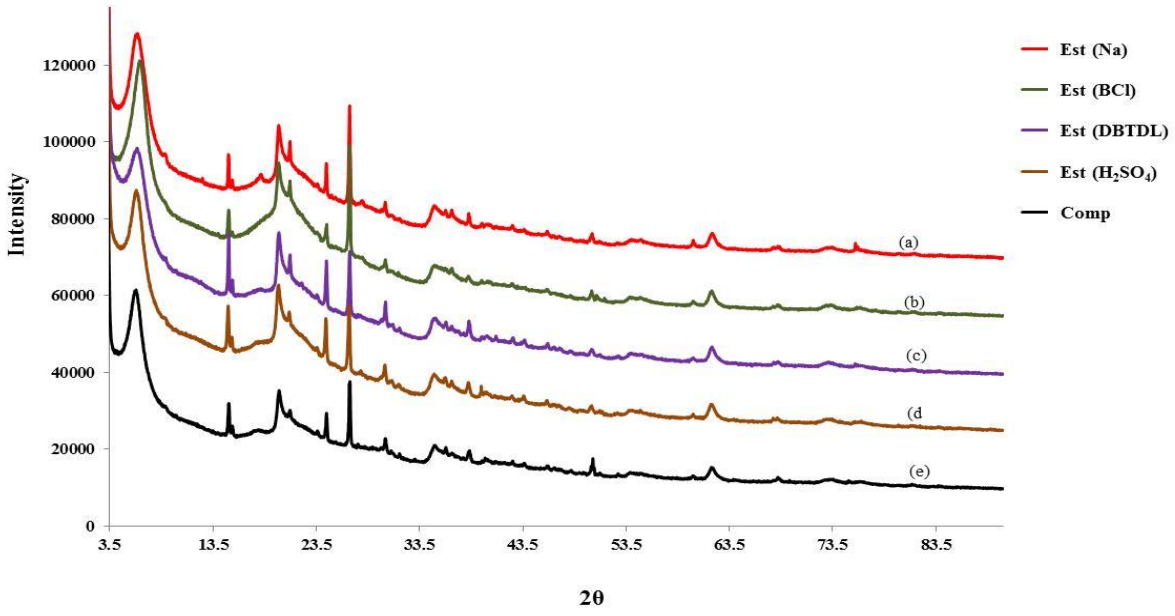

Figure 5.4: XRD Powder diffractograms for (a) Est (Na), (b) Est (BCl), (c) Est (DBTDL), (d) Est (H_2SO_4) and (e) Comp nanocomposites.

On the other hand low angle analysis showed that the basal reflection peak position and intensity varied with variation in the functionalization method and conditions used. Peak positions were observed to shift towards higher 2θ values with reference to the position of the peak in the diffractogram of the unfunctionalized parent nanocomposite as can be observed

from the values in Table 5.1. This observation implied that functionalization reactions caused a decrease in the d-spacing. Functionalization introduced a hydrophobic environment in the interlayer space of the clay structure which resulted in exclusion of water which in turn resulted in the observed reduction in d-spacing due to reduced water content which had induced swelling of the clay. This observation also helps to support the idea of successful functionalization reactions and is consistent with FTIR suggestions of exclusion of water in the nanocomposite structure. The reduction in d-spacing also appeared to be directly proportional to the functionalization extent as interpreted from FTIR analysis.

The diffractogram peak intensity changes were attributed to changes in the material crystallinity due to the functionalization conditions. However peak intensity and the d-spacing values appeared not to have any correlations which suggested that the factors bringing about variations in the two properties were independent of each other. Table 5.1 summarizes some of the parameter values obtained from the material XRD diffractograms.

Table 5.1: Values of 2θ and d-spacing values for the basal reflection peak in the ester derivative nanocomposites XRD powder diffractograms.

Sample ID	Basal reflection peak (2θ)	d-spacing (nm)	Δ d-spacing (nm)
Comp	6.05	1.462	-
Est (DBTDL)	6.13	1.441	-0.021
Est (H_2SO_4)	6.07	1.456	-0.006
Est (BCl)	6.39	1.383	-0.079
Est (Na)	6.20	1.426	-0.036

In the table Δ d-spacing represents the difference in d-spacing of the functionalized nanocomposite and that of the unfunctionalized parent nanocomposite ((functionalized nanocomposite d-spacing) – (parent d-spacing)). Delta d-spacing values were negative which

indicated a decrease in the d-spacing after functionalization (Giannelis, Krishnamoorti and Manias, 1999).

5.4.2.2 Functionalization by Etherification

Figure 5.5 shows the XRD powder diffractograms for the etherified nanocomposites.

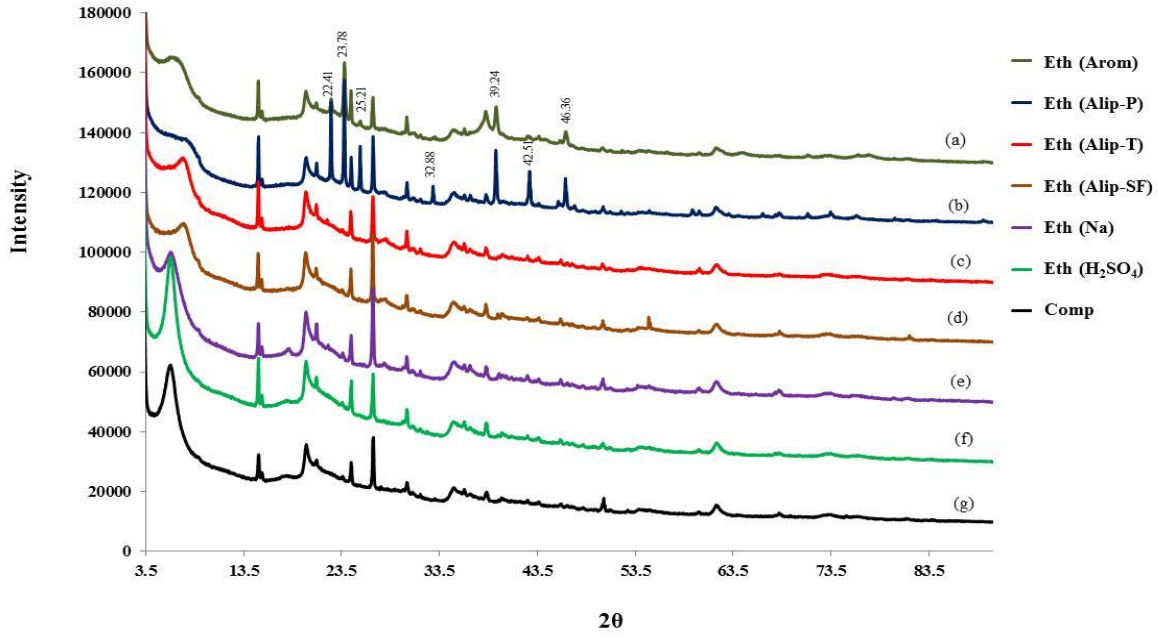

Figure 5.5: XRD Powder diffractograms of (a) Eth (Arom), (b) Eth (Alip-P), (c) Eth (Alip-T), (d) Eth (Alip-SF), (e) Eth (Na), (f) Eth (H_2SO_4) and (g) Comp nanocomposites.

Both low angle and wide range analysis of the diffractograms gave significantly interesting information about the materials. Analysis of the diffractograms for Eth (Na) and Eth (H_2SO_4) with reference to that for the unfunctionalized parent nanocomposite revealed that functionalization did not significantly affect the general structure of the nanocomposites (wide range analysis), but had an effect on the crystallinity of the phase associated with the basal reflection peak (low angle analysis) which was observed through the changes in peak intensity. The effect on crystallinity was observed to be vice versa since the peak in Eth (Na) was observed to diminish in intensity while that in Eth (H_2SO_4) became more intense.

Eth (Arom), Eth (Alip-T), Eth (Alip-P) and Eth (Alip-SF) diffractograms with reference to the parent diffractogram showed the material to be inhomogeneous which resulted in the observed broadening of the basal reflection peak in the low angle analysis. This is common in solid solutions and may imply possible contamination (Poly Crystallography, Inc., 2014). For Eth (Alip-T) and Eth (Alip-SF), broadening was accompanied by a peak shift to higher 2θ values which corresponded to the observed reduced d-spacing. No change in d-spacing was observed in the Eth (Arom) nanocomposite. However considering that the same reaction conditions were applied during functionalization as the other ethers, a similar result was expected. Failure to observe such a result was attributed to the relatively bulky nature of the functionalization moiety which is assumed to graft in the nanocomposites' NaMMT interlayers and hence maintain the d-spacing constant despite some water exclusion. Maintenance of the d-spacing was also partially attributed to the presence of minimal residual catalyst which was observed through the emergence of peaks at 22.41, 23.78, 39.24 and 46.36 2θ values as reported by other researchers (Niggli, 1922; Atta *et al*., 2014).

On the other hand the basal reflection peak in the diffractogram for Eth (Alip-P) was observed to be diminished to a shoulder while distinct new peaks were observed in the diffractogram. The additional peaks in the diffractogram were attributed to the presence of unremoved KI and Ag_2O (Niggli, 1922; Wyckoff, 1963; Ahtee, 1969; Atta *et al*., 2014). Considering that Eth (Alip-T) and Eth (Alip-SF) also underwent the same reaction conditions during functionalization except for the solvents used, the observed presence of distinctly notable amounts of KI and Ag_2O was attributed to the choice of the solvent which interfered with the efficiency of the purification process. In Eth (Alip-P) the catalyst resulted in an effect such as observed in pillaring using the catalyst. This in turn resulted in a degree of NaMMT exfoliation and hence the observed basal reflection peak loss (Dubois and

Alexandre, 2000). The observations made with Eth (Alip-P) in comparison with Eth (Alip-SF) and Eth (Alip-T) also gave strong evidence for the importance of the choice of solvent.

A notable but small difference in the Eth (Arom) diffractogram in the 2θ range of 33 – 50 from the diffractograms of the other samples in the same region was attributed to the overall difference in the functionalization moiety. Table 5.2 gives a summary of similar values as in Table 5.1 in Section 5.4.2.1.

Table 5.2: Values of 2θ and d-spacing for the basal reflection peak in the ether derivative nanocomposites XRD powder diffractograms.

Sample ID	Basal reflection peak (2θ)	d-spacing (nm)	Δ d-spacing (nm)
Comp	6.05	1.462	-
Eth (Alip-T)	7.29	1.213	-0.249
Eth (Alip-P)	-	-	-
Eth (Alip-SF)	7.31	1.209	-0.253
Eth (Arom)	6.05	1.462	0
Eth (H_2SO_4)	6.03	1.467	0.005
Eth (Na)	6.07	1.456	-0.006

No data was recorded for Eth (Alip-P) since there was no peak to derive the data from. The positive Δ d-spacing for Eth (H_2SO_4) was attributed to acid activation through partial hydrolysis of the nanocomposite lignocellulose component which made the material relatively more hydrophilic (Yang et al. 2013) and hence countering the water exclusion effect of functionalization enough to allow functionalization to result in an increase in d-spacing.

5.4.2.3 Effects of Nanocomposite Composition

Figure 5.6 shows the diffractograms of the Est (DBTDL) derivative nanocomposites of varying composition together with their corresponding parent nanocomposites. Wide angle range analysis of the diffractograms for all composition variations showed retention of the general structure of the nanocomposite after functionalization.

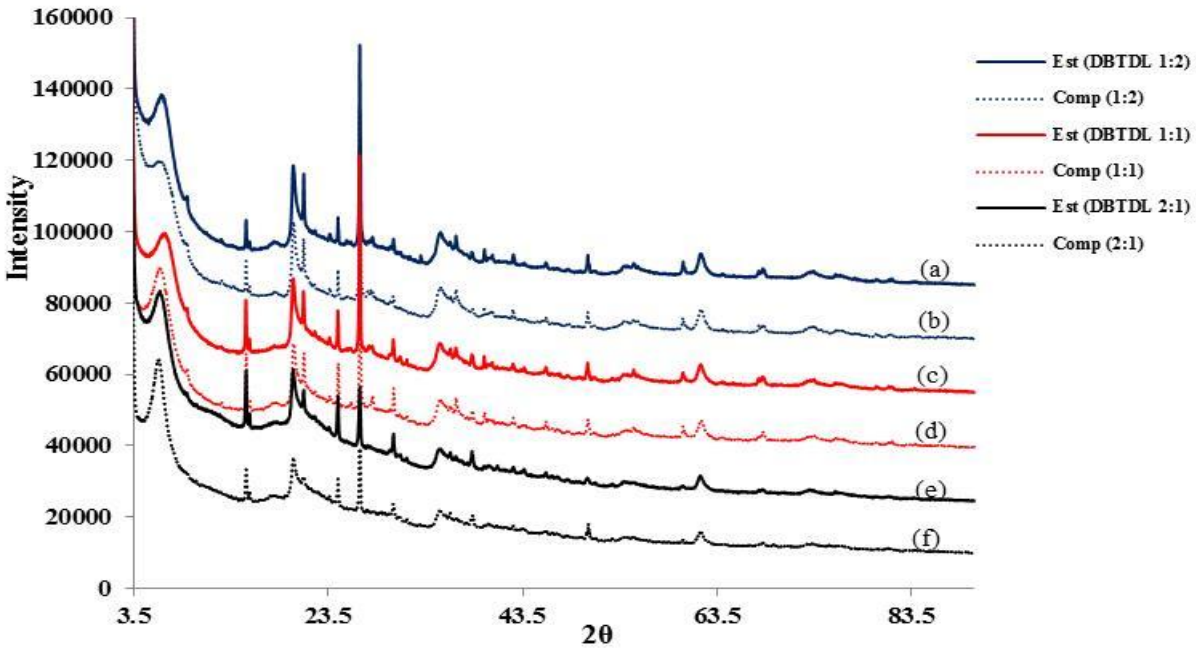

Figure 5.6: XRD Powder diffractograms of (a) Est (DBTDL 1:2), (b) Comp (1:2), (c) Est (DBTDL 1:1), (d) Comp (1:1), (e) Est (DBTDL 2:1) and (f) Comp (2:1) nanocomposites.

Low angle analysis of the diffractograms showed that basal reflection peak intensity changed after functionalization in a manner related to the material composition, but did not follow a composition trend. These relatively non-trended changes were attributed to the exclusion of water from the interlayer spaces of the NaMMT component and the amount of intercalated grafted functionalization moieties as directed by nanocomposite composition. Table 5.3 summarizes the values of parameters relating to changes in the basal reflection peak positions. The least exclusion of water was observed in Est (DBTDL 2:1) due to the least

intercalation as a result of high competition for the functionalization target posed by the larger ratio of lignocellulose in the material.

Table 5.3: Values of 2θ and d-spacing for the basal reflection peak in the Est (DBTDL) derivative nanocomposites XRD powder diffractograms.

Sample ID	Basal reflection peak (2θ)	d-spacing (nm)	Δ d-spacing (nm)
Comp (1:1)	6.09	1.451	
Est (DBTDL - 1:1)	6.69	1.321	-0.130
Comp (1:2)	6.30	1.402	
Est (DBTDL - 1:2)	6.28	1.407	0.005
Comp (2:1)	6.05	1.462	
Est (DBTDL - 2:1)	6.13	1.441	-0.021

A lower ratio of lignocellulose in Est (DBTDL 1:1) facilitated intercalation of the functionalization molecules and greater exclusion of water from the clay component to give the observed relatively large decrease in d-spacing. On the other hand an increase in d-spacing (positive Δ d-spacing value) was observed in Est (DBTDL 1:2). This observation was attributed to high organic moiety grafting in the NaMMT component motivated by the low lignocellulose ratio.

5.4.3 SEM Analysis

5.4.3.1 Functionalization by Esterification

In Figure 5.7 the micrographs for PMPS*g*Lig-NaMMT nanocomposite and its ester derivatives are displayed. All the derivative micrograms show that functionalization reaction conditions did not break down the nanocomposites as the derivatives were observed to be notably similar to the parent. However due to the limitations of the instrument, no

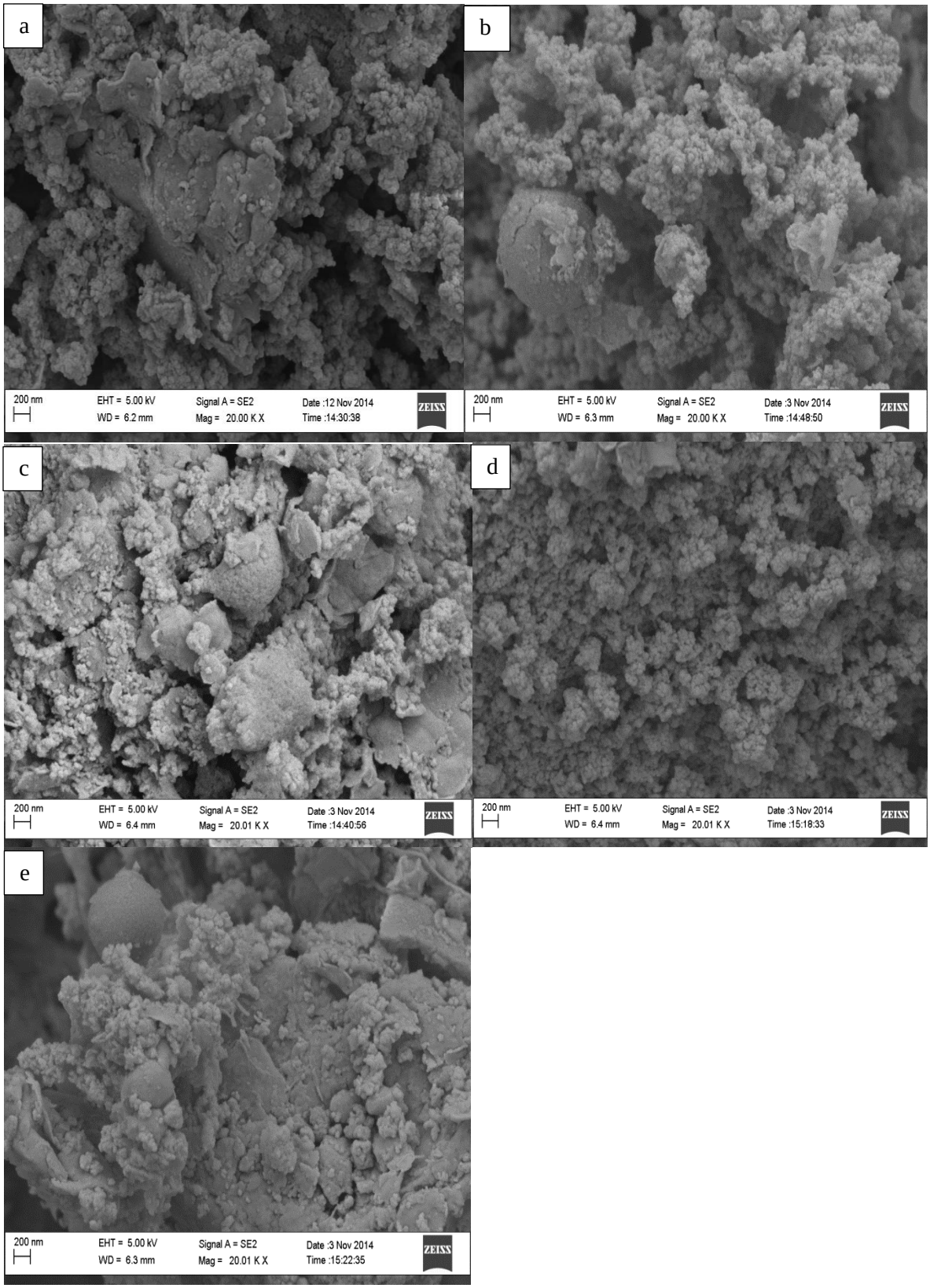

Figure 5.7: SEM micrographs of (a) Comp, (b) Est (DBTDL), (c) Est (BCl) , (d) Est (H_2SO_4) and (e) Est (Na) nanocomposites.

information directly related to the functionalization could be obtained from the micrographs. On the other hand slight variations in the micrograms can be attributed to the general inhomogeneity of the material structure. Due to the general inhomogeneity of the nanomaterial structures, the micrographs may however also not be completely and accurately representative of the whole material structure. The micrographs also did not show any features which could be attributed to the partial degradation of the nanocomposite components.

5.4.3.2 Functionalization by Etherification

The micrographs of the ether derivatives of the PMPS*g*Lig-NaMMT nanocomposite are shown in Figure 5.8. Similar to the ester derivatives the images show signs of nanocomposite structure retention although some of the micrographs show lower particle densities as compared to the ester derivatives.

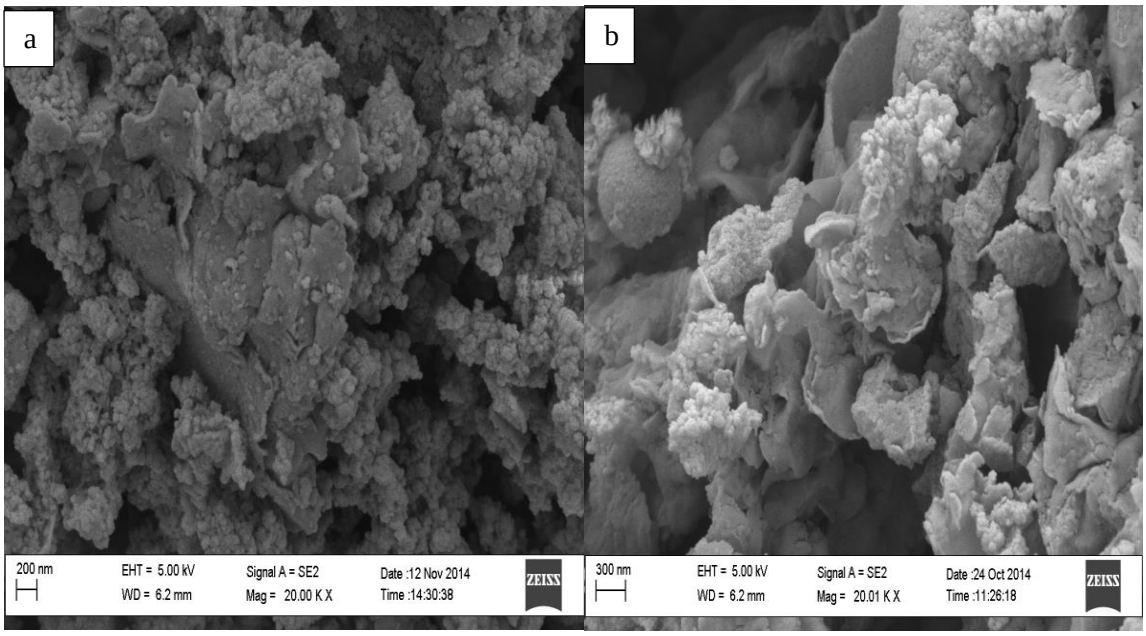

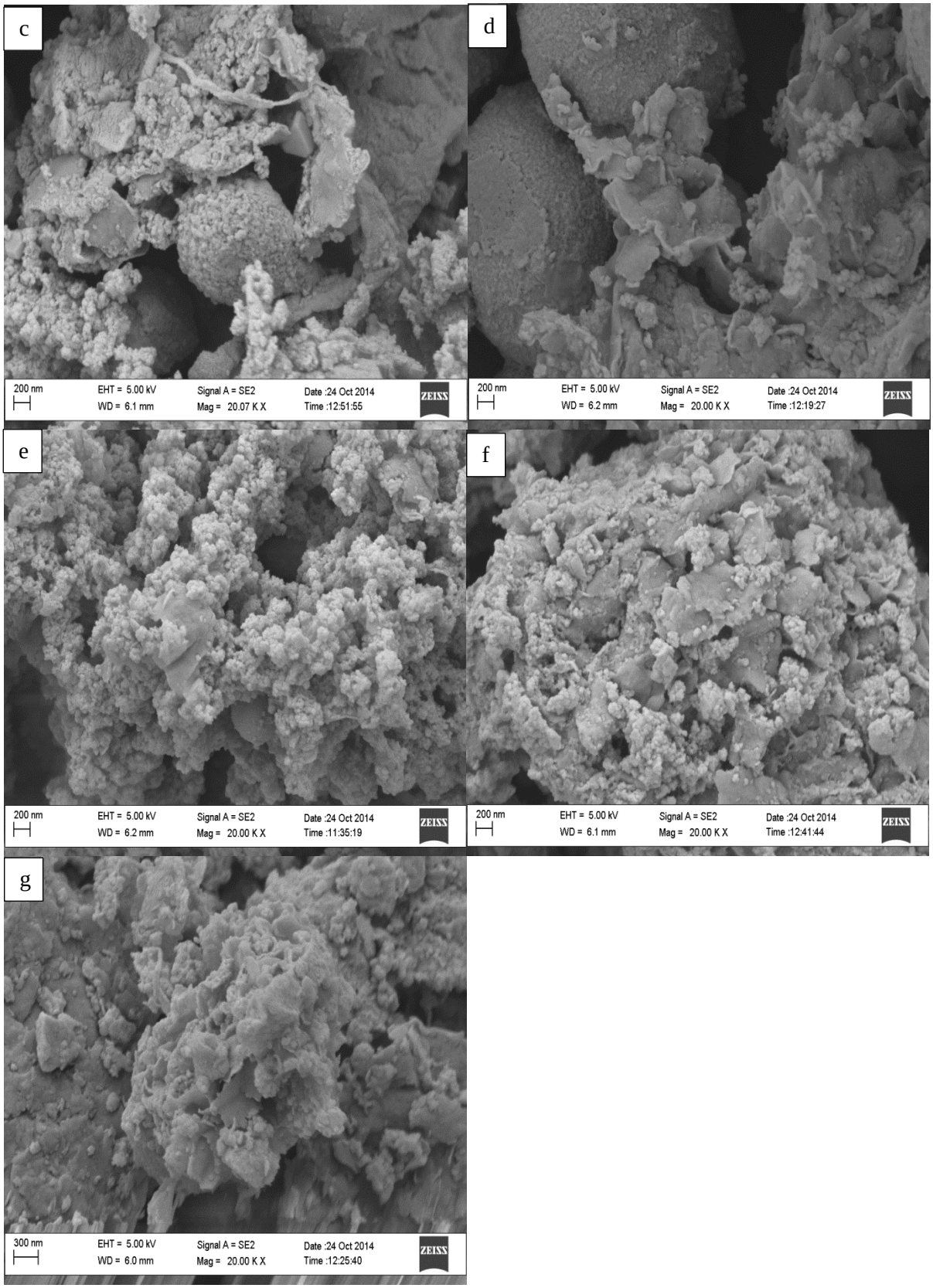

Figure 5.8: SEM micrographs of (a) Comp, (b) Eth (H_2SO_4), (c) Eth (Arom), (d) Eth (Alip-P), (e) Eth (Alip-SF), (f) Eth (Alip-T) and (g) Eth (Na) nanocomposites.

The micrographs also show that the general nanocomposite structures were nonhomogeneous.

5.4.3.3 Effects of Nanocomposite Composition

Figure 5.9 shows the micrographs of the nanocomposite composition variations together with their corresponding Est (DBTDL) derivatives. A variation in the general structures of each composition variation set (parents and derivatives) was observed. This was attributed to the differences in the nanocomposite component ratios.

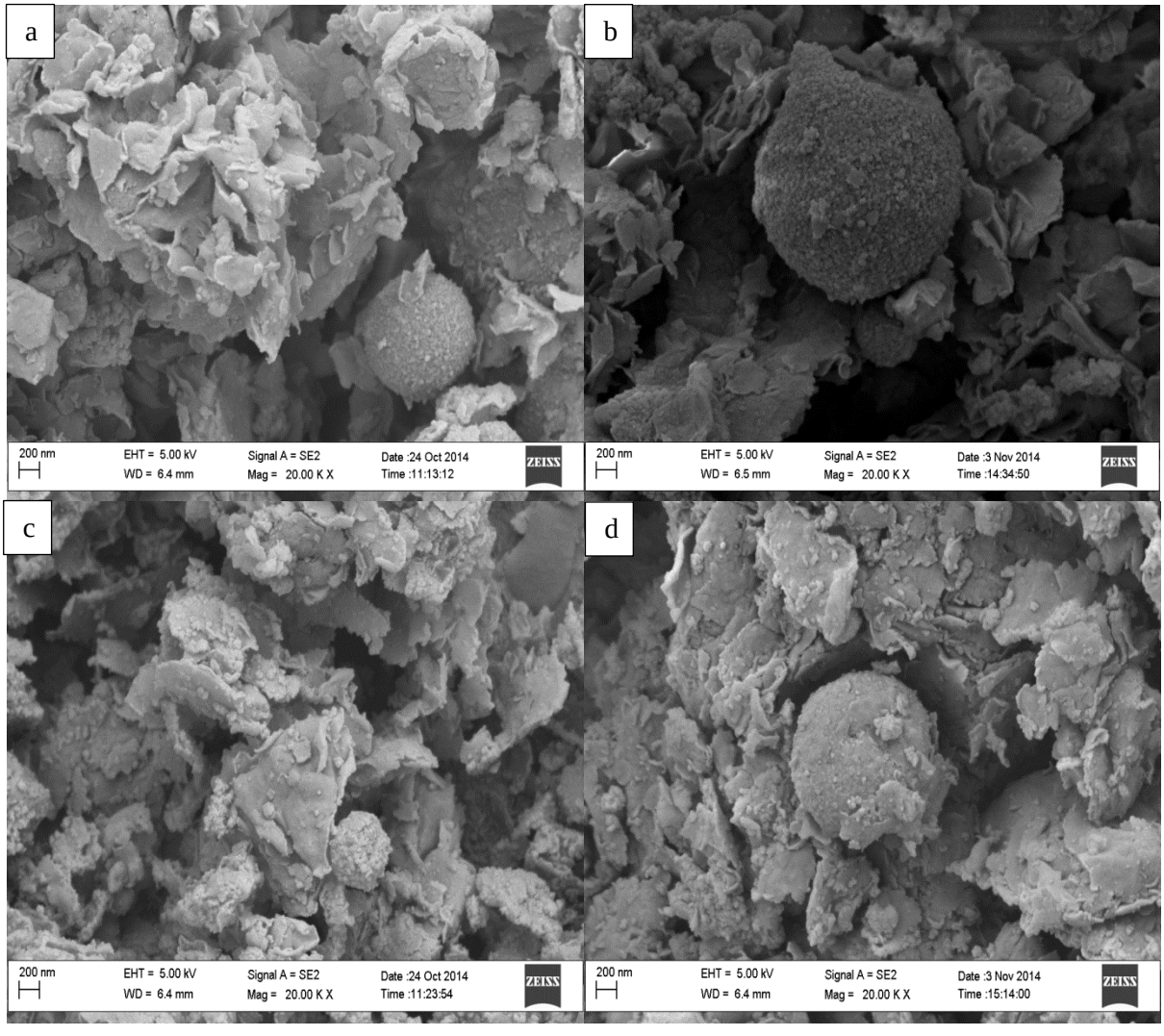

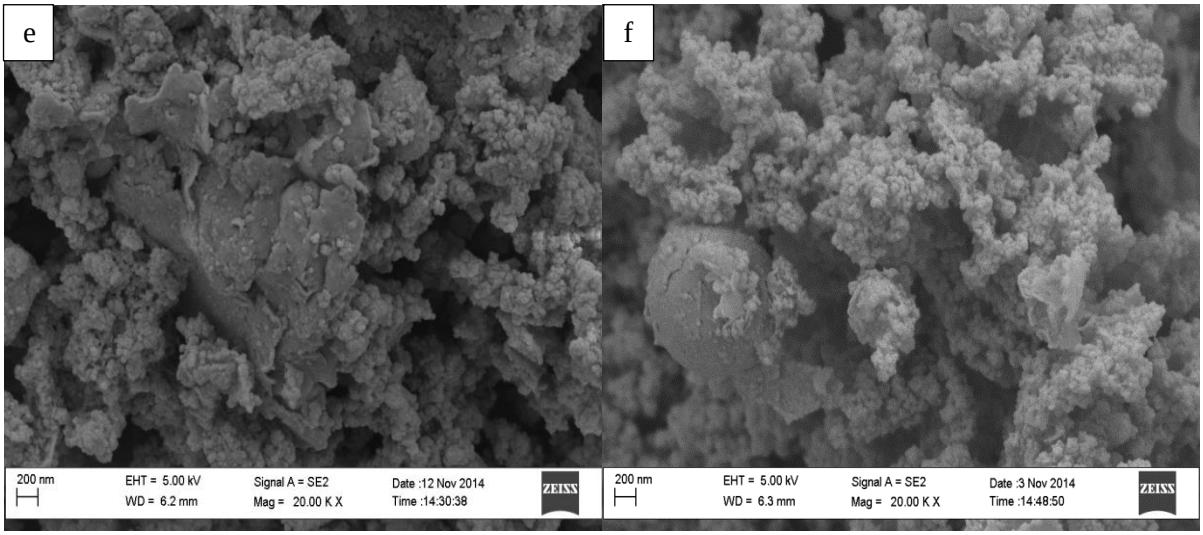

Figure 5.9: SEM micrographs of (a) Comp (1:1), (b) Est (DBTDL 1:1), (c) Comp (1:2), (d) Est (DBTDL 1:2), (e) Comp (2:1) and (f) Est (DBTDL 2:1)

For each composition ratio (parent and derivative) no notable difference was observed in the micrographs and this was consistent with the idea that functionalization conditions did not decompose the nanocomposite material and any component degradation was at a reasonable minimum if at all it did happen.

5.4.4 TG Analysis

5.4.4.1 Functionalization by Esterification

The thermal decomposition profiles of the ester derivative nanocomposites are presented in the thermograms in Figure 5.10. All derivative thermograms appeared to follow the general shape of the parent thermogram hence indicating similar decomposition patterns. However the thermogram for Est (BCl) stood out from the rest showing the least thermal stability. The auto-ignition temperatures of butane, butyric acid and 1-butanol are reported to be within the range of 343 – 452 ^{0}C (IPCS, 1998; United States of America. National Fire Protection Association, 2002; Hitech Chemicals, 2006; ScienceLab.com, Inc., 2013; WolframAlpha,

2014) which is similar to the thermal decomposition temperature range of the lignocellulose components.

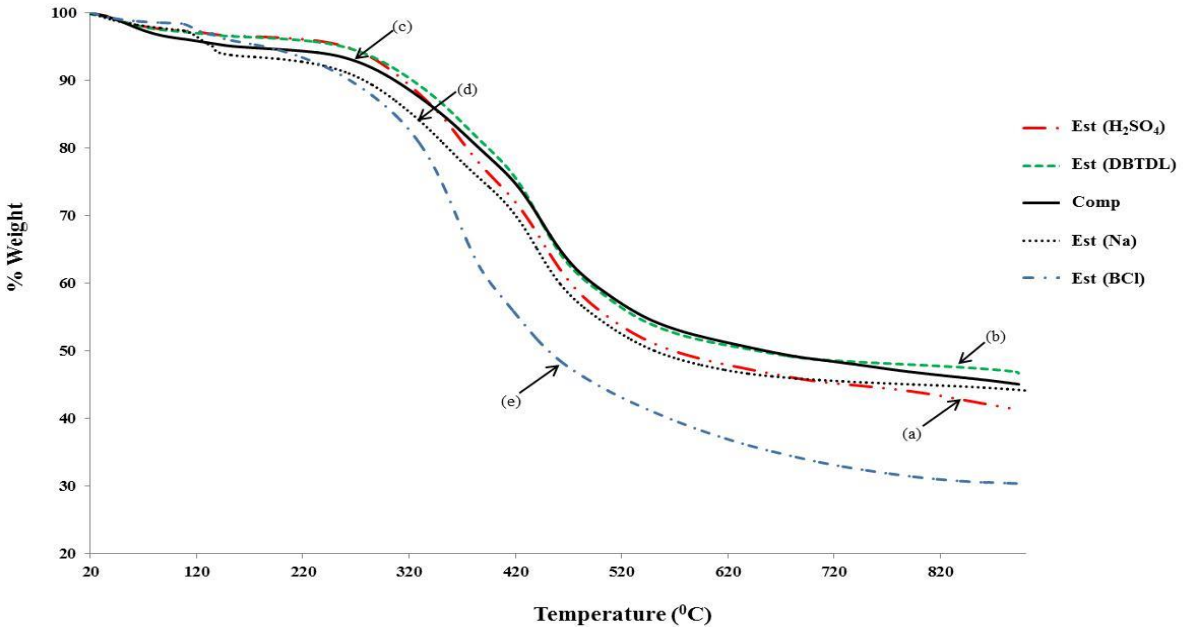

Figure 5.10: TGA thermograms of (a) Est (H_2SO_4), (b) Est (DBTDL), (c) Comp, (d) Est (Na) and (e) Est (BCl).

This may explain the observed variations in the thermograms from that of the parent without any introduction of a new distinct decomposition step. The separation of the Est (BCl) thermogram from the rest just after 200 ^{0}C suggests an increase in the decomposition of the components in the following temperature range (>200 ^{0}C), which was attributed to the pyrolysis of the grafted moiety. The separation was also consistent with FTIR analysis showing that Est (BCl) had the greatest functionalization extent. Table 5.4 summarizes some data obtained from the thermogravimetric analysis.

The % dry weight was specially taken note of as it revealed that the samples retained or excluded water to different extents after functionalization considering that all samples were equally dried and kept in sealed containers.

Table 5.4: Percentage dry weight and residual weight for the ester derivative nanocomposites.

Sample ID	% dry weight	% residual weight
Comp	94.95	47.49
Est (DBTDL)	96.47	48.43
Est (Na)	97.49	47.12
	93.71	
Est (H_2SO_4)	96.66	42.72
Est (BCl)	98.44	31.58
	96.21	

This observation was consistent with FTIR suggestions with regards to the variation in the H-O-H bending vibration peak in the nanomaterials' spectra. Est (Na) and Est (BCl) were observed to lose surface moisture in a two-step process where the first step represented simple loss from the surface similar to the other samples while the second was attributed to loss of moisture trapped between the nanocomposite surface and the hydrophobic film of functionalization. The observation of this effect only in these samples was attributed to the relatively gentle conditions of the functionalization reactions which maintained the general basic structure of the parent nanocomposite coupled with relatively high functionalization. The exclusion of water from the material was observed to be somehow directly proportional to the functionalization extent as proposed in Section 5.3.1.1.

On the other hand the % residual weight of the derivatives with comparison to the parent gives an idea of the relative balance between the functionalization extent and lignocellulose degradation during functionalization. The significantly lower % residual weight values for Est (BCl) and Est (H_2SO_4) with reference to that of the parent nanocomposite was consistent with the functionalization extent predicted in Section 5.3.1.1. On the other hand the slightly lower deviated % residual weight value for Est (Na) suggested success of the

functionalization reaction and relatively notable retention of the sodium catalyst as part of the NaMMT structure after functionalization. The observed larger % residual weight value for Est (DBTDL) coupled with a lower % dry weight value suggested significant lignocellulose degradation which gave the effect of a form of *in-situ* lignocellulose pretreatment.

5.4.4.2 Etherification Functionalization

Figure 5.11 shows the thermograms of the ether derivatives of PMPSgLig-NaMMT nanocomposites. Similar to the ester derivatives, the ether derivatives' thermograms closely resemble that of the parent nanocomposite in shape. However slight deviations from the parent thermogram were observed which can be related to the functionalization process.

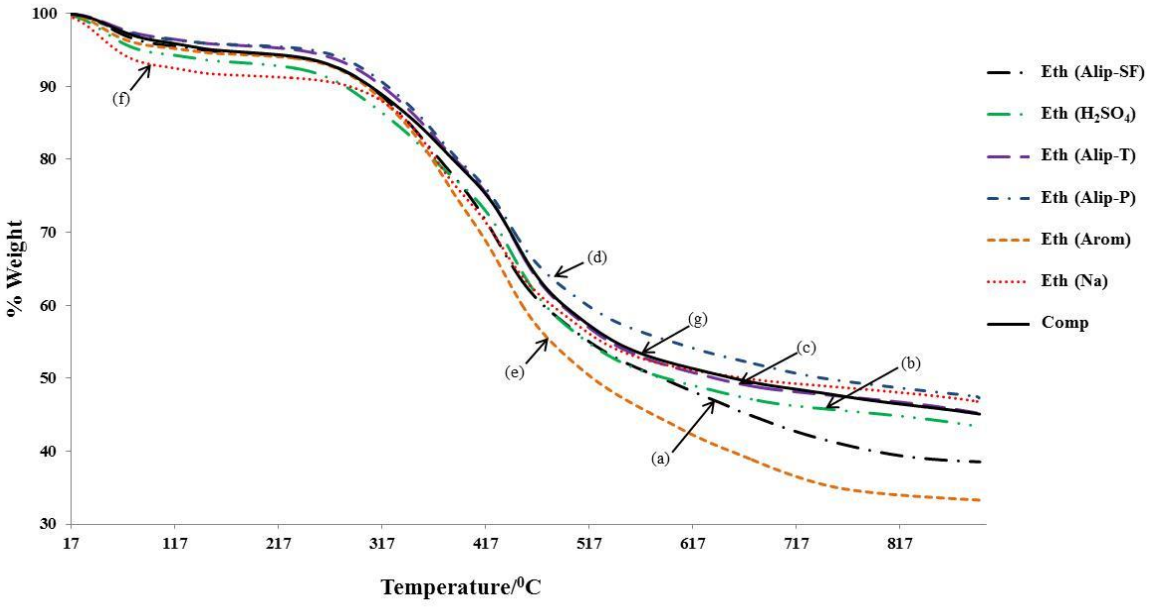

Figure 5.11: TGA thermograms of (a) Eth (Alip-SF), (b) Eth (H_2SO_4), (c) Eth (Alip-T), (d) Eth (Alip-P), (e) Eth (Arom), (f) Eth (Na) and (g) Comp nanocomposites.

Table 5.5 summarizes similar % weight data as that in Table 5.4 for the ester derivatives. The % dry weight values appeared lower than those of the esters meaning that the ethers retained more water. This observation with consideration of the explanation for the ester derivative

exclusion of water is consistent with the previously proposed idea that functionalization was more successful in the case of the ester derivatives. On the other hand the % residual weight values revealed interesting information complementary to the findings from FTIR, XRD and SEM analysis.

Table 5.5: Percentage dry weight and residual weight for the ether derivative nanocomposites.

Sample ID	% dry weight	% residual weight
Comp	94.95	47.49
Eth (Alip-T)	95.77	47.19
Eth (Alip-P)	95.79	49.37
Eth (Alip-SF)	94.88	40.61
Eth (Arom)	94.52	35.22
Eth (Na)	91.56	50.85
Eth (H_2SO_4)	93.57	46.35

Eth (Alip-T), Eth (Alip-P), Eth (Alip-SF) and Eth (Arom) were synthesized using mild conditions and therefore limited lignocellulose degradation was expected if any at all. The lower % residual weight values (with reference to the parent value) observed for Eth (Alip-SF) and Eth (Arom) supported the expected result of limited degradation and also suggested that functionalization had been achieved. However the low value for Eth (Arom) was partially attributed to the large molecular weight of the grafted moiety which was more pyrolyzed, when compared to the butyl moiety grafted on the other ether derivatives. Similar % residual weight values were expected for Eth (Alip-T) and Eth (Alip-P) but larger values were observed.

The unexpected large value for Eth (Alip-P) was the result of the presence of residual Ag_2O catalyst and KI in the samples as suggested in Section 5.3.2.2 from the diffractogram of the derivative while the slight % residual weight value deviation to a lower value was attributed

to a low degree of functionalization. The high % residual weight value observed in Eth (Alip-P) was consistent with the XRD results which suggested the highest level of residual catalyst. It should be taken into consideration that the XRD diffractogram for Eth (Arom) also suggests the presence of residual catalyst in the sample which in turn suggests that the success in the functionalization reaction may actually be more than what was reflected by the % residual weight observed.

The notable difference in % residual weight observed between Eth (Alip-T) and Eth (Alip-SF) confirmed that a higher level of functionalization is obtained in solvent free functionalization reactions considering that XRD diffractograms suggest the absence of residual catalyst in these samples. A relatively low % dry weight value for Eth (H_2SO_4) and a lower % residual weight with reference to the parent value suggested considerable lignocellulose degradation by the acid coupled with some notable functionalization. The lowest % dry weight coupled with the highest % residual weight for the Eth (Na) nanocomposite were attributed to the large NaMMT and low lignocellulose % composition in the material which was a result of relatively high free radical degradation (Carey and Sundberg, 2008) of the lignocellulose component during functionalization. Taking this into consideration, it was also possible that the free radicals generated from the chlorobutane during the functionalization reaction could have acted on the already grafted moieties hence counter-acting the functionalization reaction and contributing to the relatively large observed % residual weight.

5.4.4.3 Effects of Nanocomposite Composition

The thermograms for the Est (DBTDL) nanocomposite derivatives and their parents are presented in Figure 5.12. As expected, the thermal stability of the material was observed to increase with increase in NaMMT content of the nanocomposite. Table 5.6 summarizes some

of the thermal decomposition profile data obtained from the thermograms of the Est (DBTDL) derivatives and their parents. The % dry weight values for the parent nanocomposites with comparison to those of the derivatives revealed that the parents possessed larger amounts of moisture thereby supporting the suggestion put forward from the FTIR analysis results, that functionalization gives rise to water exclusion from the material.

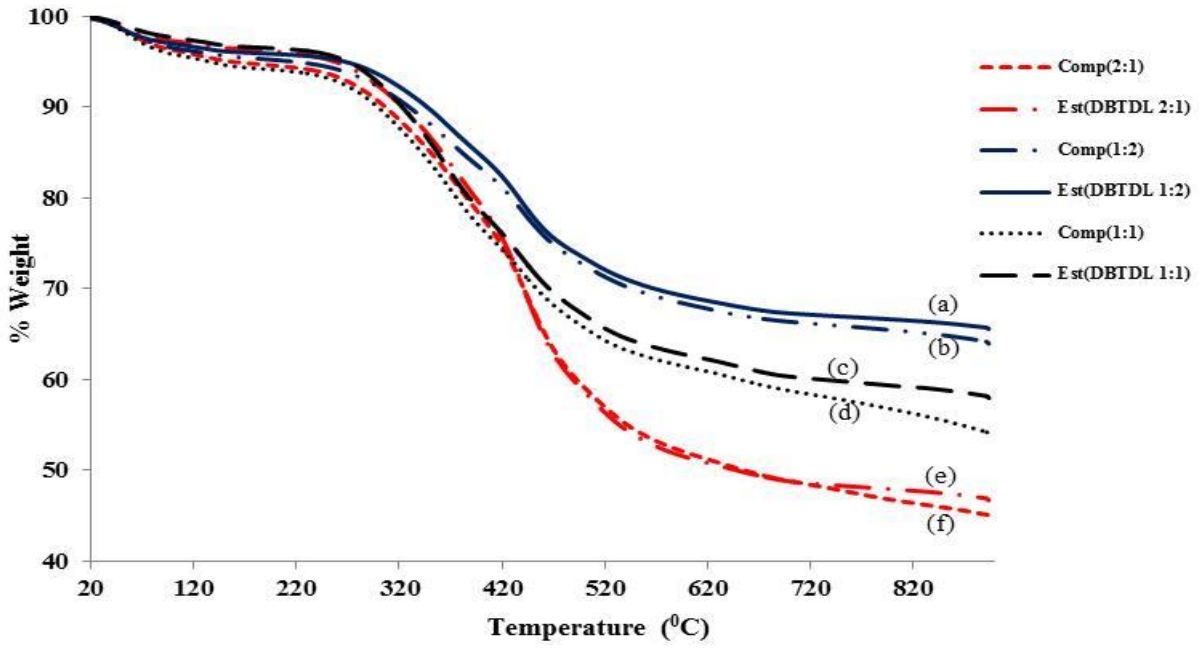

Figure 5.12: TGA thermograms of (a) Comp (2:1), (b) Est (DBTDL 2:1), (c) Comp (1:2), (d) Est (DBTDL 1:2), (e) Comp (1:1) and (f) Est (DBTDL 1:1) nanocomposites.

The % residual weight was observed to be directly proportional to the NaMMT content of the material. On the other hand, the estimated % functionalization weight deviation ([parent % residual weight] – [derivative % residual weight]) did not follow any obvious trend which may be attributed to relatively random parent weight loss during functionalization. The estimated % functionalization weight deviation values were negative due to the higher % residual weights observed for the derivatives which confirmed the occurrence of lignocellulose degradation during functionalization at all composition ratios.

Table 5.6: Percentage dry weight and residual weight for the Est (DBTDL) derivative nanocomposites

Sample ID	% dry weight	% residual weight	Estimate % functionalization weight deviation
Comp (1:1)	94.43	56.96	
Est (DBTDL 1:1)	96.66	59.97	-3.01
Comp (1:2)	95.55	66.93	
Est (DBTDL 1:2)	96.04	68.27	-1.34
Comp (2:1)	94.95	47.49	
Est (DBTDL 2:1)	96.47	48.43	-0.94

The values however do not necessarily reflect success of the functionalization reaction and were not considered for the quantification of the functionalization reaction success. The estimate % functionalization weight deviation was considered in this section since the functionalization method used was the same for the samples and any form of degradation of the parents was generally expected to be similar for the different compositions.

5.5 Conclusion

The intended modifications of the PMPSgLig-NaMMT nanocomposites were achieved using both esterification and etherification methods as confirmed by FTIR, XRD and TGA. FTIR, XRD and TGA also showed that for each type of functionalization (esterification or etherification), the different routes taken produced products with different properties which may also possibly include the adsorption properties of the nanocomposites. Functionalization was also confirmed by these characterization techniques as they showed reduced internal water content which was confirmed by XRD through variations in the d-spacing of the nanocomposite NaMMT component as the swelling of the clay reduced due to the water loss.

FTIR, XRD and SEM also confirmed that the functionalization processes did not significantly affect or decompose the general structure of the original nanocomposite.

FTIR analysis of the composition variations also confirmed the hypothesis of optimum functionalization with nanocomposites of high lignocellulose content. XRD showed that the composition of the nanocomposites plays a significant role in directing the sites for functionalization and also confirmed that functionalization occurred on both components of the nanocomposites. TGA results showed that the functionalization conditions of some of the methods used significantly degraded the lignocellulose component to give the effect of a form of *in-situ* pretreatment which may have improved both the functionalization reaction and the overall adsorption properties of the material.

In general all functionalization methods applied were successful, but to different extents depending on the specific conditions used, and assessment of the adsorption properties of the nanocomposites was crucial for the identification of the positive and negative significance of the changes brought about by functionalization.

5.6 References

Ahtee, M. **(1969)** Lattice constants of some binary alkali halide solid solutions. *Annales Academiae Scientiarum Fennicae: Physica*. 313 (A6). p. 1-11.

Atta, A. M.; Hamad A. Al-Lohedan, H. A.; Ezzat, A. O. **(2014)** Synthesis of silver nanoparticles by green method stabilized to synthetic human stomach fluid. *Molecules.* 19. p. 6737-6753.

Boyd, R. W. and Morrison, R. **(1992)** *Organic chemistry*. Englewood Cliffs, N. J: Prentice Hall.

Dubois, P. and Alexandre, M. **(2000)** Polymer-layered silicate nanocomposites: Preparation, properties and uses of a new class of materials. *Materials Science and Engineering*. 28. p. 1-63.

Hitech Chemicals. **(2006)** *Material Safety Data Sheet: n-Butanol.* [Online] December 2006. Available from: http://hitech-chemicals.com/msds2/n-butanol_msds.pdf. [Accessed: 11th November 2014].

International Programme on Chemical Safety**. (1998)** *Butyric acid (*ICSC: *1334).* [Online] Available from: http://www.ilo.org/dyn/icsc/showcard.display?p_card_id=1334. [Accessed: 11th November 2014].

McMurry, J. **(2008)** *Organic Chemistry.* 7th edition. Chicago: Thomson - Brooks/Cole.

Niggli, P. **(1922)** Die Kristallstruktur einiger Oxyde I. *Zeitschrift fur Kristallographie*. 57. p. 253-299.

Poly Crystallography, Inc. **(2014)** *XRD Analysis: An Introduction to X-ray Powder Diffraction Analysis.* [Online]. Available from: http://www.polycrystallography.com/XRDanalysis.html. [Accessed: 15th November 2014].

ScienceLab.com, Inc. **(2013)** *Material Safety Data Sheet: Butyric acid.* [Online] May 2013. Available from: http://www.sciencelab.com/. [Accessed: 11th November 2014].

United States of America. National Fire Protection Association **(2002)** *Fire Protection Guide to Hazardous Materials*. 13th edition. p. 325-327. Quincy, MA: National Fire Protection Association.

WolframAlpha. **(2014)** *Computational knowledge engine: Butane.* [Online] Available from: http://www.wolframalpha.com/input/?i=butane. [Accessed: 10th November 2014].

Wyckoff, R. W. G. **(1963)** *New York rocksalt structure*. Crystal Structures 1. 2nd edition. New York: Interscience Publishers.

Yang, H.; Chen, Q.; Wang, K.; Sun, R. C. **(2013)** Correlation between hemicelluloses-removal-induced hydrophilicity variation and the bioconversion efficiency of lignocelluloses. *Bioresour Technol.* 147. p. 539-544.

Carey, F. A. and Sundberg, R. J. **(2008)** *Advanced Organic Chemistry*. Part A: Structure and Mechanisms. 5th edition. New York: Springer.

CHAPTER 6

ADSORPTION STUDIES

6.1Introduction

Application of adsorbent materials for any process in industry or at a commercial level requires efficiency screening to avoid slowing down processes. Such screening involves accessing and quantifying the capacity and rate of adsorption, predicting the activity of the adsorbent material in varying adsorbate concentration environments and the effects of conditions such as temperature and pH on the adsorbent activity. A detailed understanding of the adsorption process by an adsorbent is essential in establishing relevant predictions on the fitness for industrial and commercial application of the adsorbent in question. Such relevant adsorption data may be obtained from adsorption isotherms, application of adsorption modelling equations and kinetic modelling.

Adsorption isotherms may be interpreted using the method of visual inspection as proposed by Giles *et al.* (1960) and further explained by Hinz (2001), while the use of isotherm models complements this method. Two commonly used adsorption models are the Langmuir and Freundlich models of which both together with the visual inspection method were applied in this study. On the other hand, kinetic modelling is accomplished by fitting the appropriate adsorption data into adsorption kinetic model equations. In this study, experimental adsorption data was fitted into the two commonly used adsorption kinetic models, the pseudo first-order and pseudo second-order models.

This chapter gives details of the procedures, conditions and results from batch adsorption experiments for the evaluation of the synthesized adsorbent materials. In carrying out these experiments the effects of the various methods of functionalization together with the effect of

varying the nanocomposite composition, on the adsorbent performance were determined. In the experiments 1,10-phenanthroline was used as the model organic pollutant while maintaining adsorption conditions of temperature and pH at 25 ^{0}C and 7.35 – 7.95 respectively. Quantification of 1,10-phenanthroline adsorption in water was achieved using UV/Vis spectroscopy at an experimentally observed λ_{max} of 285 nm in water. All experiments were carried out in triplicate and the average considered for statistical reasons (precision and accuracy). Adsorption data was then used to plot adsorption isotherms, fitted into Langmuir and Freundlich adsorption models, and also fitted into pseudo first and second-order kinetic models. The results and discussions after following these procedures were reported in Section 6.4.

6.2 Experimental Procedures

6.2.1 Adsorption Isotherms

Solutions of 1,10-phenanthroline in the range 20-100 ppm were prepared by dissolution of the chemical in deionized water. Adsorbent (0.1g) was added to each 250 mL conical flask of 100 mL solution and agitated for 8 hours. After 8 hours, aliquots were collected and filtered through acrodisc syringe filters (0.45 μm supor membrane) of low protein binding. UV/Vis spectroscopy was then used to determine the unadsorbed pollutant from the aliquots. The adsorbed amount, Q_e(mg/g), was then calculated and plotted against equilibrium concentration, C_e(mg/L) to give the adsorption isotherms. Data was also fitted into the Langmuir and Freundlich adsorption model equations.

6.2.2 Adsorption Kinetics

Adsorbent (0.1g) was added to 250 conical flasks of 100 mL of 100 ppm 1,10-phenanthroline solutions and the resulting suspensions agitated. Aliquots (5 ml) were collected from each

flask at time intervals of 15 mins, 30 mins, 1 hr, 2 hrs, 4 hrs and 8 hrs. Adsorbent was then separated from aliquots by filtration through 0.45 µm acrodisc syringe filters. UV/Vis spectroscopy was then used to determine the amount of adsorbate left in each aliquot. Solutions were agitated for 40 hrs but there was no significant change in the adsorbed amount of the adsorbate so only the results up to 8 hours of agitation are reported. Adsorbed amount Q_e (mg/g) values were calculated and plotted against time, and appropriate obtained data fitted into the kinetic modelling equations.

6.3 Analysis of Adsorption Data

6.3.1 Adsorption Isotherms and Model Application

6.3.1.1 Graphical Inspection

Figure 6.1 summarizes the four major classes of isotherms and their sub-groups, S-type (S-shaped); L-type (Langmuir type); H-type (high affinity) and C-type (constant partition).

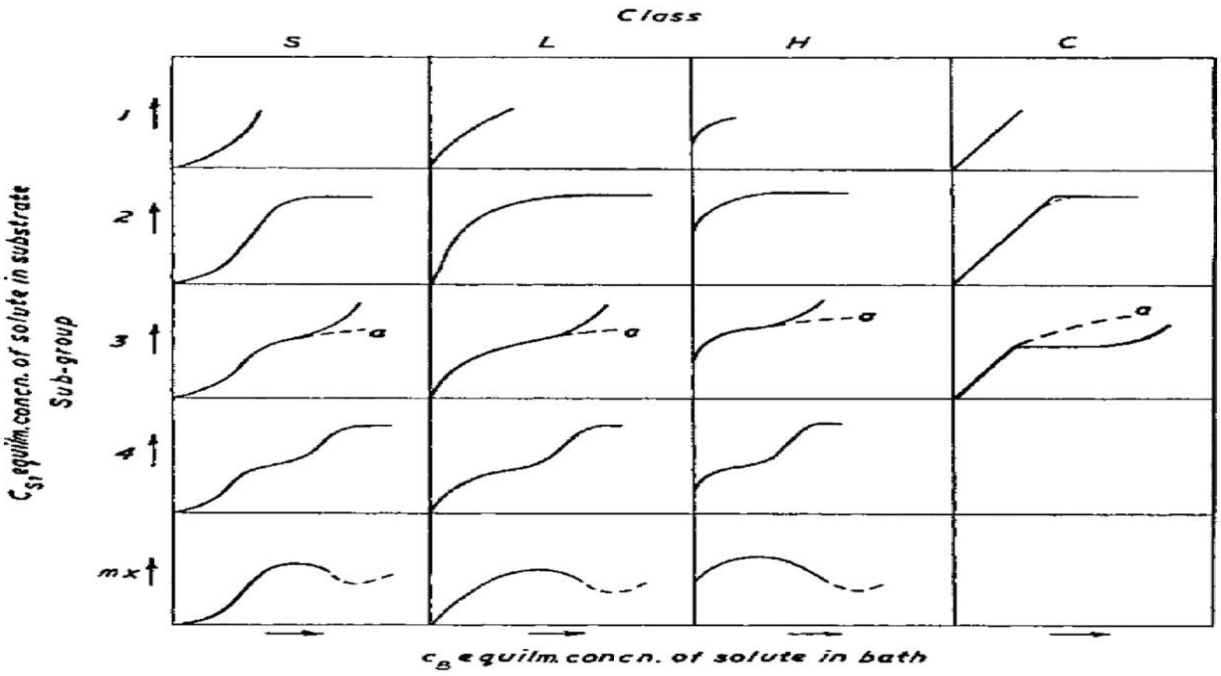

Figure 6.1: System of isotherm classification (Giles et al., 1960).

Adsorption isotherms were classified based on the slope of the initial curve of the equilibrium adsorbed amount (Q_e (mg/g)) versus equilibrium adsorbate concentration (C_e (mg/L)) as proposed by Giles *et al.* (1960) and Hinz (2001).

6.3.1.2 Langmuir Model

The linear Langmuir equation is expressed as follows:

$$(C_e/Q_e) = (1/Q_0 b) + (C_e/Q_0) \quad (6.1)$$

where C_e is the equilibrium amount of adsorbate in solution (mg/L); Q_e is the equilibrium adsorbed amount of adsorbate per unit mass of adsorbent (mg/g); Q_0 (mg/g) and b (L/mg) are the Langmuir constants related to the adsorption capacity and the rate of adsorption, respectively (Kumar *et al.*, 2008). A plot of C_e/Q_e against C_e should give a straight line if the adsorption data conforms to the Langmuir adsorption model. The model assumes that the adsorbent has a fixed (limited) number of adsorption sites, all adsorption sites are equal, each site retains one adsorbate molecule and all sites are energetically and sterically independent of the adsorbed amount (Limousin *et al.*, 2007). The Langmuir model describes monolayer adsorption onto homogeneous surfaces.

6.3.1.3 Freundlich Model

The empirical form of the Freundlich model equation is given by:

$$Q = FC^n \quad (6.2)$$

where Q (mg/g) is the adsorbed amount; C (mg/L) the remaining adsorbate concentration and F (L/g) and n (dimensionless) are constants. The equation may also be expressed in a linear form as follows:

$$\text{Log } Q_e = \log K_f + (1/n)\log C_e \quad (6.3)$$

where Q_e (mg/g) is the equilibrium adsorbed amount; C_e (mg/L) is the equilibrium concentration of the adsorbate (mg/L); K_f and *n* are the Freundlich constants related to the adsorption capacity and the rate of adsorption respectively (Namane *et al.*, 2005; Rawajfih *et al.*, 2006; Kumar *et al.*, 2008; Wang *et al.*, 2009; Kul *et al.*, 2010). A plot of Log Q_e against Log C_e yields a straight line if the adsorption data conforms to the Freundlich model (Limousin *et al.*, 2007). High values of *n* suggest good adsorption over the concentration range studied while steep slopes (small *n*) suggest good adsorption at high concentrations and poor at low adsorbate concentrations (Rawajfih *et al.*, 2006). The Freundlich model describes multilayer adsorption onto heterogeneous surfaces (Annadurai *et al.*, 2002) where uptake of adsorbate occurs onto different types of adsorption sites on the adsorbent, with adsorption on each type following the Langmuir model.

6.3.2 Kinetic Model Application

6.3.2.1 Pseudo First-order Kinetics Model

The linear pseudo first-order equation is expressed as:

$$\text{Log } (Q_e - Q_t) = \text{Log } Q_e - (k_1/2.303)t \quad (6.4)$$

where Q_e (mg/g) is the amount of solute adsorbed at equilibrium per unit mass of adsorbent; Q_t (mg/g) is the amount of solute adsorbed at time t, and k_1 is the pseudo first-order rate constant in min^{-1}. Due to chemisorption being immeasurably slow (King *et al.*, 2007) Q_e in this study was taken as the amount of adsorbate adsorbed after 8 hours. If adsorption data conforms to the pseudo first-order kinetic model, a plot of Log (Q_e-Q_t) against time (t) yields a straight line.

6.3.2.2 Pseudo Second-order Kinetics Model

The pseudo second-order equation is expressed as:

$$t/Q_t = (1/k_2Q_e^2) + (t/Q_e) \quad (6.5)$$

where Q_e (mg/g) is the amount of solute adsorbed at equilibrium per unit mass of adsorbent; Q_t (mg/g) is the amount of solute adsorbed at time t; k_2 is the pseudo second-order rate constant with units of $gmg^{-1}min^{-1}$. A plot of t/Q_t versus time t, gives a straight line if adsorption data is consistent with the pseudo second-order kinetic model (Delval *et al.*, 2002; Kumar, 2006). The pseudo second-order model assumes chemisorption and can be used to describe the adsorption mechanism for the whole sorption process.

6.4 Results and Discussion

6.4.1 Effects of Functionalization

6.4.1.1 Adsorption Isotherms of Esterified Material

Figure 6.2 shows the adsorption isotherms for the ester functionalized nanocomposites. Isotherms were all classified as Langmuir of the type L_{mx} by visual inspection (Giles *et al*., 1960; Hinz, 2001) and showed that beyond a certain equilibrium adsorbate concentration, the adsorbed amount decreases. This observation may be attributed to gradual saturation of the adsorbent adsorption sites at high concentrations, which is consistent with monolayer adsorption and the Langmuir adsorption model. All functionalized nanocomposite adsorption isotherms except for Est (BCl) were observed to be above and further to the left as compared to that for the unfunctionalized adsorbent which indicated enhanced adsorption after functionalization.

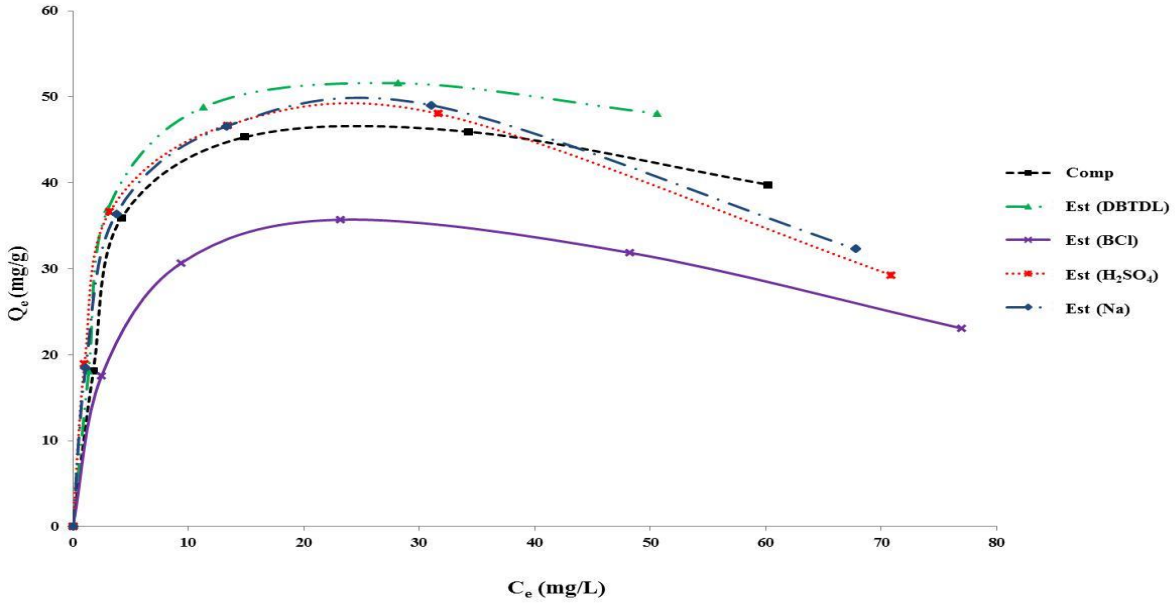

Figure 6.2: Isotherms for 1,10-phenanthroline adsorption by ester derivative nanocomposites adsorbents.

On the other hand the surprisingly lower adsorption observed with Est (BCl) considering the fact that characterization indicated highest functionalization, may be explained by the observed difficulty of the adsorbent to mix with water as a result of high hydrophobicity due to high functionalization extent. In general the order of adsorption was as follows: Est (DBTDL)> Est (Na) > Est (H_2SO_4) > Comp > Est (BCl).

Figure 6.3 and Figure 6.4 show the Langmuir and Freundlich plots respectively, for the adsorbents in question and Table 6.1 summarizes the data from the plots. Correlation coefficient (R^2) value comparison for the two adsorption models indicated that the Langmuir model was the best fit for all esterified together with the unmodified adsorbent samples. Also Q_0 values for the samples corresponded to the adsorbed amounts while k_f values failed to exhibit a corresponding trend, which further supported the idea that adsorption followed the Langmuir model.

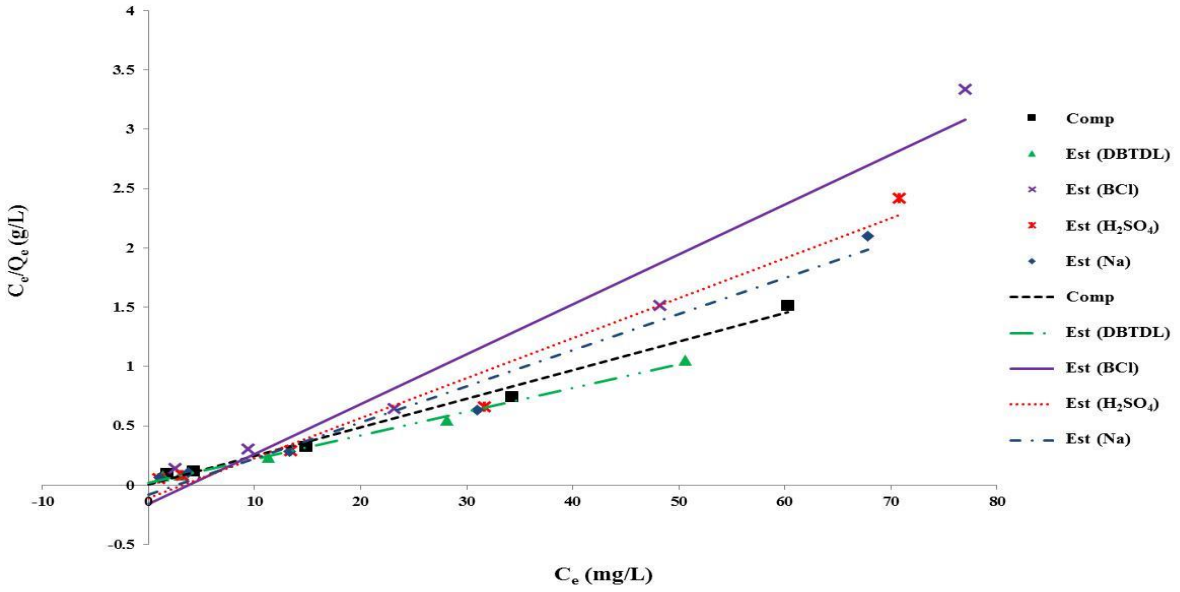

Figure 6.3: Langmuir plots for the adsorption of 1,10-phenanthroline onto ester derivative nanocomposite adsorbents.

However, a negative *b* value for Est (H_2SO_4) discredited its consistency with the Langmuir model (Igwe and Abia, 2007; Alves Fungaro *et al*., 2009) despite the high R^2 value and other consistencies.

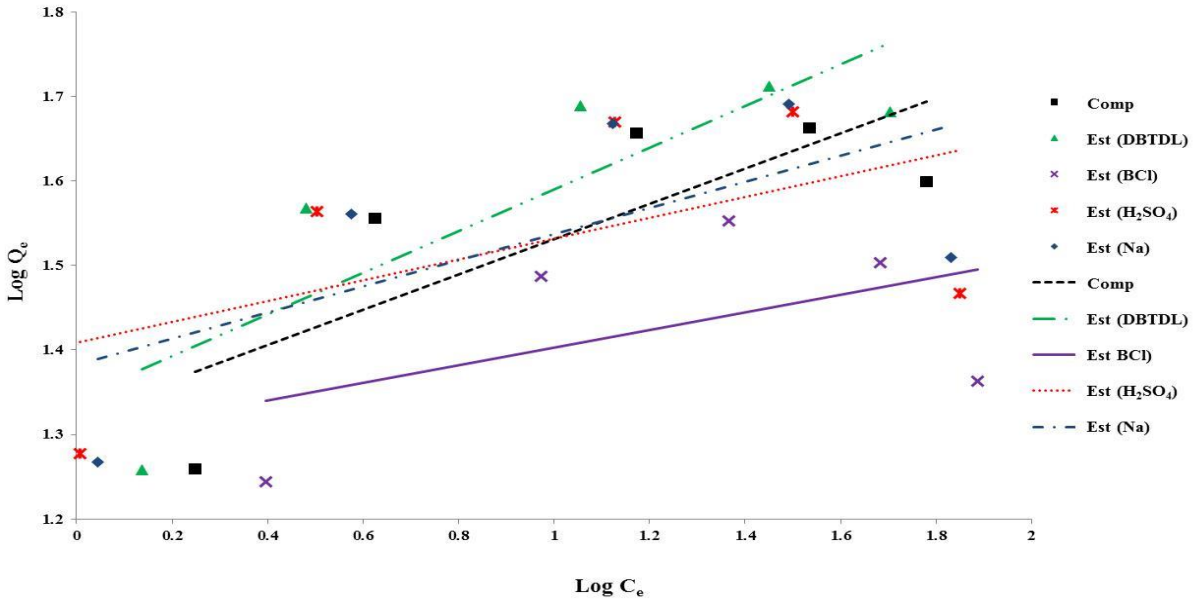

Figure 6.4: Freundlich plots for the adsorption of 1,10-phenanthroline onto ester derivative nanocomposite adsorbents.

The source of the negative *b* value was observed to be the intercept of the Langmuir plot which shifted the R^2 value from 0.9996 to the observed 0.9910. Taking this into consideration Est (H_2SO_4) may be considered to be consistent with the Langmuir model although the accuracy of some values may be shifted.

Table 6.1: Summary for isothermal plots for ester derivative adsorbents adsorption studies.

Adsorbent	Isotherm Class	Isotherm	Slope	R^2	Q_0/K_f	Intercept	*b*/*n*
Comp	L_{mx}	Langmuir	0.0242	0.9898	41.322	0.0026	9.3077
		Freundlich	0.2090	0.6303	21.009	1.3224	4.7847
Est (DBTDL)	L_{mx}	Langmuir	0.0199	0.9958	50.251	0.0207	0.9614
		Freundlich	0.2466	0.7252	22.070	1.3438	4.0551
Est (H_2SO_4)	L_{mx}	Langmuir	0.0238	0.9910	42.017	-0.0094	-2.5319
		Freundlich	0.1878	0.6751	23.779	1.3762	5.3248
Est (BCl)	L_{mx}	Langmuir	0.0282	0.9920	35.461	0.0523	0.5392
		Freundlich	0.1952	0.7644	16.773	1.2246	5.1230
Est (Na)	L_{mx}	Langmuir	0.0223	0.9935	44.843	0.0056	3.9821
		Freundlich	0.2162	0.7456	22.341	1.3491	4.6253

6.4.1.2 Adsorption Kinetics of Esterified Material

Q_t versus time was plotted for the esterified nanocomposites to observe the variation of amount adsorbed with time. These plots are presented in Figure 6.5. Plots were observed to correspond to observations made from isothermal data where they clearly showed the predicted adsorption trends together with better relative approximations between the adsorbents' capacities. Adsorption data was also fitted into the pseudo first-order and pseudo-second order kinetic models and corresponding plots made (Figure 6.6 and Figure 6.7). Data from the kinetic plots was summarized in Table 6.2.

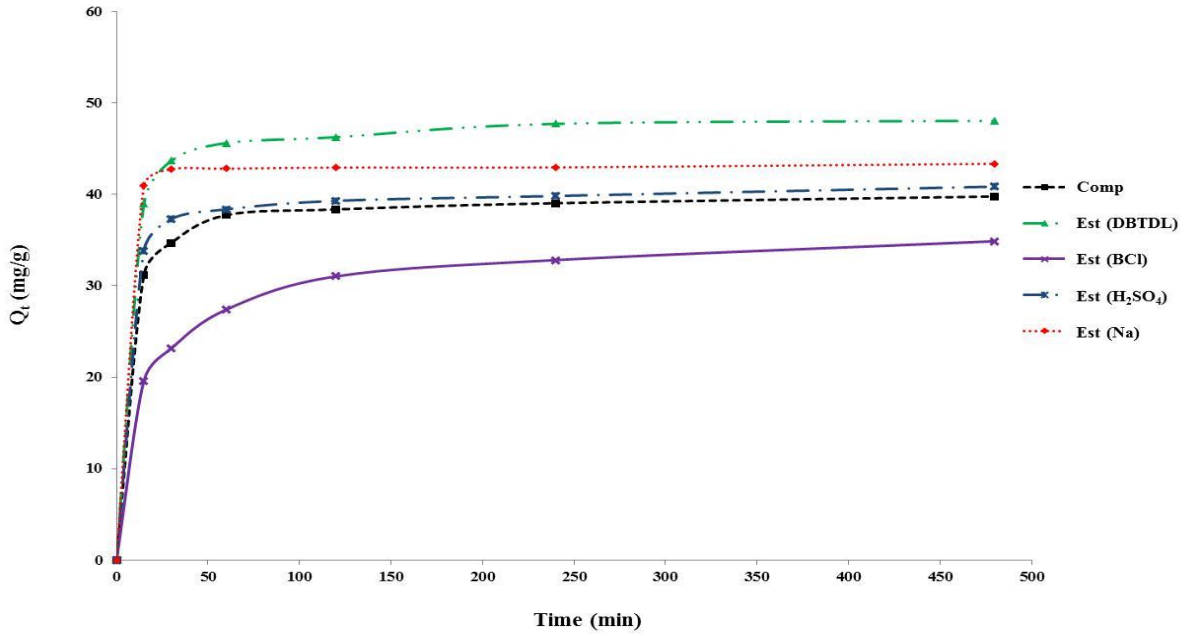

Figure 6.5: Plots for the adsorbed amount (mg/g) of 1,10-phenanthroline onto ester derivative nanocomposite adsorbents against time (min).

All adsorbents were observed to have distinctly high R^2 values for the pseudo second-order kinetic model which was further supported by observation of Q_e values which corresponded to maximum Q_t values observed in Figure 6.5 and corresponded to isothermal findings.

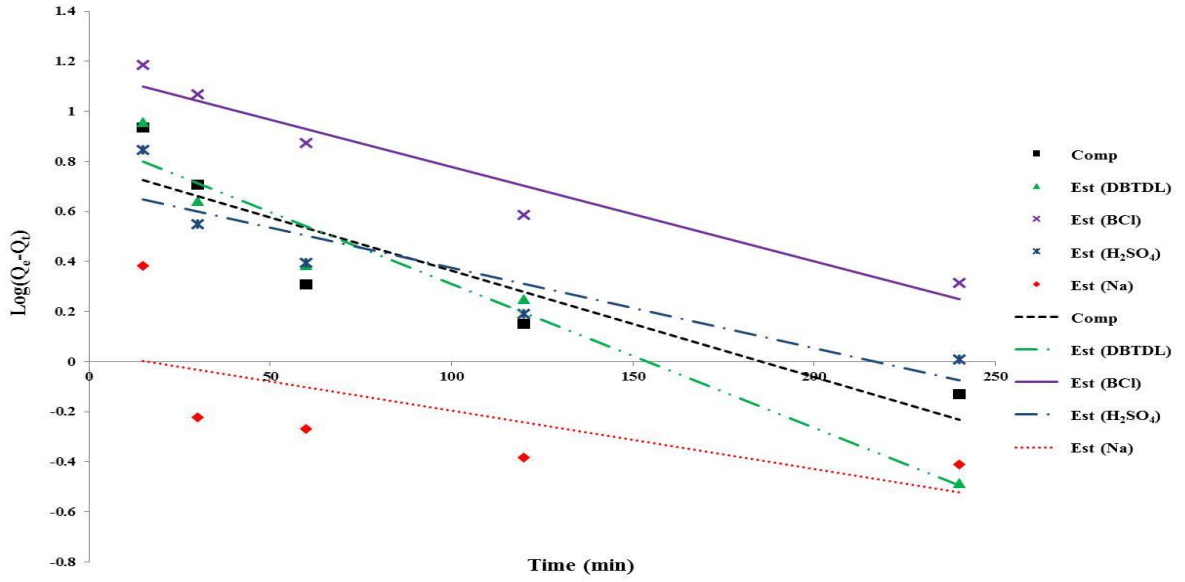

Figure 6.6: Pseudo first-order kinetic model plots for the adsorption of 1,10-phenanthroline onto ester derivative nanocomposite adsorbents.

Although Est (DBTDL) and Est (BCl) had notably high R^2 values for the pseudo first-order kinetic model, their values for the pseudo second-order model were even higher. Therefore all esterified samples together with the non-functionalized nanocomposite conform to the pseudo-second order kinetic model.

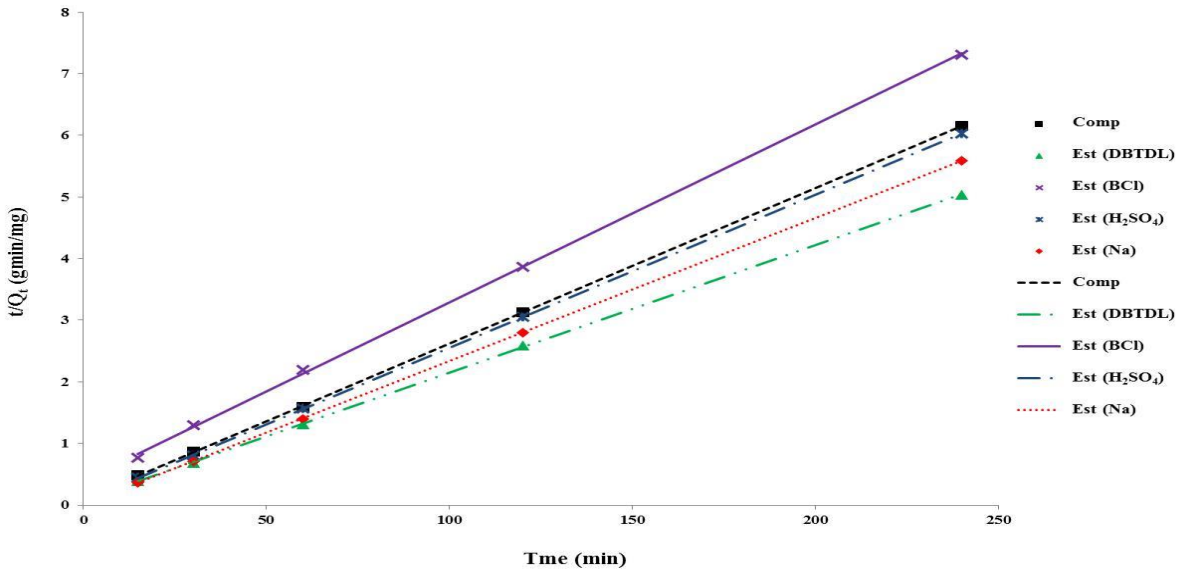

Figure 6.7: Pseudo second-order kinetic model plots for the adsorption of 1,10-phenanthroline onto ester derivative nanocomposite adsorbents.

Table 6.2: Summary for kinetic plots for ester derivative adsorbents adsorption studies.

Adsorbent	Model	Slope	R^2	Intercept	k_1/k_2	Q_e
Comp	1st	-0.0043	0.8330	0.7905	0.0099	6.1731
	2nd	0.0252	1.0000	0.0986	0.0064	39.683
Est (DBTDL)	1st	-0.0057	0.9505	0.8843	0.0131	7.6613
	2nd	0.0207	0.9999	0.0780	0.0055	48.309
Est (H_2SO_4)	1st	-0.0032	0.8213	0.6959	0.0074	4.9648
	2nd	0.0248	1.0000	0.0688	0.0089	40.323
Est (BCl)	1st	-0.0038	0.9429	1.1571	0.0088	14.358
	2nd	0.0288	0.9997	0.4037	0.0021	34.722
Est (Na)	1st	-0.0023	0.4282	0.0359	0.0053	1.0862
	2nd	0.0232	1.0000	0.0102	0.0528	43.103

6.4.1.3 Adsorption Isotherms of Etherified Material

Similarly to the esterified nanocomposites, etherified nanocomposite adsorption isotherms were plotted in comparison to the unfunctionalized nanocomposite (Figure 6.8). All etherified samples were observed to decrease in their adsorption capabilities although at low concentrations Eth (H_2SO_4) showed the best adsorption character. The etherified adsorbents were observed to also fall into the Langmuir (L_{mx}) classification. The base catalyzed etherification products, Eth (Alip-T), Eth (Alip-P) and Eth (Alip-SF) were observed to have closely related isotherms as would have been expected since the only variation was the solvent in the reactions. Although there were closely related some deviations were still observed which confirmed the suspicions that the type of the functionalization solvent may have an influence on the structure and overall performance of the final product adsorbent.

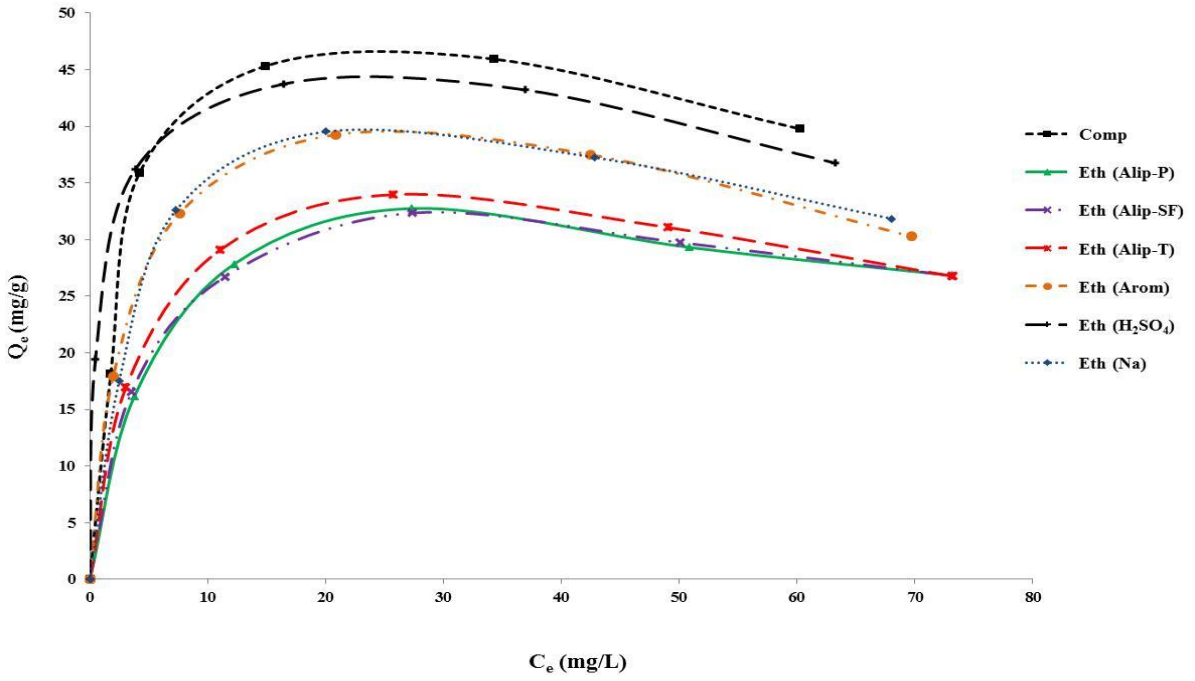

Figure 6.8: Isotherms for 1,10-phenanthroline adsorption by ether derivative nanocomposite adsorbents.

Functionalization using an aromatic moiety in Eth (Arom) with comparison to the corresponding Eth (Alip-T) showed superior adsorption properties.

Adsorption by Eth (H_2SO_4) and Eth (Na) may however not be equally compared with that of the other adsorbents since the functionalization conditions of the adsorbents were different from those of the others. These two samples were however observed to have relatively higher adsorption capabilities and these may be attributed to the pH environment during adsorbent synthesis where the acidic environment seemed to yield superior adsorbents even with esterification. Eth (Na) was synthesised in an environment which was relatively neither acidic nor basic hence its adsorption properties were observed to be between the two extremes. In general the relatively lower adsorption properties of the etherified nanoadsorbents may be attributed to relatively poor dispersion in water as compared to the esterified adsorbents due to lack of the extra ester oxygen which may be used to enhance interaction with water coupled with relatively low functionalization. Adsorption data was also fitted into the Langmuir and Freundlich adsorption model equations and corresponding plots made (Figure 6.9 and Figure 6.10).

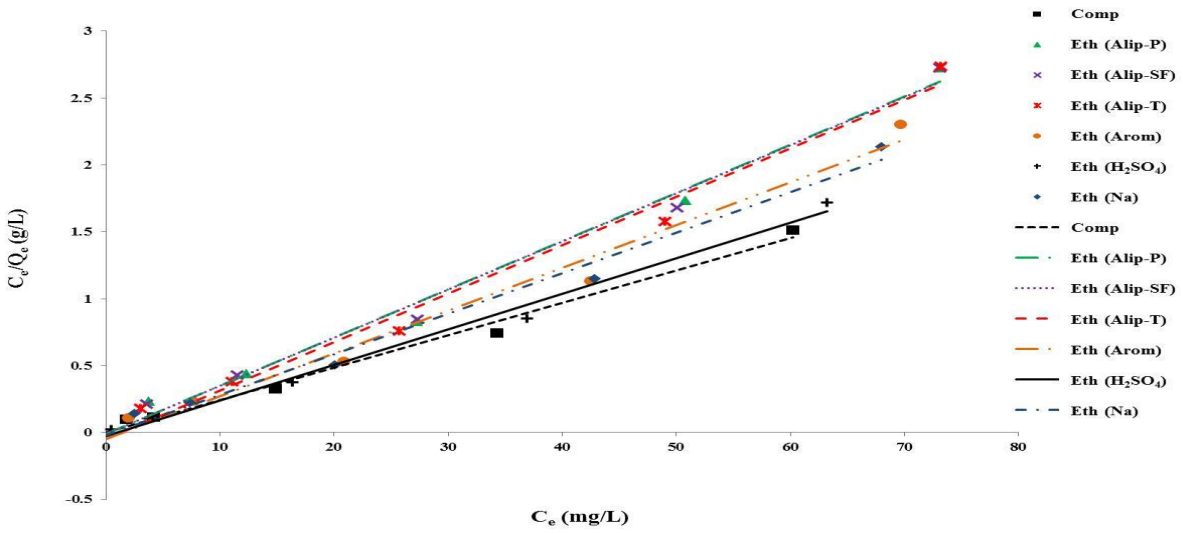

Figure 6.9: Langmuir plots for the adsorption of 1,10-phenanthroline onto ether derivative nanocomposite adsorbents.

Values from the plotted data were summarized in the Table 6.3. All adsorbents in question exhibited high R^2 values for the Langmuir model as compared to the Freundlich model and the Q_0 values gave a trend which corresponded to the adsorption capacities of the adsorbents which both support the prediction by visual inspection in support of conformation to the Langmuir model.

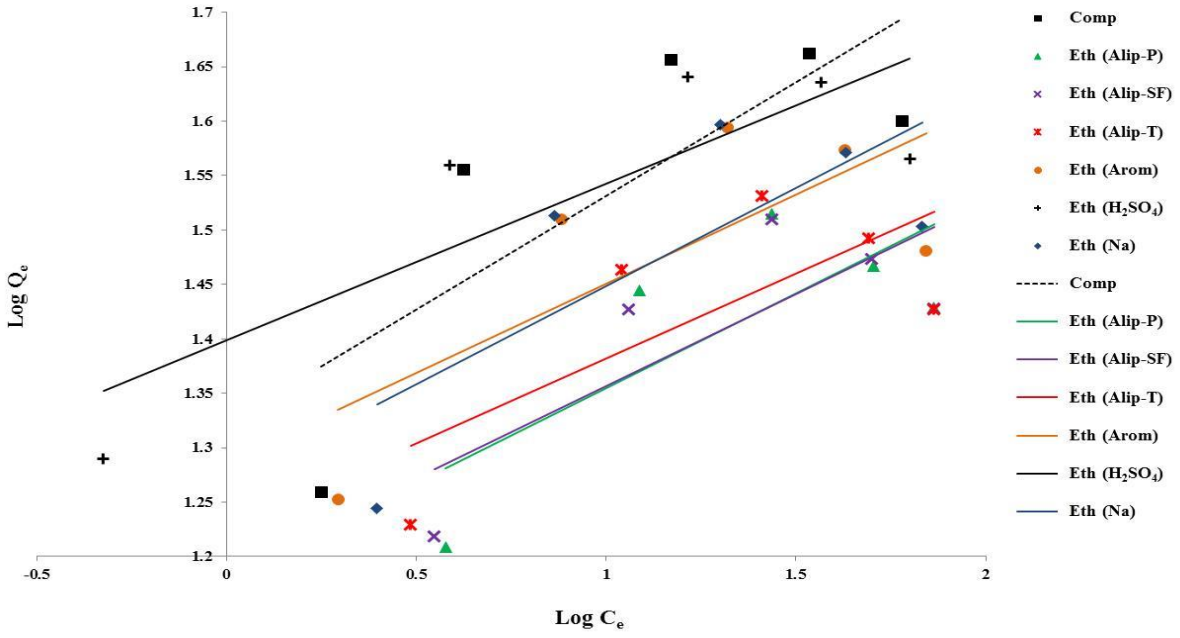

Figure 6.10: Freundlich plots for the adsorption of 1,10-phenanthroline onto ether derivative nanocomposite adsorbents.

On the other hand negative values of *n* were observed for all the etherified adsorbents which did not fit the Langmuir model. However a second look at the adsorption data showed that the last value in the plotting data appeared as an outlier which gave rise to negative intercept values in addition to lowering the R^2 values. Taking this observation into consideration, all the adsorbents were observed to follow the Langmuir adsorption model.

Table 6.3: Summary for isothermal plots for ether derivative adsorbents adsorption studies.

Adsorbent	Isotherm Class	Isotherm	Slope	R^2	Q_0/K_f	Intercept	*n/b*
Comp	L_{mx}	Langmuir	0.0242	0.9898	41.322	0.0026	9.3077
		Freundlich	0.2090	0.6303	21.009	1.3224	4.7847
Eth (Alip-T)	L_{mx}	Langmuir	0.0361	0.9839	27.701	-0.0449	-0.8040
		Freundlich	0.1558	0.5303	16.834	1.2262	6.4185
Eth (Alip-P)	L_{mx}	Langmuir	0.036	0.9885	27.778	-0.0117	-3.0769
		Freundlich	0.1746	0.5750	15.132	1.1799	5.7274
Eth (Alip-SF)	L_{mx}	Langmuir	0.0359	0.9884	27.855	-0.0088	-4.0795
		Freundlich	0.1693	0.6242	15.399	1.1875	5.9067
Eth (Arom)	L_{mx}	Langmuir	0.0319	0.9799	31.348	-0.0481	-0.6632
		Freundlich	0.1638	0.5534	19.355	1.2868	6.1050
Eth (H2SO4)	L_{mx}	Langmuir	0.0266	0.9907	37.594	-0.0269	-0.9888
		Freundlich	0.1435	0.7248	25.061	1.3990	6.9686
Eth (Na)	L_{mx}	Langmuir	0.0303	0.9855	33.003	-0.0195	-1.5538
		Freundlich	0.1801	0.5559	18.561	1.2686	5.5525

6.4.1.4 Adsorption Kinetics of Etherified Material

Kinetics plots similar to those made for the esterified adsorbents were made (Figure 6.11, Figure 6.12 and Figure 6.13) and relevant values are summarized in Table 6.4. The plot of Q_t versus time confirmed and clarified some of the isothermal predictions and adsorption relationships. On the other hand similar to the esterified adsorbents, pseudo first-order and second-order kinetic model plots indicated that all etherified adsorbents conformed to the pseudo-second–order kinetic model with distinctly high R^2 values.

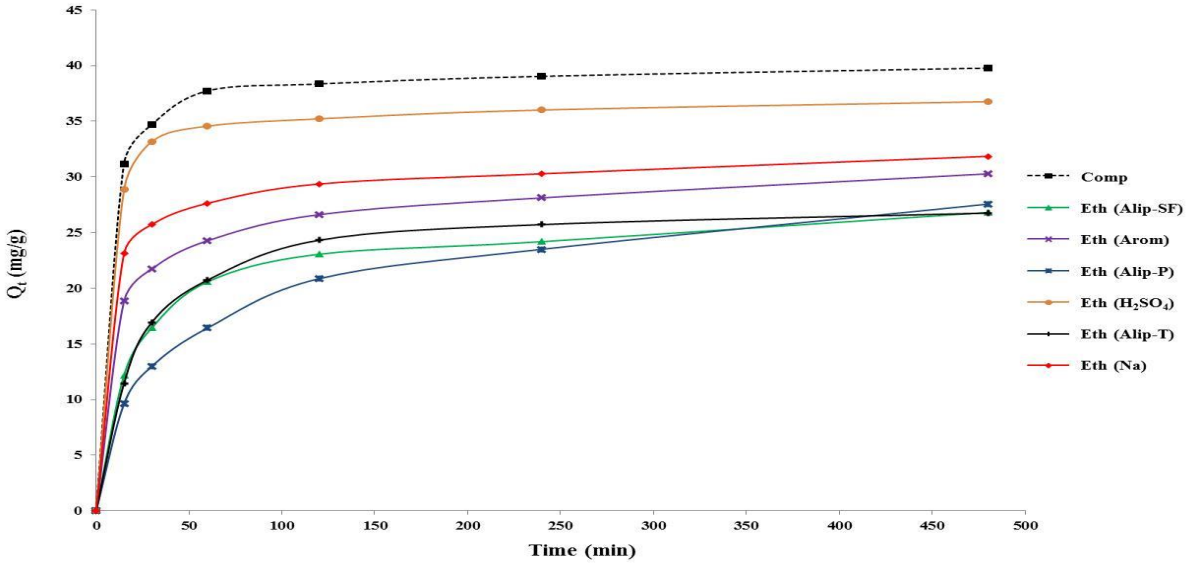

Figure 6.11: Plots for the adsorbed amount (mg/g) of 1,10-phenanthroline onto ether derivative nanocomposite adsorbents against time (min).

Pseudo first-order model R^2 values were relatively high as compared to those of the esterified adsorbents.

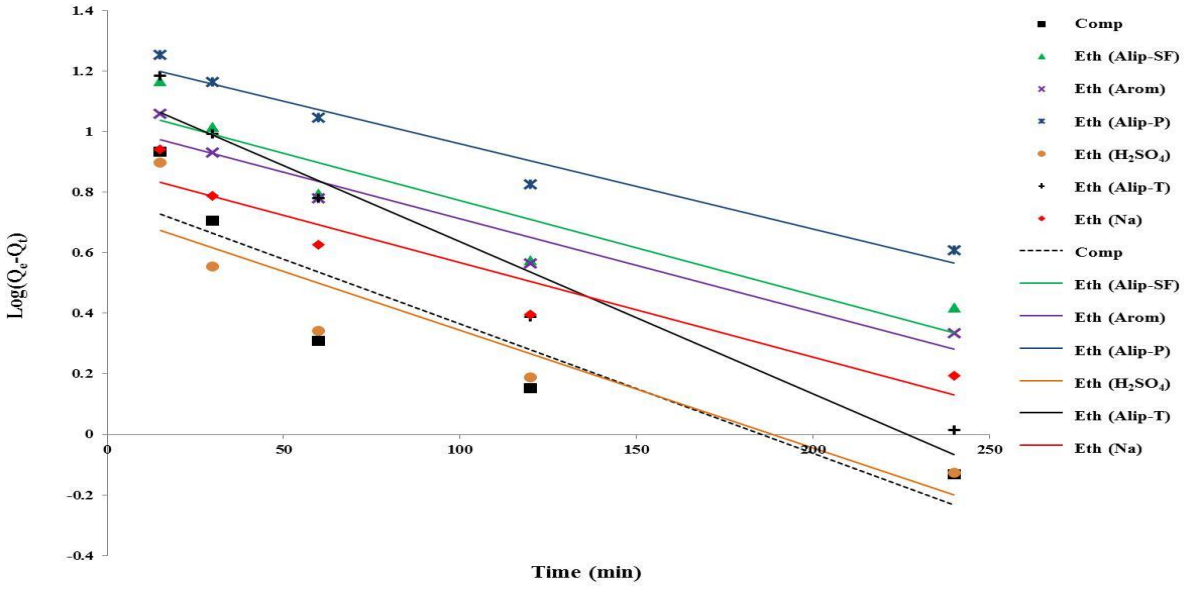

Figure 6.12: Pseudo first-order kinetic model plots for the adsorption of 1,10-phenanthroline onto ether derivative nanocomposite adsorbents.

Also in support of pseudo-second order conformation, Q_e values corresponded to isothermal and Q_t versus time plot predictions.

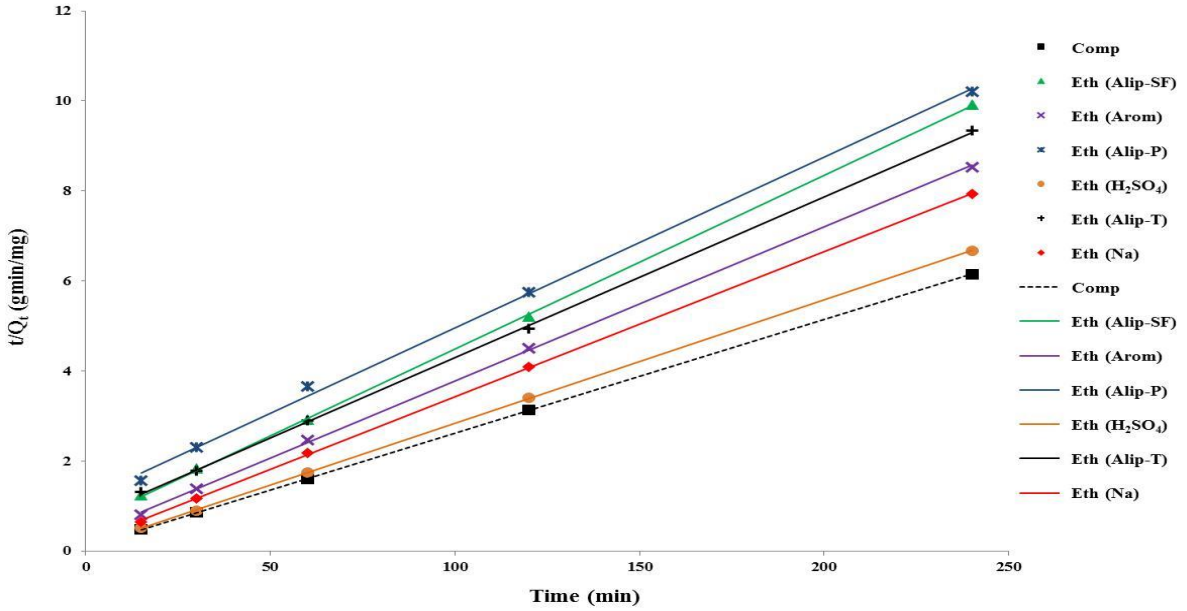

Figure 6.13: Pseudo second-order kinetic model plots for the adsorption of 1,10-phenanthroline onto ether derivative nanocomposite adsorbents.

Table 6.4: Summary of kinetic plots for ether derivative adsorbents adsorption studies.

Adsorbent	Model	Slope	R^2	Intercept	k_1/k_2	Q_e
Comp	1st	-0.0043	0.8330	0.7905	0.0099	6.1731
	2nd	0.0252	1.0000	0.0986	0.0064	39.683
Eth (Alip-T)	1st	-0.0050	0.9477	1.1384	0.0115	13.753
	2nd	0.0357	0.9998	0.7266	0.0018	28.011
Eth (Alip-P)	1st	-0.0028	0.9580	1.2406	0.0064	17.402
	2nd	0.0379	0.9984	1.1739	0.0012	26.385
Eth (Alip-SF)	1st	-0.0031	0.8603	1.0828	0.0071	12.100
	2nd	0.0386	0.9999	0.6316	0.0024	25.907
Eth (Arom)	1st	-0.0031	0.9385	1.0184	0.0071	10.433
	2nd	0.0342	0.9997	0.3561	0.0033	29.240
Eth (H_2SO_4)	1st	-0.0039	0.8471	0.7312	0.0090	5.3852
	2nd	0.0274	1.0000	0.0994	0.0076	36.496
Eth (Na)	1st	-0.0031	0.9096	0.8786	0.0071	7.5614
	2nd	0.0322	0.9999	0.2009	0.0052	31.056

6.4.2 Effects of Nanocomposite Composition

The effect of nanocomposite composition on functionalization and adsorption was accessed using the method of functionalization through esterification by DBLDT catalysis on nanocomposite samples of Lig:NaMMT ratios of 1:1, 1:2 and 2:1. Similar adsorption studies as those described in the previous sections were carried out on the 3 variations.

6.4.2.1 Adsorption Isotherms

Figure 6.14 shows adsorption isotherms for the three variations of the PMPSgLig-NaMMT nanocomposite and their corresponding ester derivatives. As determined inSection 6.4.1.1, Est (DBTDL) samples all conformed to the Langmuir model.

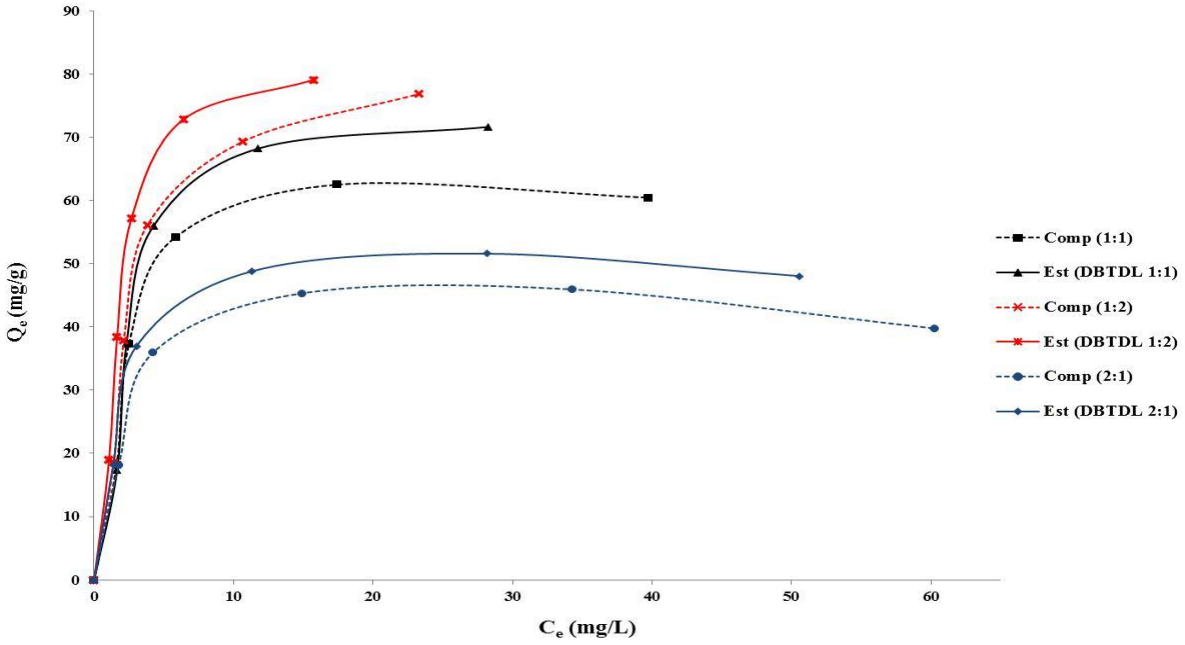

Figure 6.14: Isotherms for 1,10-phenanthroline adsorption by Est (DBTDL) derivative nanocomposites.

However the adsorbents were observed to fall into different types, where Comp (1:1), Comp (2:1) and Est (DBTDL 2:1) were observed to fall in the L_{mx} type while Est (DBTDL 1:1), Comp (1:2) and Est (DBTDL 1:2) fell into the L_2 type subgroup.

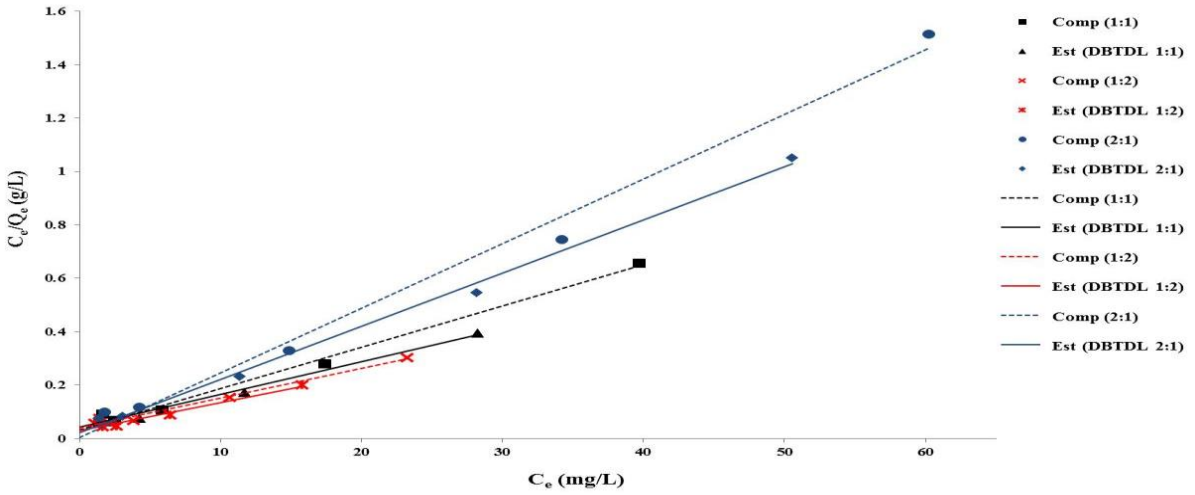

Figure 6.15: Langmuir plots for the adsorption of 1,10-phenanthroline onto Est (DBTDL) derivative nanocomposite adsorbents.

Functionalization was observed to enhance adsorbent activity for all the composition variations with the most significant enhancement being observed with the Comp (1:1) nanocomposite as it resulted in a shift of the adsorption type from L_{mx} to L_2 type which is well in consistency with enhanced adsorption properties.

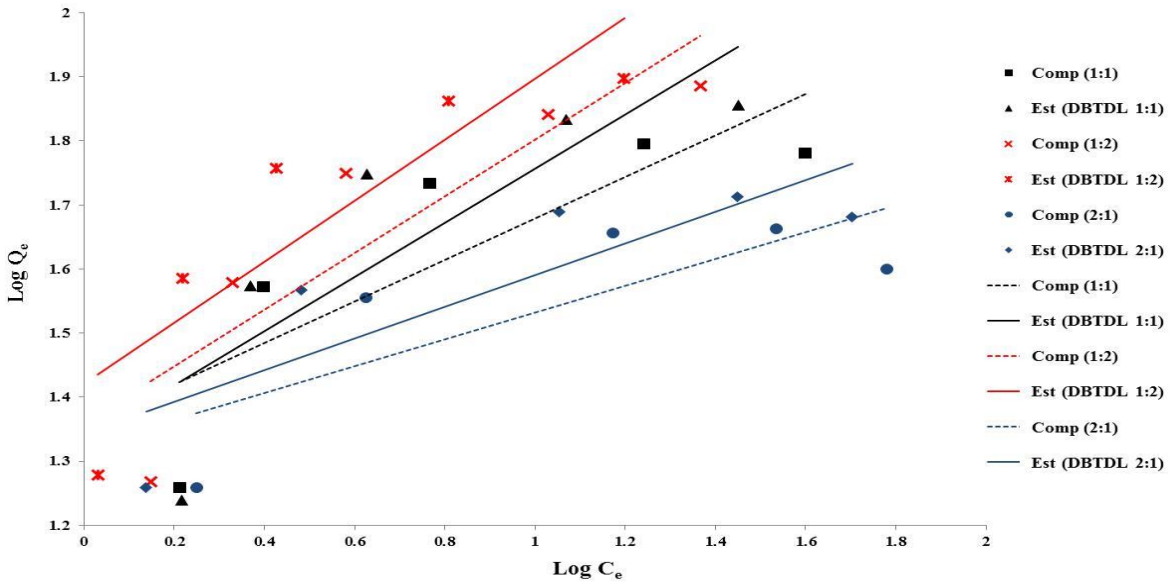

Figure 6.16: Freundlich plots for the adsorption of 1,10-phenanthroline onto Est (DBTDL) derivative nanocomposite adsorbents.

Langmuir and Freundlich plots (Figure 6.15 and Figure 6.16) showed that all variations conformed to the Langmuir model in a similar manner as predicted in Section 6.4.1.1. as can be observed from the data summary in Table 6.5.

Table 6.5: Summary for isothermal plots for Est (DBTDL) derivative adsorbents adsorption studies.

Adsorbent	Isotherm Class	Isotherm	Slope	R^2	Q_0/K_f	Intercept	*b*/*n*
Comp (1:1)	L_{mx}	Langmuir	0.0154	0.9922	64.935	0.0329	0.4681
		Freundlich	0.3245	0.6939	22.646	1.3550	3.0817
Est(DBTDL 1:1)	L_2	Langmuir	0.0122	0.9774	81.967	0.0422	0.2890
		Freundlich	0.4226	0.7123	21.592	1.3343	2.3663
Comp (1:2)	L_2	Langmuir	0.0112	0.9836	89.286	0.0389	0.2879
		Freundlich	0.4420	0.7844	22.872	1.3593	2.2624
Est(DBTDL 1:2)	L_2	Langmuir	0.0106	0.9724	94.340	0.0284	0.3732
		Freundlich	0.4758	0.7748	26.357	1.4209	2.1017
Comp (2:1)	L_{mx}	Langmuir	0.0242	0.9898	41.322	0.0026	9.3077
		Freundlich	0.2090	0.6303	21.009	1.3224	4.7847
Est(DBTDL 2:1)	L_{mx}	Langmuir	0.0199	0.9958	50.251	0.0207	0.9614
		Freundlich	0.2466	0.7252	22.070	1.3438	4.0551

6.4.2.2 Adsorption kinetics

Adsorption data was similarly treated as in Section 6.4.1.1 and Section 6.4.1.3 (Figure 6.17, Figure 6.18 and Figure 6.19) and kinetic model plot data are summarized in Table 6.6. All adsorbent variations and their derivatives were observed to conform to the pseudo second-order kinetic model with high R^2 values although the R^2 values for the pseudo first-order model for all derivatives and the Comp (1:1) samples were also significantly high. The plot of Q_t versus time (Figure 6.17) graphically and clearly presented the equilibrium adsorption capacity relationship between the adsorbent variations and their derivatives.

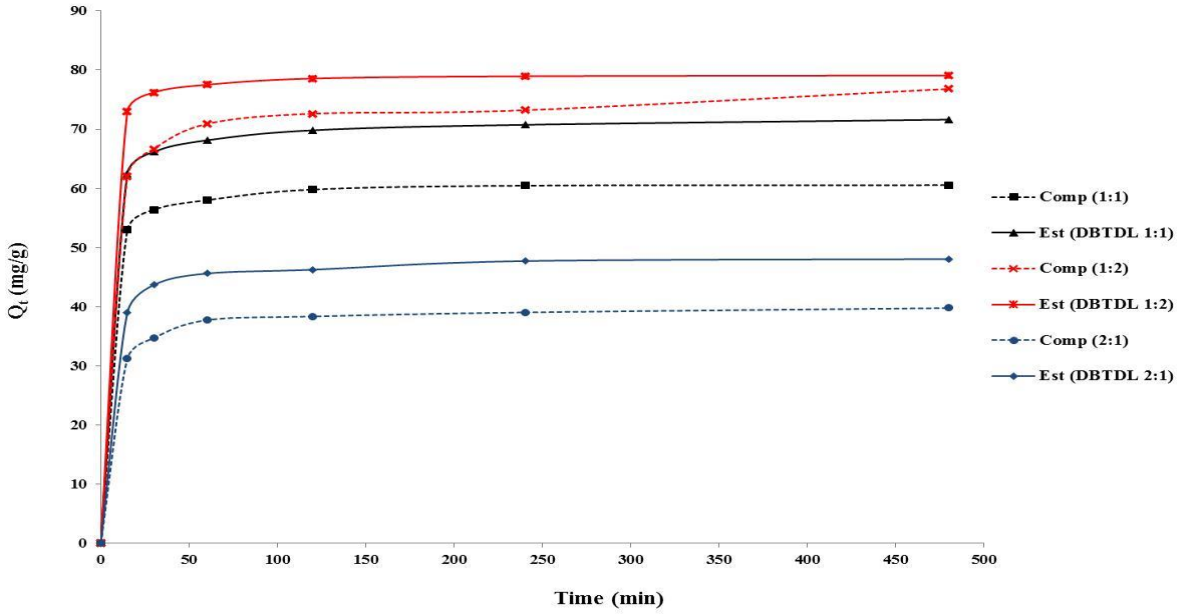

Figure 6.17: Plots for the adsorbed amount (mg/g) of 1,10-phenanthroline onto Est (DBTDL) derivative nanocomposite adsorbents against time (min).

This plot also revealed that the greatest composition influence on adsorbent was observed in the move from the 2:1 to the 1:1 ratio adsorbents (both parent and derivative).

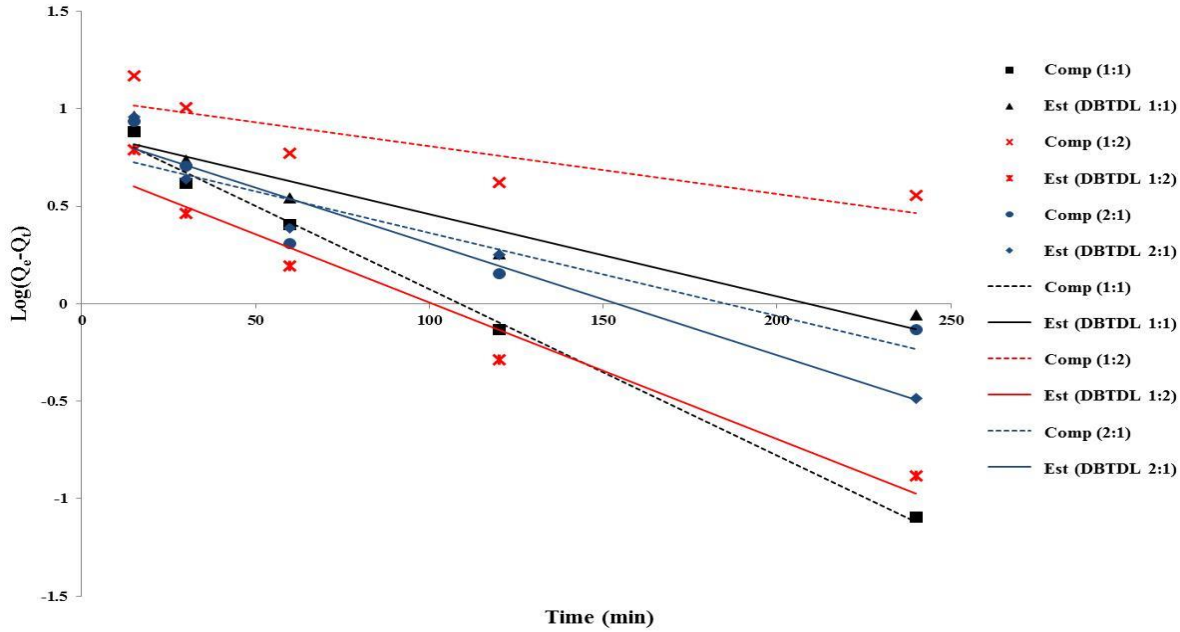

Figure 6.18: Pseudo first-order kinetic model plots for the adsorption of 1,10-phenanthroline onto Est (DBTDL) derivative nanocomposite adsorbents.

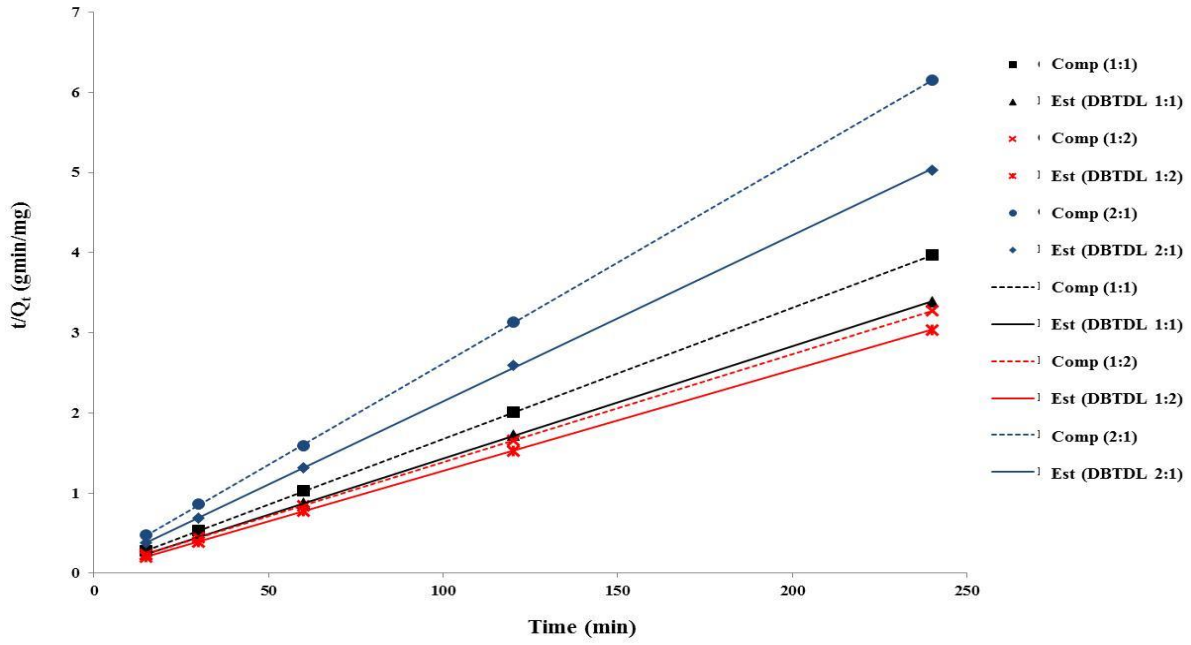

Figure 6.19: Pseudo second-order kinetic model plots for the adsorption of 1,10-phenanthroline onto Est (DBTDL) derivative nanocomposite adsorbents.

Table 6.6: Summary for kinetic plots for Est (DBTDL) derivative adsorbents adsorption studies.

Adsorbent	Model	Slope	R^2	Intercept	k_1/k_2	Q_e
Comp (1:1)	1st	-0.0085	0.9954	0.9282	0.0196	8.4762
	2nd	0.0164	1.000	0.0431	0.0062	60.976
Est(DBTDL 1:1)	1st	-0.0042	0.9255	0.8794	0.0097	7.5753
	2nd	0.0140	1.000	0.0350	0.0056	71.429
Comp (1:2)	1st	-0.0024	0.7420	1.0518	0.0055	11.267
	2nd	0.0135	1.0000	0.0400	0.0046	74.074
Est(DBTDL 1:2)	1st	-0.0070	0.9550	0.7052	0.0161	5.0722
	2nd	0.0126	1.0000	0.0167	0.0095	79.365
Comp (2:1)	1st	-0.0043	0.8330	0.7905	0.0099	6.1731
	2nd	0.0252	1.0000	0.0986	0.0064	39.683
Est(DBTDL 2:1)	1st	-0.0057	0.9505	0.8843	0.0131	7.6613
	2nd	0.0207	0.9999	0.0780	0.0055	48.309

6.5 Conclusion

Although only two products (esters and ethers) were targeted during functionalization, the reaction conditions proved to be highly influential on the properties of the end product including the adsorption capacity. Functionalization via Esterification proved to enhance adsorbent activity while etherification lowered the activity. It was also established that efficiency of the functionalization reaction does not necessarily result in optimum adsorption capacity, but a balance between high functionalization, and adsorbent dispersion and compatibility with water needs to be established as was observed with Est (BCl). The pH environment of the functionalization medium for both esterification and etherification is significantly important as acidic environments gave superior adsorbents.

On the other hand some relatively uncommon reaction catalysis for the functionalization such as the use of DBTDL and Na may prove to give superior active products as was observed in this study of the Est (DBTDL) and Est (Na) nanocomposite adsorbents which had the highest adsorption capacities amongst all the adsorbents studied. The nature of the functionalization moiety had significant influence with aromatic moieties yielding better adsorbing products. When solvents are used in the functionalization reaction, their nature especially their molecular structure may give rise to some slightly notable influence on the adsorption properties of the product with small molecular sizes give results similar to solvent free reactions. However of most notable importance was the effect of nanocomposite composition on the adsorption properties of the adsorbents. The adsorption capacity of the adsorbents proved to be directly proportional to the NaMMT loading.

In general all adsorbents studied conform to the Langmuir adsorption isothermal model and the pseudo-second order kinetic model, and exhibit monolayer adsorption for the adsorption of 1,10-phenanthroline.

6.6 References

Alves Fungaro, D.; Bruno, M. and Grosche, L. C. **(2009)** Adsorption and kinetic studies of methylene blue on zeolite synthesized from fly ash. *Desalination and Water Treatment.* 2. p. 231–239.

Annadurai, G.; Juang, R. S. and Lee, D. J. **(2002)** Use of cellulose-based wastes for adsorption of dyes from aqueous solutions. *Journa of Hazardous Materials*. B92. p. 263–274.

Delval, F.; Crini, G.; Morinc, N.; Vebrel, J.; Bertini, S.; Torri, G. **(2002)** The sorption of several types of dye on crosslinked polysaccharides derivatives. *Dyes and Pigments*. 53. p. 79–92.

Giles, C. H.; Macewans, T. H.; Nakhwa, N.; Smith, D. **(1960)** Studies in adsorption Part XI. A system of classification of solution adsorption isotherms, and its use in diagnosis of adsorption mechanisms and in measurement of specific surface areas of solids. *Journal of Chemical Society*. 111. p. 3973-3993.

Hinz, C. **(2001)** Description of sorption data with isotherm Equations. *Geoderma*. 99. p. 225–243.

Igwe, J. C. and Abia, A. A. **(2007)** Equilibrium sorption isotherm studies of Cd(II), Pb(II) and Zn(II) ions detoxification from waste water using unmodified and EDTA-modified maize husk. *Electronic Journal of Biotechnology*. [Online] 10 (4). Available from: http://www.ejbiotechnology.info/content/vol10/issue4/full/15/ [Accessed: 13 November 2014]

King, P.; Rakesh, N.; Beenalahari S.; Kumar, Y. P.; Prasad, V. S. R. K. **(2007)** Removal of lead from aqueous solution using *Syzygium cumini* L.: Equilibrium and kinetic studies. *Journal of Hazardous Materials*. 142 (1-2). p. 340-347.

Kul, A. R. and Koyuncu, H. **(2010)** Adsorption of Pb(II) ions from aqueous solution by native and activated bentonite: kinetic, equilibrium and thermodynamic study. *Journal of Hazardous Materials*. 179. p. 332–339.

Kumar, D.; Singh, A. and Gaur, J. P. **(2008)** Mono-component versus binary isotherm models for Cu(II) and Pb(II) sorption from binary metal solution by the green alga Pithophora oedogonia. *Bioresource Technology*. 99. p. 8280–8287.

Kumar, K. V. and Sivanesan, S. **(2006)** Pseudo second order kinetic models for safranin onto rice husk: Comparison of linear and non-linear regression analysis. *Process Biochemistry*. 41. p. 1198–1202.

Limousin, G.; Gaudet, J. P.; Charlet, L.; Szenknect, S.; Barthès, V.; Krimissa, M. **(2007)** Sorption isotherms: A review on physical bases, modelling and measurement: Review. *Applied Geochemistry*. 22. p. 249–275.

Namane, A.; Mekarzia, A.; Benrachedi, K.; Belhaneche-Bensemra, N.; Hellal, A. **(2005)** Determination of the adsorption capacity of activated carbon made from coffee grounds by chemical activation with ZnCl2 and H3PO4. *Journa of Hazardous Materials*. B119. p. 189–194.

Rawajfih, Z. and Nsour, N. **(2006)** Characteristics of phenol and chlorinated phenols sorption onto surfactant-modified bentonite. *Journal of Colloid and Interface Science*. 298. p. 39-49.

Wang, S.; Dong, Y.; He, M.; Chen, L.; Yu, X. **(2009)** Characterization of GMZ bentonite and its application in the adsorption of Pb(II) from aqueous solutions. *Applied Clay Science*. 43. p. 164-171.

CHAPTER 7

CONCLUSIONS AND RECOMMENDATIONS

7.1 Conclusion

PMPSgLig-NaMMT nanocomposite adsorbent was successfully functionalized by both esterification and etherification methods, but only the esterification functionalization methods achieved the aim of the study which was, to enhance adsorption of organic pollutants from water. Ester functionalization of the nanoadsorbents was to different extents proportional to the adsorption activity of the adsorbents in the absence of other factors. However the source of adsorption enhancement (hydrophobicity) opposed an essential factor (adsorbent dispersion in water) vital to the adsorbent activity. Therefore optimum enhancement of the adsorbent activity goes beyond functionalization alone, and dispersion of the functionalized adsorbent in water should hence be critically considered.

Other factors such as pH environment of the functionalization reaction, use of solvents and nature of functionalization moiety were influential as acidic environment and solvent-free grafting of aromatic moieties gives high performance adsorbents. On the other hand, of great importance was the nanocomposite composition, where high NaMMT content enhanced adsorbent performance which was attributed to enhanced adsorbent dispersion in water (increase in available surface area) which was important since the adsorption process occurred in a monolayer fashion.

7.2 Recommendations for further work

In this study the conditions used for functionalization were theoretically optimum based on literature of similar material which may not be the case for the nanocomposite in question, hence optimization using practically determined conditions may be necessary to verify the results obtained. The effect of chain length of the functionalization moiety on the functionalization and overall adsorption activity of the adsorbent needs to be investigated for the selection of the most appropriate functionalization molecule since the overall hydrophobic nature of the material has a notable effect on the dispersion in water. For the different functionalization methods investigated, different nanocomposite components may be preferentially targeted for functionalization and as observed in this study, the composition may facilitate grafting onto a particular component hence the effect of composition may need to be investigated for all methods used.

The base catalyzed etherification method was observed to be prone to contamination mainly due to the relatively low solubility of the Ag_2O catalyst hence the use of more soluble bases may be assessed. On the other hand the use of halogenoalkanes for ether functionalization using Na as a catalyst proved to be possible, but with great need for optimization to limit lignocellulose attack by free radicals and possibly avoid free radical attack of grafted moieties. Est (BCl) showed the most efficiency in functionalization but adsorption properties were negatively affected due to poor dispersion in water, and study of the specific parameters and conditions to limit functionalization to an optimum level may be useful as this method may provide an efficient route for introduction of selective functionalization moieties. The effect of varying methods of lignocellulose pretreatment before nanocomposite synthesis, on functionalization and the adsorption properties of the product need to be accessed as this may reveal means of optimizing nanoadsorbent activity.

The concept of functionalization can be fine-tuned to introduce selectivity and specificity hence it may be interesting to establish the relevant parameters such as the functionalization moiety for application on specific pollutants. The fate of the heavy metal adsorption properties of the original material needs to be established including investigation of simultaneous adsorption of different pollutants from water. Desorption studies may also provide an insight into the potential for reuse of the material after an adsorption cycle hence such studies need to be carried out. The effects of temperature and pH on the adsorption by the functionalized nanocomposites were not investigated in this study hence establishing these effects may prove essential for practical application of the material. Assessment of the application in a continuous flow system needs to be carried out to establish the potential practical application of the material, as a step towards commercial application.